PRACTICAL DESIGN GUIDELINES FOR SYNTHETIC MULTIVALENT NANOPARTICLES AS TARGETED BIOMEDICAL NANODEVICES

by

Ming-Hsin Li

A Dissertation submitted in partial fulfillment
of the requirement for the degree of
Doctor of Philosophy
(Biomedical Engineering)
in the University of Michigan
2013

Doctoral Committee:

Professor James R. Baker, Jr., Chair
Professor Ronald G. Larson
Professor Xudong Fan
Professor David S. Sept

DEDICATION

To my parents, Deng-Jye Lee and Chi-Ying Chiu, my wife Pei-Ling, and my little boy, Isaac.

ACKNOWLEDGMENTS

I would like to express my appreciation to my advisor Prof. James Baker, Jr. Without his support, encouragement and advice, this study could not be accomplished. Form the conception of this project to its completion; Dr. Baker fully dedicated himself to teaching me how to become a real scientist. All the while, he created a perfect role model that I could learn from. I also would like to sincerely thank Prof. Ronald Larson for his support from the EFRI project and the enormous scientific inspiration he provided me during the NSF project. My other committee members, Prof. Sherman Fan and Prof. David Sept also guided me throughout this study and generously gave of their time and provided valuable suggestions.

It was a great pleasure to work with a number of incredibly supportive collaborators in the Baker group. I would like to give special recognition to Dr. Seok Ki Choi for his encouragement and training in the initial part of my PhD studies. I also obtained a extensive help from Dr. Hong Zong, Dr. Baohuang Huang, Dr. Pascale Leroueil, Shengzhuang Tang, Ankur Desai and Cheryl Bradshaw. Their expertise in chemistry, analytical techniques and biological sciences provided knowledge that facilitated this study.

Finally, I would like to thank my family members. My wife Pei-Ling is always with me during this journey, even when times were difficult. My parents also made incredible sacrifices that allowed me to chase my dream. I am truly fortunate to have the support of my remarkable family.

TABLE OF CONTENT

LIST OF TABLES

LIST OF FIGURES

LIST OF ABBREVIATIONS

Ac	Acetyl amide
CAM	Cell adhesion molecule
CuAAc	Cu (I)-catalyzed alkyne azide 1.3-dipolar cycloaddition
DCC	Dicyclohexylcarbodiimide
DIEPA	*N*,*N*-Diisopropylethylamine
DMSO	Dimethyl sulfoxide
DNA	Deoxyribonucleic acid
EDC	1-ethyl-3-(3-dimethylaminopropyl)carbodiimide)
G	Generation
GA	Glutaric acid
HPLC	High performance liquid chromatography
K_D	Dissociation constant
k_{off}	Dissociation rate constant
k_{on}	Association rate constant
MALDI	Matrix assisted desorption/ionization-
MS	Mass Spectrometry
MTX	Methotrexate
MWCO	Molecular Weight Cut Off
NGR	Asparagine-glycine-arginine
NHS	N-hydroxysuccinimide

OD_{260}	Optical density at 260 nm
PAMA	Poly(methyl methacrylate)
PAMAM	Poly(amidoamine)
PBS	Phosphate buffered saline
PEG	Poly(ethylene glycol)
PLGA	Poly(lactic-*co*-glycolic acid)
RGD	Arginine-glycine-aspartic acid
RU	Response unit
scFv	Single chain Fv antibody fragment
SEC	Size-exclusion chromatography
SPAAC	strain-promoted alkyne-azide cycloaddition
SPR	Surface plasmon resonance
ss	Single-stranded
UV-Vis	Ultraviolet-visible

ABSTRACT

This dissertation explores the heterogeneity of synthetic nanoparticles and systematically investigates factors that regulate the multivalent binding avidity of these particles. We aim to establish parameters for designing multivalent nanoparticles, and define the role the heterogeneity of nanoparticles plays in this process from both structural and kinetic perspectives. In these studies, the kinetic and thermodynamic binding parameters of heterogeneous nanoparticle populations are identified and evaluated. We assess the effect of varied design parameters on the function of multivalent nanoparticles to provide these design guidelines. In the end, we prove the binding avidity of nanoparticles can be optimized using this approach.

We first developed a novel method for evaluating the avidity distribution of nanoparticles. This involved the design and synthesis of a model multivalent nanoparticle system and a unique kinetic analysis to quantify the avidity distribution. We used mono-dispersed PAMAM dendrimers functionalized with ssDNA oligonucleotides as a platform, and used complementary oligonucleotides as targeted receptors to create this well-controlled model nanoparticle system and an SPR biosensor to evaluate their binding. We found the binding curves were characterized by heterogeneity, including fast- and slow-dissociation subpopulations. By using a parallel initial rate analysis and dual-Langmuir analysis, the

avidity distribution of nanoparticles were determined and compared to the chemical diversity of ligand distribution.

Second, we probed the avidity distributions resulting from a variety of parameters, including the number and the affinity of functionalized ligands. Based on both experimental and simulation results, we showed that multivalent interactions were dependent on these design parameters and developed strategies to enhance the binding avidity of ligand-functionalized nanoparticles and the frequency of high-avidity subpopulations in the heterogeneous nanoparticles.

Finally, we tested the principles defined in our prior studies by synthesizing ligand-functionalized nanoparticles that demonstrated homogeneous high-avidity interactions with SPR surfaces. This was accomplished by using copper-free click chemistry, which allowed us to synthesize uniform and densely ligand-functionalized nanoparticles. As hypothesized, these nanoparticles demonstrated uniform binding to the targeted surface with pM-level avidity. This avidity is comparable to the avidity of antigen-antibody interaction, suggesting that these guidelines can be used in the design of nanoparticles in targeting drugs *in vivo*.

CHAPTER 1

INTRODUCTION

1.1 Ligand-functionalized nanoparticle-based targeted delivery systems

More than one hundred years ago, Paul Ehrlich postulated the idea of a "magic bullet" and depicted the vision of targeted drug therapy. [1] Over these decades, researchers have been dedicated to the concept of "side effect-free" therapy achieved by using specific molecular interactions to target biomarkers on cells associated with diseases.[2-8] This "active" targeting has been extensively studied using both antibodies and ligand-functionalized nanoparticles as targeted delivery systems. In particular, nanoparticle-based targeting systems bring advantages that could not be achieved with antibodies. These advantages include 1) low immunogenicity, 2) high chemical stability, 3) prolonged circulation time, 4) high drug payload, and 5) multi-functionality. In particular, nanoparticles with multiple numbers of ligands have been developed as carriers for targeted therapeutics and diagnostics. Currently, ligand-functionalized nanoparticles have demonstrated promise in targeting drugs in preclinical development. Moreover, some targeted nanoparticles have even entered early phases of clinical studies, as listed in Table 1.1.[9-14]

Given the tremendous therapeutic potential of ligand-functionalized nanoparticles, a wide variety of biological ligands have been coupled to nanoparticles for drug targeting. As listed in Table 1.2, peptides, nutrients, aptamers, and fragments to antibodies have all been

explored as targeting molecules to treat serious illnesses such as cancer and autoimmune diseases.[15-21] The explosive growth of novel types of nanoparticles also expands the opportunities of nanoplatforms for targeted delivery. Researchers can select nanoparticles based on the size (1-100 nm), material (organic or inorganic), or other physical properties such as geometry and fluorescence sensitivity. [2-8] Examples include dendrimers, liposomes, nanoemulsions, micelles, quantum dots and non-spherical nanoparticles; in short, a wide variety of nanoparticles have demonstrated their potential to serve as platforms in targeted nanocarriers.

PAMAM dendrimers were developed during the 1980's, and this family of polymer nanoparticles has attracted attention due to its unique characteristics for biomedical applications, including 1) high water solubility, 2) well-defined chemical structure, and 3) excellent biocompatibility.[22-24] Additionally, abundant surface amino groups on PAMAM dendrimers offer the potential for surface modification with biological molecules to create functionalized nanoparticles. Recently, a variety of natural and synthetic ligands have been coupled to the surface of PAMAM dendrimers to promote the ligand-mediated targeting. These molecules include folic acid, methotrexate, RGD peptides, and aptamers.[25-28] PAMAM dendrimers can also be coupled to drug molecules, antisense RNA, fluorescent dyes, and inorganic contrast agents for use in targeted therapeutics or imaging agents.[29-31] These macromolecules have the potential to form the basis for the next generation of therapeutics.

1.2 Multivalency in ligand-functionalized nanoparticles

Multivalency is characterized by the simultaneous interaction of multiple ligand-receptor pairs, which is believed to collectively result in stronger binding avidities than the interaction between a single ligand-receptor pair.[32,33] (Fig. 1.1) Utilizing this mechanism, a variety of biological molecules and cells can effectively recognize their targets on multivalent surfaces. For instance, viruses use multivalent interactions to recognize membrane binding proteins or antigens presented on cells. Synthetic multivalent ligands with enhanced binding avidity based on this biological phenomenon have also been developed as a means to target nanoparticles. To evaluate this multivalent enhancement, the quotient of dissociation constant between the monovalent free ligand and the multivalent ligand, $\beta = \frac{K_{D,monovalent}}{K_{D,multivalent}}$, is conventionally used as a quantitative indicator. According to reports, this synthetic multivalent enhancement can be as high as a million-fold improvement over the affinity of a single ligand-receptor pair.

In addition, multivalency offers a unique advantage over other approaches of targeting, which is a better selectivity of recognition. Multivalent interactions are, in fact, highly sensitive to the density of counter interacting molecules or moieties. That is, multivalent targeting would only be effective on tissue expressing a sufficient density of receptors. When the surface density of a receptor is not sufficient, the possibility to form simultaneous interactions between ligand-receptor pairs would dramatically decrease, leading to the loss of a multivalent interaction. [34,35] The capability to determine receptor density would actually benefit targeted delivery by avoiding the undesired interaction on tissues expressing just a normal level of receptors. This concept was proved by a statistical thermodynamic simulation that demonstrated that multivalent interactions would undergo a

very sharp transition at the “cut-off” receptor density required to support enhanced binding avidity. Below that concentration, multivalent interactions essentially would just disappear.

With assets from both bionanotechnology and multivalent architecture, synthetic multivalent nanoparticles promise to serve as an ideal targeting delivery system. In general scenarios, the key to successfully developing multivalent nanoparticles is to have an adequate process of fabrication. Particularly, the process to add multiple, stably coupled ligands onto the nanoparticle platforms is crucial to the ability to target. On the one hand, harsh chemical methods should be avoided to maintain the biological activity of the ligand. On the other hand, the chemistry should also be an efficient reaction in order to ensure multiple ligands can be “squeezed” onto the small surface of nanoparticles. A variety of conjugation chemistries have been applied to achieve this purpose, including amide bond and ester bond, thiourea bond, gold-sulfur bond, and cycloaddition chemistries.[36-39] After the synthesis, the interaction of these nanoparticles could be examined with a variety of bioanalytical methods, such as SPR, ITC and ELISA.[35,40,41]

1.3 Design strategies of ligand-functionalized multivalent nanoparticles

The targeting avidity of synthetic, multivalent nanoparticles is the result of a variety of design factors, such as the number of attached ligands on the nanoparticles (valence), the length and flexibility of the ligated linkers, and the size of the nanoparticle platforms.[42-44] Due to the ease of varying the number of ligands, valence has become the most studied factor that alters the avidity of nanoparticles.[45,46] Hong and co-workers utilized a series of folic acid-functionalized G5 PAMAM dendrimers with a variety of ligand numbers to evaluate the

effect of valence on the binding avidity of synthetic multivalent nanoparticles. Their results showed that multivalent enhancement, β, of the functionalized dendrimers reached its maximum and saturated when the nanoparticles had an average of 5 or more folic acids. This result suggests that when synthesizing folic acid-functionalized G5 dendrimers as targeted carriers, the ideal valence number of folic acids on the dendrimers would be 5. Similarly, Tassa and co-workers conducted an extensive survey on the binding avidity of a combinatorial library of ligand-functionalized iron oxide nanoparticles. They consistently found that nanoparticles functionalized with 4 or more ligands can show multivalent enhancement. Taken together, this work suggests that there is a threshold for the number of ligands required to obtain multivalent binding.

However, other nanoparticle systems failed to reach a consensus on the ideal valence for synthetic multivalent systems. This is best exemplified with a series of carbohydrate-functionalized dendrimers developed to target lectins.[40,47,48] The results showed their interaction with the lectin hardly showed saturation due to increases in the number of carbohydrates on the nanoparticles. Additionally, the enhancement of binding avidity was also not as significant as that observed with folic acid-functionalized dendrimers. The discrepancy due to the effect of valence suggests the mechanism involved in multivalent interactions could be variable and dependent on the properties of functionalized ligands. Some of the additional results in Tassa's studies likely confirmed this trend of ligand-dependence. They found that β of nanoparticles functionalized with 4 different ligands can range from 10 to more than 1000. Interestingly, it was also found that the intensity of the avidity of synthetic multivalent nanoparticles is inversely proportional to the intrinsic affinity

of ligand, further highlighting the importance of physical properties in the synthetic multivalency.

1.4 Heterogeneous ligand distribution on multivalent nanoparticles

The number of functionalized ligands on nanoparticles is characterized by a variety of analytical techniques. These measurements provide the number of functionalized ligands, either based on the change of molecular weight that occurs during the ligand conjugation process as measured by MALDI MS and GPC or the change in the intensity of characteristic spectroscopic signals generated by the functionalized ligands using techniques such as NMR and UV-Vis.[18,26,29] These measurements, however, in most cases provide simply an arithmetic mean of distributed numbers, and a single molecular population value derived from bulk analysis cannot comprehensively reflect the properties of the composition of single molecules in a population of synthetic multivalent nanoparticles. Thus, while most synthetic materials are heterogeneous, especially after modified or functionalized, the quantitative analysis of the heterogeneity is still insufficient. This prevents an understanding of whether the binding characteristics observed for nanoparticles are representative of all particles in a population or indicative of only subpopulations of molecules with higher affinity binding.

Recently, our laboratory and others have attempted to address this problem by examining the distribution of ligands chemically coupled to nanoparticles. Statistical thermodynamic simulations predicted the distribution of functionalized ligand on nanoparticles would present not as a uniform population but as a Poisson-distributed pattern.[49,50] An experimental assessment of the distribution of a series of ligand-

functionalized dendrimers displayed as a Poisson distribution, thus confirming this prediction of the simulation. To further confirm this finding, the number of ligands was directly measured on HPLC fractionated populations of functionalized dendrimers, and the result of this analysis correlated to a Poissonian distribution. Together, these results convey two important messages that should guide the rational design of synthetic multivalent nanoparticles: 1) the distribution of functionalized ligands is broad and not at all uniform, varying widely from zero to more than double the mean, and 2) the portion of molecules in a nanoparticle distribution having the mean number of ligands is limited (less than 20% of the population). More remarkable, in a study of a dual ligand-nanoparticle system, where two separate materials were ligated to the dendrimer, the subpopulation that bears the mean number of each of the two ligands represented roughly only 5% of the population. (Figure 1.2) These considerations need to be kept in mind whenever testing or evaluating populations of nanoparticles and make the assessment of the activities of these molecules difficult.

Given the markedly heterogeneous distribution of multivalent ligands on nanoparticles, one must assume that there are marked heterogeneous ligand-receptor interactions that yield distributed binding avidities with target surfaces. In this scenario, only the small portion of nanoparticles with higher levels of ligand functionalization would demonstrate avidity and lead to strong binding. This would suggest that in applications such as drug delivery, only a portion of the nanoparticles would work and would thus require increasing the overall dose required for a desired therapeutic effect. Also, the weaker-avidity subpopulations would cause safety concerns because their carried drugs or imaging agents would not be efficiently targeted and could potentially lead to side effects. Clearly, the reduction or even the removal of weak-avidity nanoparticles would increase the binding

specificity of synthetic multivalent nanoparticles. While these concerns are real, there remains a poor understanding of the concept of multivalent nanoparticle binding and the role that different variables play in binding, such as the number of ligands, the intrinsic affinity of functionalized ligands, and the distributed binding avidity of synthetic multivalent nanoparticles. Therefore, it would be extremely important to establish methods to investigate the avidity distribution of nanoparticle binding. This is the focus of my thesis.

1.5 Outline of Dissertation Organization

This dissertation explores the heterogeneity of synthetic nanoparticles and systematically investigates factors that regulate the multivalent binding avidity distributions of these systems. In Chapter 2, a novel method that was developed for evaluating avidity distribution will be introduced. The procedures underlying this method will also be discussed. These methods involved the design, synthesis, and characterization of a model multivalent nanoparticle system, kinetic measurements of the binding in this system using a SPR biosensor, and a unique kinetic analysis to quantify the avidity distribution. In Chapter 3, we use this novel kinetic method to probe the dependence of an avidity distribution on a number of functionalized ligands. Based on both experimental and simulation results, we show the relationship of multivalent interactions to the valence number on the nanoparticle and develop a strategy using this factor to design high-avidity ligand-functionalized nanoparticles. In Chapter 4, the effect of physical factors that alter specific affinity of ligands, including temperature, was used to assess the effect of the intrinsic affinity of ligands on the binding heterogeneity of synthetic multivalent nanoparticles. After revealing the effect of a variety of factors on multivalent binding, in Chapter 5 we test principles learned from prior studies by

synthesizing homogeneous, ligand-functionalized nanoparticles showing homogeneously strong binding avidity. This is accomplished by using high-reaction-yield copper-free click chemistry, which allowed us to synthesize densely, ligand-functionalized nanoparticles which strongly and uniformly bound to the targeted surface. In this final chapter, the synthesis, purification, and characterization of the click-chemistry linker will also be reported.

Table 1.1 Ligand-functionalized nanoparticles that have been conducted with clinical trials.

Platforms	Ligands	Indication	Status	References
Cyclodextrin-coating polymeric nanoparticles	Transferrin	Solid tumor	Phase I	10
Liposome	Transferrin	Gastric,esophageal, gastricophageal adenocarcinoma	Phase Ib/II	11
Liposome	$F(ab')_2$ fragment	Metastatic stomach cancer	Phase I	12
Liposome	Transferrin receptor-specific-scAb	Solid tumor	Phase I	13
PLGA-PEG nanoparticles	PSMA-specific peptide	Solid tumor	Phase I	14

Table 1.2 Classification of targeting ligands in ligand-nanoparticles.

Targeting ligands	Targeted receptors	Indication	References
RGD	αvβ3 intergrin	Vascular endothelial cells in solid tumors	15
NGR	Aminopeptidase N (CD13)	Vascular endothelial cells in solid tumors	16
Transferrin	Transferrin receptor	Cancer cells overexpressing transferrin receptor	17
Folate	Folate receptor	Cancer cells overexpressing folate receptor	18
Galactosamine	Galactosamine receptor in hepatocyte	Hepatoma	19
scFv	Her-2 receptor	Breast, ovarian cancer	20

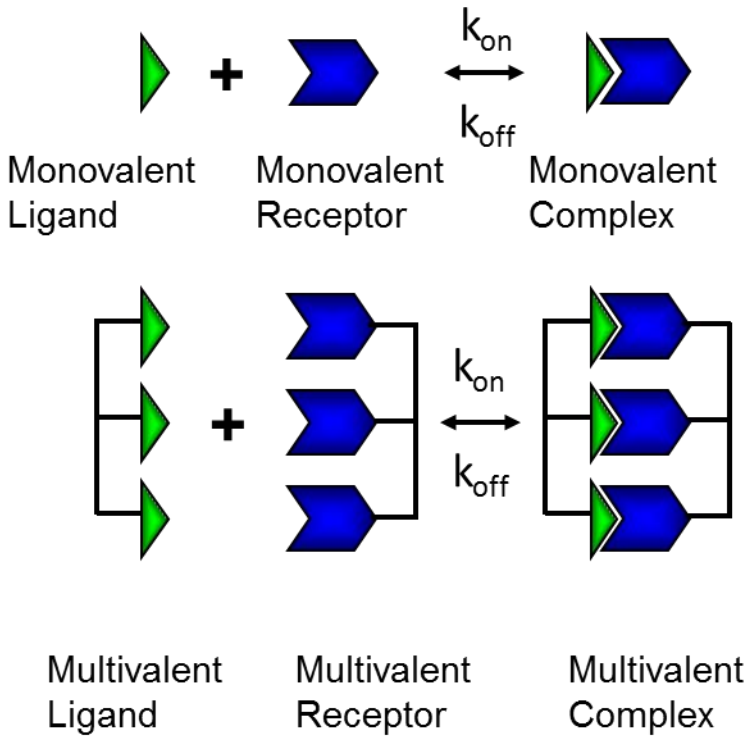

Fig. 1.1 Illustration of multivalency.

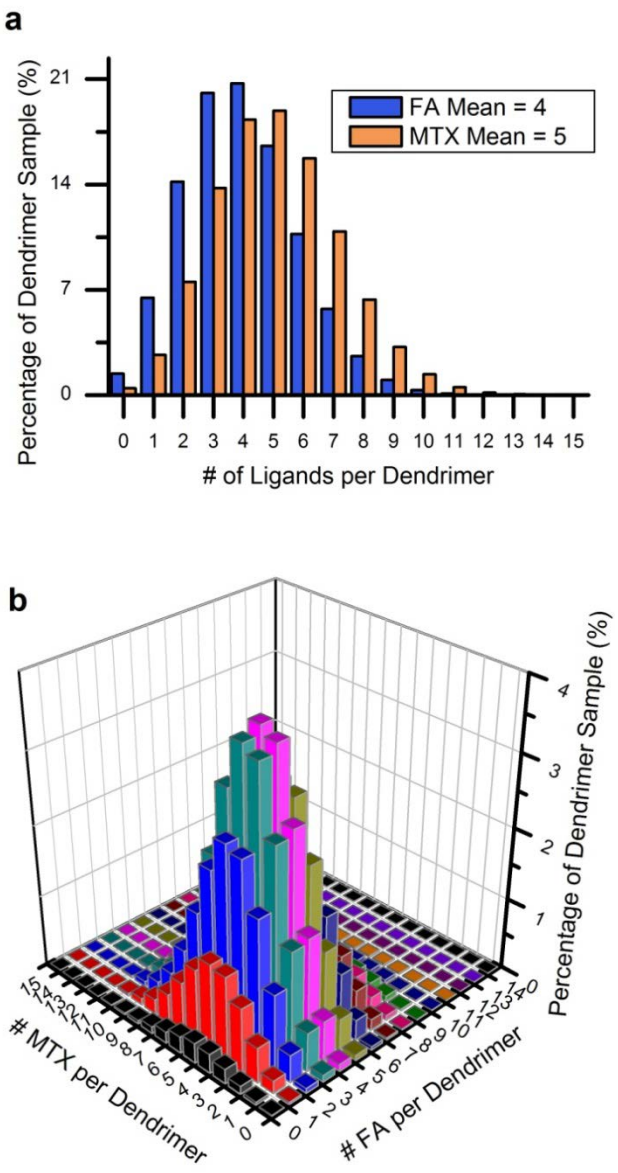

Fig. 1.2 Ligand-to-dendrimer distribution based on Poisson simulation (a) single-ligand model (b) dual-ligand model.

1.6 References

1. Strebhardt, K. & Ullrich, A. Paul Ehrlich's magic bullet concept: 100 years of progress. *Nat Rev Cancer* **8**, 473-480 (2008).

2. Brannon-Peppas, L. & Blanchette, J.O. Nanoparticle and targeted systems for cancer therapy. *Adv Drug Deliv Rev* **56**, 1649-1659 (2004).

3. Peer, D., *et al.* Nanocarriers as an emerging platform for cancer therapy. *Nat Nanotechnol* **2**, 751-760 (2007).

4. Debbage, P. Targeted drugs and nanomedicine: present and future. *Curr Pharm Des* **15**, 153-172 (2009).

5. Kamaly, N., Xiao, Z., Valencia, P.M., Radovic-Moreno, A.F. & Farokhzad, O.C. Targeted polymeric therapeutic nanoparticles: design, development and clinical translation. *Chem Soc Rev* **41**, 2971-3010 (2012).

6. Mahon, E., Salvati, A., Baldelli Bombelli, F., Lynch, I. & Dawson, K.A. Designing the nanoparticle-biomolecule interface for "targeting and therapeutic delivery". *J Control Release* **161**, 164-174 (2012).

7. Zhang, X.Q., *et al.* Interactions of nanomaterials and biological systems: Implications to personalized nanomedicine. *Adv Drug Deliv Rev* **64**, 1363-1384 (2012).

8. Rizzo, L.Y., Theek, B., Storm, G., Kiessling, F. & Lammers, T. Recent progress in nanomedicine: therapeutic, diagnostic and theranostic applications. *Curr Opin Biotechnol* (2013).

9. Yu, M.K., Park, J. & Jon, S. Targeting Strategies for Multifunctional Nanoparticles in Cancer Imaging and Therapy. *Theranostics* **2**, 3-44 (2012).

10. Sarris, A.H., *et al.* Liposomal vincristine in relapsed non-Hodgkin's lymphomas: Early results of an ongoing phase II trial. *Ann Oncol* **11**, 69-72 (2000).

11. Petrelli, F., Borgonovo, K. & Barni, S. Targeted delivery for breast cancer therapy: the history of nanoparticle-albumin-bound paclitaxel. *Expert Opin Pharmaco* **11**, 1413-1432 (2010).

12. Lim, W.T., *et al.* Phase I pharmacokinetic study of a weekly liposomal paclitaxel formulation (Genexol (R)-PM) in patients with solid tumors. *Ann Oncol* **21**, 382-388 (2010).

13. Davis, M.E. The First Targeted Delivery of siRNA in Humans via a Self-Assembling, Cyclodextrin Polymer-Based Nanoparticle: From Concept to Clinic. *Mol Pharmaceut* **6**, 659-668 (2009).

14. Sankhala, K.K., *et al.* A phase I pharmacokinetic (PK) study of MBP-426, a novel liposome encapsulated oxaliplatin. *J Clin Oncol* **27**(2009).

15. Kim, Y.H., *et al.* Tumor targeting and imaging using cyclic RGD-PEGylated gold nanoparticle probes with directly conjugated iodine-125. *Small* **7**, 2052-2060 (2011).

16. Chen, Y., Wu, J.J. & Huang, L. Nanoparticles targeted with NGR motif deliver c-myc siRNA and doxorubicin for anticancer therapy. *Mol Ther* **18**, 828-834 (2010).

17. Pitek, A.S., *et al.* Transferrin coated nanoparticles: study of the bionano interface in human plasma. *PLoS One* **7**, e40685 (2012).

18. Li, M.H., *et al.* Dendrimer-based multivalent methotrexates as dual acting nanoconjugates for cancer cell targeting. *Eur J Med Chem* **47**, 560-572 (2012).

19. Shen, Z., *et al.* A galactosamine-mediated drug delivery carrier for targeted liver cancer therapy. *Pharmacol Res* **64**, 410-419 (2011).

20. Vigor, K.L., *et al.* Nanoparticles functionalized with recombinant single chain Fv antibody fragments (scFv) for the magnetic resonance imaging of cancer cells. *Biomaterials* **31**, 1307-1315 (2010).

21. Farokhzad, O.C., *et al.* Targeted nanoparticle-aptamer bioconjugates for cancer chemotherapy in vivo. *Proc Natl Acad Sci U S A* **103**, 6315-6320 (2006).

22. Esfand, R. & Tomalia, D.A. Poly(amidoamine) (PAMAM) dendrimers: from biomimicry to drug delivery and biomedical applications. *Drug Discov Today* **6**, 427-436 (2001).

23. Svenson, S. & Tomalia, D.A. Dendrimers in biomedical applications--reflections on the field. *Adv Drug Deliv Rev* **57**, 2106-2129 (2005).

24. Tomalia, D.A. Interview: An architectural journey: from trees, dendrons/dendrimers to nanomedicine. Interview by Hannah Stanwix. *Nanomedicine (Lond)* **7**, 953-956 (2012).

25. Goonewardena, S.N., *et al.* Design considerations for PAMAM dendrimer therapeutics. *Bioorg Med Chem Lett* **23**, 2872-2875 (2013).

26. Huang, B., *et al.* The facile synthesis of multifunctional PAMAM dendrimer conjugates through copper-free click chemistry. *Bioorg Med Chem Lett* **22**, 3152-3156 (2012).

27. Lesniak, W.G., *et al.* Synthesis and characterization of PAMAM dendrimer-based multifunctional nanodevices for targeting alphavbeta3 integrins. *Bioconjug Chem* **18**, 1148-1154 (2007).

28. Pednekar, P.P., Jadhav, K.R. & Kadam, V.J. Aptamer-dendrimer bioconjugate: a nanotool for therapeutics, diagnosis, and imaging. *Expert Opin Drug Deliv* **9**, 1273-1288 (2012).

29. Cline, E.N., *et al.* Paclitaxel-conjugated PAMAM dendrimers adversely affect microtubule structure through two independent modes of action. *Biomacromolecules* **14**, 654-664 (2013).

30. Arima, H., *et al.* Folate-PEG-appended dendrimer conjugate with alpha-cyclodextrin as a novel cancer cell-selective siRNA delivery carrier. *Mol Pharm* **9**, 2591-2604 (2012).

31. Chen, Q., *et al.* Targeted CT/MR dual mode imaging of tumors using multifunctional dendrimer-entrapped gold nanoparticles. *Biomaterials* **34**, 5200-5209 (2013).

32. Mammen, M., Choi, S.K. & Whitesides, G.M. Polyvalent interactions in biological systems: Implications for design and use of multivalent ligands and inhibitors. *Angew Chem Int Edit* **37**, 2755-2794 (1998).

33. Pieters, R.J. Maximising multivalency effects in protein-carbohydrate interactions. *Org Biomol Chem* **7**, 2013-2025 (2009).

34. Martinez-Veracoechea, F.J. & Frenkel, D. Designing super selectivity in multivalent nano-particle binding. *Proc Natl Acad Sci U S A* **108**, 10963-10968 (2011).

35. Choi, S.K., *et al.* Dendrimer-based multivalent vancomycin nanoplatform for targeting the drug-resistant bacterial surface. *ACS Nano* **7**, 214-228 (2013).

36. Shakya, A.K., Sami, H., Srivastava, A. & Kumar, A. Stability of responsive polymer-protein bioconjugates. *Prog Polym Sci* **35**, 459-486 (2010).

37. Le Guevel, X., Spies, C., Daum, N., Jung, G. & Schneider, M. Highly fluorescent silver nanoclusters stabilized by glutathione: a promising fluorescent label for bioimaging. *Nano Res* **5**, 379-387 (2012).

38. Jain, P.K., Qian, W. & El-Sayed, M.A. Ultrafast cooling of photoexcited electrons in gold nanoparticle-thiolated DNA conjugates involves the dissociation of the gold-thiol bond. *Journal of the American Chemical Society* **128**, 2426-2433 (2006).

39. Li, N.W. & Binder, W.H. Click-chemistry for nanoparticle-modification. *J Mater Chem* **21**, 16717-16734 (2011).

40. Mangold, S.L. & Cloninger, M.J. Binding of monomeric and dimeric Concanavalin A to mannose-functionalized dendrimers. *Org Biomol Chem* **4**, 2458-2465 (2006).

41. Bowman, M.C., *et al.* Inhibition of HIV fusion with multivalent gold nanoparticles. *Journal of the American Chemical Society* **130**, 6896-+ (2008).

42. Duncan, R. Polymer conjugates as anticancer nanomedicines. *Nat Rev Cancer* **6**, 688-701 (2006).

43. Kumar, P., Khan, R.A., Choonara, Y.E. & Pillay, V. A prospective overview of the essential requirements in molecular modeling for nanomedicine design. *Future Med Chem* **5**, 929-946 (2013).

44. Sengupta, S. & Kulkarni, A. Design principles for clinical efficacy of cancer nanomedicine: a look into the basics. *ACS Nano* **7**, 2878-2882 (2013).

45. Hong, S., *et al.* The binding avidity of a nanoparticle-based multivalent targeted drug delivery platform. *Chem Biol* **14**, 107-115 (2007).

46. Tassa, C., *et al.* Binding affinity and kinetic analysis of targeted small molecule-modified nanoparticles. *Bioconjug Chem* **21**, 14-19 (2010).

47. Woller, E.K., Walter, E.D., Morgan, J.R., Singel, D.J. & Cloninger, M.J. Altering the strength of lectin binding interactions and controlling the amount of lectin clustering using mannose/hydroxyl-functionalized dendrimers. *Journal of the American Chemical Society* **125**, 8820-8826 (2003).

48. Wolfenden, M.L. & Cloninger, M.J. Carbohydrate-functionalized dendrimers to investigate the predictable tunability of multivalent interactions. *Bioconjugate Chem* **17**, 958-966 (2006).

49. Mullen, D.G., *et al.* A Quantitative Assessment of Nanoparticle-Ligand Distributions: Implications for Targeted Drug and Imaging Delivery in Dendrimer Conjugates. *ACS Nano* **4**, 657-670 (2010).

50. Mullen, D.G., *et al.* Isolation and Characterization of Dendrimers with Precise Numbers of Functional Groups. *Chem-Eur J* **16**, 10675-10678 (2010).

CHAPTER 2

KINETIC ANALYSIS DEMONSTRATING DISTRIBUTED AVIDITIES OF LIGAND-FUNCTIONALIZED NANOPARTICLES

2.1 Introduction

One confounding factor associated with multivalent interactions involving ligand-functionalized nanoparticles is the heterogeneity of the number of ligands on the particles.[1,2] It has been possible to characterize the number of ligands attached to nanoparticles by different analytical techniques, based on different aspects of their physiochemical properties. For instance, the NMR and UV-Vis utilize spectroscopic information to characterize the change in ligand chemical structure after conjugation. Mass spectrometry and GPC provide differences in carrier molecular weight before and after ligand functionalization.[3-5] Information from these measurements can readily be converted to the number of functionalized ligands. Although it seems these techniques can provide well-characterized information on the valence of the nanoparticles, the properties measured by these techniques in fact only represent the average ligand number of the tested nanoparticles.

The extent of this heterogeneity was recently revealed by extensive analyses of a variety of functionalized nanoparticles. With both theoretical calculation and experimental results, this work demonstrated that, among an extensively distributed number of functionalized ligands per particle, the average number of ligands was only a portion, and often a small portion, of the entire population of macromolecules. This was first proved using

a statistical thermodynamic method to elucidate the mechanism of ligand conjugation and estimate the quantity of ligands attached to nanoparticles.[6] The result showed that the distribution of attached ligands would display as a Poissonian distribution, meaning the ligands were completely randomly attached to the particle surface. Meanwhile, Mullen developed a method of HPLC separation to isolate nanoparticles and recover fractions of purified nanoparticles with a single defined number of ligand.[1,2] This experimental work validated the concept of random distribution in a Poissonian simulation and proved the complexity and heterogeneity of multivalent nanoparticles. In this report, the number of ligands per dendrimer of the modular nanoparticles, which consisted of PAMAM dendrimers and alkyne ligands with the mean at 7, actually spread from 0 to 17. In the dual ligand-nanoparticle system, the nanoparticles with exactly the mean of ligand per nanoparticle for both ligands were less than 5% of the entire population.

This heterogeneous distribution of multivalent ligands on the nanoparticles is presumed to result in heterogeneous ligand-receptor interactions, potentially yielding distributed binding avidities with targeted surfaces. This avidity distribution also infers that, in synthetic ligand-functionalized nanoparticles, potentially only a portion of highly functionalized particles with stronger avidity would accomplish targeting, thus increasing the overall dose required for a desired therapeutic effect. In contrast, the weaker-avidity subpopulations would cause safety concerns because the drugs and imaging agents they carry would not be active in a site-specific manner and could potentially lead to side effects. While this is a concern, there is a poor understanding of this concept at this time. Therefore, it is important to develop model systems and analytical strategies that can assess avidities of distributed populations of ligand-bearing nanoparticles.

In the current studies, a well-controlled model system, composed of monodispersed PAMAM dendrimers and ssDNA oligonucleotides as nanoparticles and ligands, respectively, was established to clarify the complexity of ligand-receptor interactions of synthetic multivalent nanoparticles. Using an SPR biosensor, the kinetic behaviors of non-uniform synthetic multivalent nanoparticles were also recorded and evaluated. During the SPR kinetic analysis, we demonstrated the heterogeneous binding of the ligand-functionalized nanoparticles that show discreet binding affinities. More importantly, we developed a means to perform a kinetic analysis to quantify the subpopulations in the heterogeneous synthetic ligand-functionalized nanoparticles and evaluate the avidity distribution of our materials. We proved that only a small portion of ligand-functionalized nanoparticles really gain avidity enhancement due to their multivalent structure.

2.2 Experimental Methods

Chemicals and materials: Single-stranded DNA oligonucleotides (ssDNA oligos) were synthesized with 5'-end modifications and purified with a standard desalting process at Integrated DNA Technologies (Coralville, IA), including an 8-mer amino-terminated oligo, 5'-NH_2-C_6-TGCTGAGG, and a 25-mer biotinylated oligo 5'-biotin-TTTCTTCAGCATCTTATCCGAGTTTT. The generation 5 poly(amidoamine) (G5 PAMAM) dendrimer was purchased from Dendritech Inc. (Midland, MI) and was purified as described in the synthesis section. All organic solvent, reagents and titration volumetric solutions (0.1M HCl and 0.1M NaOH) were purchased from Sigma Aldrich (St. Louis, MO) and used without further purification. Phosphate buffer saline (PBS) without calcium and

magnesium was purchased from Thermo Scientific (Logan, UT). 10K molecular weight cutoff (MWCO) centrifugal filters (Amicon Ultra-4) were purchased from Millipore (Billerica, MA). 10K MWCO dialysis membrane was purchased from Spectrum Laboratories (Rancho Dominquez, CA). SPR sensor chips SA and HBS-EP (pH 7.4) buffer were purchased from GE Healthcare (Piscataway, NJ).

Synthesis of G5 PAMAM dendrimer-based multivalent nanoparticles: The purchased G5 PAMAM dendrimer was purified with 10K MWCO dialysis, as previously described, to remove lower molecular weight impurities.[3] The purified G5 PAMAM dendrimer (G5-NH_2) was then chemically modified for reducing nonspecific electrostatic interactions or providing functional groups in the subsequent coupling reaction of ligands. (Scheme 2.1) Briefly, the purified amine-terminated G5 PAMAM dendrimers (200.01 mg, 7.41 μmole) were reacted with 85 equivalents of acetic anhydride (59.43 μL, 629.85 μmole) which was slowly added to amine-terminated dendrimers in anhydrous MeOH (20 ml) in the presence of triethylamine (105.43 μL, 755.82 μmole) for 16 hours at room temperature. The excessive solvent and reagents in the reaction were removed by rotary evaporation, followed by 10K MWCO dialysis against PBS and deionized water (DIW), respectively, for 3 cycles. The recovered partial acetylated dendrimer (G5-Ac-NH_2) was lyophilized for 3 days to yield a white solid (193.40 mg, 87%). The G5-Ac-NH_2 was subsequently modified to convert the residual primary amines to primary carboxylic groups, using glutaric anhydride. In brief, 50 equivalents of glutaric anhydride (10.14 mg, 88.87 μmole) was added to G5-Ac-NH_2 (53.32 mg, 1.78 μmole) dissolved in anhydrous DMSO (5mL) in the presence of triethylamine (12.40 μL, 88.87 μmole) for 16 hours at room temperature. The mixture was purified with 10K MWCO centrifugal filters and dissolved in PBS and DIW for 4 cycles each. The

recovered partially acetylated and carboxylated dendrimer (G5-Ac-NH_2-COOH) was lyophilized for 3 days to yield a white solid (47.21 mg, 83%). The amide-coupling reaction of the ssDNA oligo to the dendrimers was slightly modified from the previous reaction. G5-Ac-NH_2-COOH (6.1 mg, 0.19 μmole) was dissolved in DMSO (0.6 mL) and activated using coupling reagents, 1-Ethyl-3-[3-dimethylaminopropyl]carbodiimide hydrochloride (EDC) (1.05 mg, 5.56 μmole) and N-hydroxysuccinimide (NHS) (0.77 mg, 6.67 μmole), for 2 hours at room temperature to form intermediate NHS-ester activated dendrimer. The mixture was evenly divided into three aliquots and then reacted with amino-terminated ssDNA oligos. 20 equivalent ssDNA oligos (1.28 μmole) were added into one aliquot with the NHS-ester activated dendrimer mixture in 0.4 mL pH 9 carbonate buffer for 16 hours at room temperature. The mixture of the coupling reaction was purified using 10K MWCO centrifugal filters in PBS and DIW for 4 cycles each. The recovered dendrimer-ssDNA conjugates were lyophilized for 3 days to yield a white solid with yield ~ 80%.

Characterization of G5 PAMAM dendrimer-based multivalent nanoparticles: The mean number of primary amines of original and partially acetylated G5 PAMAM (G5-NH_2 and G5-Ac-NH_2) was determined by potentiometric titration using a Mettler Toledo (MP) meter and an inlab®micro electrode at room temperature as previously described.[1] Briefly, 10 mg of dendrimer was dissolved in 1mL 0.1N NaCl solution. After adjustment to pH 2.5, the dendrimer solution was titrated with 0.1N NaOH and the number of primary amines was determined by the titration curve of acidification.

The molecular weight of G5 PAMAM dendrimer-based ssDNA oligo nanoparticles was determined by MALDI-TOF MS using a Micromass TofSpec-2E with positive ion mode as previous described.[7] The number of attached ssDNA oligonucleotides was determined by

UV-Vis spectra analysis that was performed using a 1-mL quartz cuvette with a Perkin Elmer Lamda 20 spectrophotometer. The equivalent concentration of ssDNA was calibrated using OD_{260} of the specific DNA sequence. The mean number of conjugated ssDNA oligo per G5 PAMAM dendrimer was determined by using the quotient of an equivalent concentration of ssDNA that the oligonucleotide-functionalized dendrimer presented and the concentration of the nanoparticles that was calculated based on the MS-determined molecular weight of the functionalized nanoparticles.

SPR measurements: The kinetic analysis was conducted using a BIAcore X (Pharmacia Biosensor AB, Uppsala, Sweden), equipped with sensor chip SA, which was pre-coated with streptavidin on the surface, for the capture of biotinylated ssDNA oligos. Before the immobilization process, the SA surface was pre-conditioned with exposure to three 1-minute injections containing 50mM NaOH. The 25-mer biotinylated ssDNA oligo solution (1 mg/mL) in HBS-EP buffer was then injected only into flow channel 1 for 10 minutes, resulting in 1300 RU (1.3 ng/mm^2) of immobilized ssDNA oligos. After the capturing process, a 1-minute injection of 10mM NaOH was used to reduce the non-specific binding that occurred during prior injections. A control flow channel without immobilization of 25-mer oligonucleotides was used as a reference.

During SPR measurement, the 8-mer ssDNA oligo and the oligo-functionalized dendrimer dissolved in HBS-EP buffer were injected into both flow channels of the sensor chip, including the ssDNA oligo-immobilized channel and the reference channel, at a flow rate of 10 μL/min. After each measurement, the chip surface was regenerated using 5μL injections of pH 2 HCl-glycine buffer or 5-10 μL pH 11 NaOH for the sample of 8-mer ssDNA oligo or the G5 ssDNA oligo-functionalized nanoparticles, respectively, to ensure

complete removal of bound molecules before the next measurement. The final SPR sensograms were obtained by using the measurement after subtraction of the signal on the reference channel from the signal on the oligo-immobilized channel. After this process of referencing, the kinetic parameters, including, k_{on}, k_{off} and K_D, of the free ssDNA oligo were determined using the Langmuir 1:1 kinetic model with default setting in BIAevaluation software.

Evaluation of avidity distribution: The first step in determining the avidity distribution is to quantify the molar fraction of the two subpopulations presenting different binding avidities. The process to quantify this fraction involved a unique parallel initial rate kinetic analysis, including a directly measured initial rate analysis of the entire population and an extrapolated initial rate analysis just for the subpopulation with enhanced avidity. The acquisition of the directly measured initial rate from SPR sensograms was clearly described previously, and the equation of initial rate analysis was presented as Eqn. 1, where R represents the measured RU, R_{max} is the maximum capacity of the RU of the immobilized receptor, and C stands for the concentration of the overall particles.[8] By using BIAevaluation software, the initial $\frac{dR}{dt}$ was extracted by the first-order derivative at the initial point of the measured sensogram. In contrast, the equation of extrapolated initial rate analysis was presented as Eqn. 2 where C_s stands for the concentration of particles showing slow dissociation and the extrapolated initial rate, $\frac{dRs}{dt}$, was extracted by using the average $\frac{dR}{dt}$ after association time at 2 minutes. Based on Eqn. 1 and 2, the fraction of the enhanced-avidity subpopulation, $\frac{Cs}{C}$, was extracted by using the ratio of $\frac{dRs}{dt}$ and $\frac{dR}{dt}$.

$\frac{dR}{dt}|_0 = R_{max} * k_{on} * C$ Eqn.1

$\frac{dRs}{dt}|_0 = R_{max} * k_{on} * C_s$ Eqn. 2

Kinetic parameters, including k_{on}, k_{off} and K_D of the ssDNA oligo-functionalized nanoparticles, were determined using the dual Langmuir kinetic-binding model with BIAevaluation software. In the dual Langmuir analysis, the concentrations of the two tested ligands were defined as the product of the concentration of the total dissolved ssDNA oligo-functionalized dendrimer and the molar fractions acquired by parallel initial rate analysis described above.

2.3 Results and Discussions

Design and Synthesis of PAMAM dendrimer-based multivalent nanoparticles: The goal of this study is to offer practical and comprehensive guidelines for designing ligand-functionalized multivalent-targeted nanoparticles. Therefore, it is crucial to develop these guidelines using materials that represent the binding properties of most ligands and nanoparticles. Also, it is important that these materials be well-defined and characterized, in order to alleviate difficulty in the analysis of their chemical structure and physical properties. In this report, we employed 8-mer ssDNA oligonucleotides as the ligands and G5 PAMAM dendrimers as the nanoparticles to meet our purposes. Given the feasibility of designing the sequences and being synthesized, ssDNA oligos are already one of the most-used biological molecules in developing novel biomedical platforms and devices.[9-11] Additionally, the 8-mer ssDNA oligo used in this study is promising as the ideal model ligand for two reasons. First,

the sequence was designed for demonstrating a μM affinity (K_D) which is comparable to the binding capacity that most biological ligands utilized in multivalent targeting. [12-15] Second, an 8-mer ssDNA oligo also approximates the median size among most targeting ligands implemented in multivalent nanoparticle systems. For instance, the molecular weight of targeting ligands can be as small as carbohydrate-based ligands or as large as aptmer-based ligands with more than 10 kD in size.[16,17] We intend to take advantage of the median affinity and size of the ssDNA oligo as the ligand to enhance the applicable extent of the guidelines, derived experimentally and based on the observations made in our model system. In addition to the unique model ligand, the platform nanoparticle, G5 PAMAM dendrimer, also aids our purpose in developing broadly applicable guidelines. This nanoparticle has been proven to have extensive biomedical utilities and is characterized by superb monodispersity, biocompatibility, and water-solubility.[18,19] More importantly, its abundant accessible terminal functional groups and its flexible structure further suggest that G5 PAMAM dendrimers are an ideal platform in multivalent nanoparticle systems. In fact, there are already a number of examples of the use of conjugates of oligo and dendrimer in developing drug delivery systems and detective devices.[20-22]

The synthesis of ssDNA oligo-functionalized multivalent nanoparticles is shown in Scheme 2.1. The functionalization of amino-terminated G5 PAMAM dendrimers (G5-NH_2) was carried out with serial reactions of partial acetylation and carboxylation, giving the G5 dendrimer a bifunctional surface. This predominantly neutral surface was tailored to both reserve the yield of amide-bond coupling chemistry and reduce non-specific interactions attributed to the protonated primary amines. Subsequent to the surface modification, the coupling reaction between the carboxylic groups on dendrimers and the amino-terminated

ssDNA oligos was carried out using EDC and NHS catalyzed chemistry. With 80% acetylated and 20% carboxylic functional groups on the surface, the G5 PAMAM dendrimers were reacted with 20 equivalences of amino-terminated ssDNA oligos, resulting in 6, on average, covalently linked ssDNA oligos onto the dendrimers, based on the results of UV-Vis spectroscopy at OD_{260}. In other words, the reaction yield of this EDC/NHS coupling reaction was just 30%. We tried to improve the reaction yield by increasing the carboxylic groups on the dendrimer surface, but the reaction was actually inversely associated with the number of COOH, meaning an increase in the number of COOH would just decrease the reaction yield, rather than offering enhancement.

SPR measurement of synthetic multivalent nanoparticles: The interactions of ssDNA oligo-functionalized multivalent nanoparticles, G5-$(oligo)_6$, and free ssDNA oligos with the targeted surface were measured using an SPR biosensor in which the detection sensor chip was immobilized with 25–mer ssDNA oligos. This 25-mer-oligo model receptor included a segment with 8 nucleotides complementary to the 8-mer ssDNA oligo on the dendrimer, while the rest of the nucleotides served as a linker. During SPR measurements, G5-$(oligo)_6$ showed enhanced binding, which featured remarkably slow dissociation and significantly differed from the complete dissociation presented by free ssDNA oligo. (Fig. 2.1) After 2 minutes of association and a 5-minute dissociation phase, more than 1/3 of the surface-bound nanoparticles were still stably adhered to the complimentary surface. In addition, we found an unusual phenomenon–that the SPR association binding curve of the multivalent nanoparticle did not reach equilibrium after 2 minutes of association but showed a trend of a gradual increase. To understand this unusual binding curve, we conducted a series of SPR tests with varied association times in order to observe equilibrated binding of

the nanoparticles. (Fig. 2.2) Surprisingly, none of these binding curves plateaued as expected, even if the association time was increased 5-fold and had reached the limit of the instrumental setting. This apparent non-equilibrated binding strongly suggests there were nearly "irreversible" interactions taking place in the synthetic multivalent nanoparticle system.

By examining the series of binding curves with increasing association times, we observed these binding curves were consistently initiated by a sharp increase, were then presented with transitions showing a clear inflection point, and eventually were followed by a slower and linear increase. We also found that the time of transitions and the accumulation of bound nanoparticles until those transitions were all similar among tests with varied association times. In contrast, the final accumulation of bound nanoparticles after injections was highly positively associated with the duration of the association. Considering the time-independent binding by synchronizing transition points and the time-dependent binding after the transition, it was clear that this synthetic multivalent nanoparticle is a binary system that demonstrated distinguishable binding behaviors. During association, the subpopulation presenting weaker avidity would reach equilibrium of binding at transition; another subpopulation with stronger avidity processed a nearly irreversible binding.

In particular, the linear increase during the association phase is characteristic evidence supporting the existence of strong binding. Based on the simulation using the Langmuir kinetic model, the dissociation rate constant (k_{off}) should be lower than 10^{-3} ML^{-1}, which is significantly slower than the k_{off} of the free ssDNA oligo, and the association curve can be apparently straight. (Fig. 2.3) To my knowledge, the linear binding curve is rarely observed and has not been examined in previous studies of multivalent nanoparticles. Most

of molecular interactions show association curves straying from the initial slope and bending toward the horizontal axis. Until the association-dissociation equilibrium is reached, the binding mass would not change and the binding curve would be flat and steady at the equilibrated number.

In addition to the binding behavior seen during the association phase of the binding curve, binary binding behavior was also demonstrated by the synthetic multivalent nanoparticles during the dissociation phase. The dissociation curves that were preceded by varied association times displayed similar patterns that involved a leading fast dissociation and a following drastically slow dissociation. Within the fast dissociation phase, we found that the duration of these fast dissociations and the amount of nanoparticles dissociated from the surface during fast dissociation were identical among varied binding curves. (Fig 2.2) The association of fast dissociation and the identical amounts of fast-dissociation nanoparticles, again, strongly suggested the existence of a subpopulation with weaker binding avidity. In contrast, the net nanoparticles bound to the surface after fast dissociation increased approximately linearly with the association time of the sample injections, suggesting the nearly irreversible binding as previously described. Taken together, evidence on both the association and the dissociation phases indicated this synthetic multivalent nanoparticle system was composed of two classes of nanoparticles: one demonstrated strong interaction and nearly irreversible binding; another showed weak interactions with a rapid binding equilibrium and fast dissociation.

Evaluating avidity distribution of multivalent nanoparticles: Based on the parallel initial rate analysis described in the Methods section, the binary composition of G5-$(oligo)_6$ was successfully evaluated using this graphic-orientated method. (Fig. 2.4) The directly

measured initial rate, $\frac{dR}{dt}|_0$, and the extrapolated initial rate, $\frac{dRs}{dt}|_0$, were extracted, and they were 2.18 and 0.217 (RU/s), respectively. With the ratio of these two rates, we demonstrated there was about 10% of the G5-$(oligo)_6$ showing nearly irreversible binding. This result provides experimental evidence to prove the hypothesis that heterogeneous structures would lead to heterogeneous interactions. The low portion of enhanced-avidity nanoparticles also indicates that the current design of this multivalent particle is ineffective in promoting multivalent interactions and requires further improvement.

The proposed parallel initial rate analysis would be valid with certain assumptions, including 1) that the variation of association rate constant, k_{on}, within the nanoparticle system can be neglected and 2) that the slope of association during the linearly increasing region can be regarded as the initial rate of slow-dissociation nanoparticle, that is $\frac{dRs}{dt}|_0 = \frac{dRs}{dt}_{, t > ti}$, where ti stands for the inflection point of the binding curve. In fact, the reliability of these assumptions has been either experimentally or theoretically proven. First, prior studies have already demonstrated that synthetic multivalent nanoparticles functionalized with identical ligands but with a varied number of ligands that showed significantly different K_D would still show an insignificant variation of the association rate constant, k_{on}. Additionally, the soundness of another assumption was also proven with a simulation method using Langmuir kinetic analysis to conduct a systematic survey of kinetic curves featuring a broad range of the association and dissociation rate constants k_{on} and k_{off}. (Fig. 2.3) By using $\frac{dR}{dt}$ of the linear segment in the association curve as the initial rate, the deviation between the extrapolated initial rate and the real initial rate was less than 5%. This assessment was based on the simulation result with k_{off} at 10^{-3} ML^{-1}. Additionally, this simulation also indicates the

deviation between two initial rates would decrease with the k_{off} of the binding. Once the system presented with the high-avidity component, it would be accurate to use the extrapolated initial rate in a parallel initial rate analysis. Because G5-$(oligo)_6$ showed a stable and linear increase during associations suggesting the k_{off} is smaller than 10^{-3} ML^{-1}, the method of parallel rate initial analysis would be valid in this system.

Dual-Langmuir analysis of synthetic multivalent nanoparticles: With the quantified composition of varied subpopulations, the binary interaction of a synthetic multivalent nanoparticle system was able to be interpreted by a more analytical kinetic model. With this dual-Langmuir kinetic analysis, the kinetic parameters of interaction presented by the G5-$(oligo)_6$ were determined. (Table 2.1) In particular, including k_{on}, k_{off} and K_D, the kinetic parameters of both the fast- and slow-dissociation nanoparticles were individually evaluated. Based on the results of the kinetic analysis, we demonstrated an approximately two-order-of-magnitude enhancement of binding avidity was obtained by the slow-dissociation G5-$(oligo)_6$ and the avidity was about 10nM. In contrast, the fast-dissociation nanoparticles simply produced a weaker avidity at about 1μM, which is relatively similar to the affinity of the free ssDNA oligo.

The exceptional fitting goodness also demonstrated that this two-component Langmuir kinetic model perfectly interpreted the binding process of the synthetic multivalent nanoparticle system. The excellent chi square value, χ^2, was 10-fold less than the criterion of a solid fitting and mathematically proved that the nanoparticles interacted with the complementary surface as a binary system. In contrast, when using a simple 1:1 Langmuir kinetic model to analyze the interaction of this nanoparticle, the fitted curve was highly deviated from the measured reading and, moreover, the χ^2 was larger than 300, which is 100-

fold larger than the acceptable χ^2 of a non-linear regression, also suggesting this synthetic nanoparticle system would not simply perform a single mode of interaction.

This kinetic information offers a quantitative evaluation of the avidity distribution in synthetic multivalent nanoparticles, which is unachievable by using typical Langmuir kinetic analysis. We found that the "monovalent-level" interaction performed by fast-dissociation showed insignificant avidity enhancement and the "multivalent-level" interaction performed by slow-dissociation nanoparticles showed a 100-fold stronger avidity, compared to the majority in this nanoparticle system. Additionally, the discreet avidity distribution suggests that the multi-valent driven avidity enhancement may be a step-wise augmentation rather than a continuous increase. In the G5-$(oligo)_6$ system, 90% of the nanoparticles stayed in a mode where they only perform interactions comparable to monovalent interactions. Another subpopulation, however, reached the "on" mode and actually gained stronger interactions due to multivalent interactions. This on-off mechanism also suggested that the energy gap to activate the multivalent interactions seems to be formidably high so that there were rarely in-between interactions that existed in this system. Taken together, this heterogeneity of binding avidity enlightens that the multivalent structure on nanoparticles would not guarantee the multivalent interactions presented by the nanoparticles.

Practical evaluation of multivalent nanoparticles as a targeted delivery system: In addition to providing comprehensive kinetic information about synthetic multivalent nanoparticles, our analyses are informative for the real-world biopharmaceutical development process. The key is that this technique can rapidly evaluate the targeting potential of ligand-functionalized nanoparticles by assessing the information of avidity distribution. As described previously, only ligands showing stable binding to the targeted

surface are able to achieve a targeting effect. Therefore, we believe the fractions of enhanced-avidity nanoparticles could be practical indicators reflecting the targeting potential of a synthetic multivalent nanoparticle system. The simulation results using the two-component Langmuir kinetic model further support this concept. This simulation suggests that the fraction of slow-dissociation nanoparticles highly regulated the amount of ligand-nanoparticles that attached to the receptor surface. The 2 to 3-fold increase in slow-dissociation nanoparticles would lead to doubled and tripled specific binding. (Fig. 2.5) Additionally, this fraction is sufficient enough to assess the targeting potential, without the extraction of kinetic parameters.

The parallel initial rate analysis also can provide the percentage of enhanced-avidity nanoparticles in real time with limited post-processing and without complex numerical or mathematical processing. Although the initial rate analysis is originated from solutions of ordinary differential equations, the acquisition of this fraction is basically just a graphic method involving two slopes of a kinetic binding curve in a series. Practical users can efficiently extract the fraction of slow-dissociation (targeting-potential) nanoparticles, just from apparent observation of the biosensor-measured kinetic curve without processing difficult math such as an accurate first-order derivative. Our results suggest this user-friendly indicator and technique would be valuable in future applications of high-throughput screening of synthetic multivalent targeting nanoparticles.

Table 2.1 Rate constants (k_{on} / k_{off}) and dissociation constant (K_D) of free oligo and oligo-functionalized dendrimers determined by SPR kinetic analysis.

Ligands	**k_{on} ($M^{-1}s^{-1}$)**	**k_{off} (s^{-1})**	**K_D (M)**
Free oligo	$5.36x10^{4}$	$4.34x10^{-2}$	$8.11x10^{-7}$
Fast-dissociation G5-$(oligo)_6$	$3.31x10^{4}$	$4.61x10^{-2}$	$1.39x10^{-6}$
Slow-dissociation G5-$(oligo)_6$	$3.10x10^{4}$	$3.37x10^{-4}$	$1.09x10^{-8}$

The kinetic parameters of free oligo were determined by 1:1 Langmuir kinetic model.

The kinetic parameters of G5-$(oligo)_6$ were determined by dual Langmuir kinetic model.

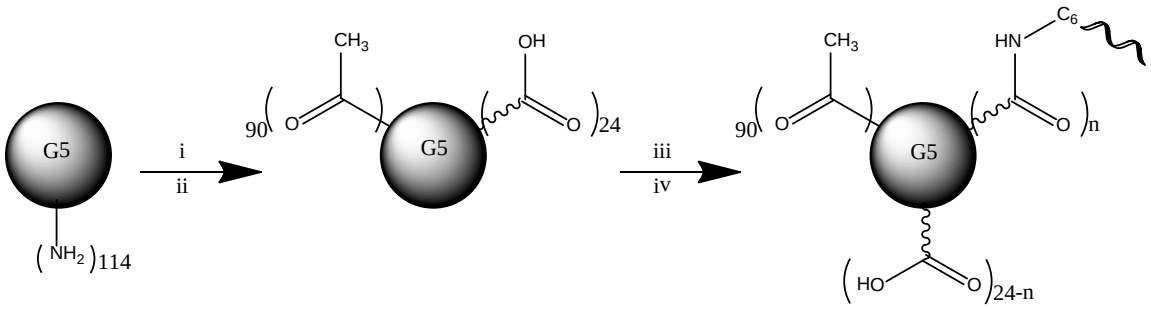

Scheme 2.1 Synthesis of oligonucleotide-functionalized G5 PAMAM dendrimers with amide-bond ligation. Reagents and conditions: (i) acetic anhydride, triethylamine, MeOH, rt, 16 hours; (ii) glutaric anhydride, triethylamine, DMSO, rt, 16 hours; (iii) EDC, NHS, DMSO, rt, 2 hours; (iv) 8-mer amino-terminated oligonucleotide, pH 9 carbonate buffer, rt, 16 hours.

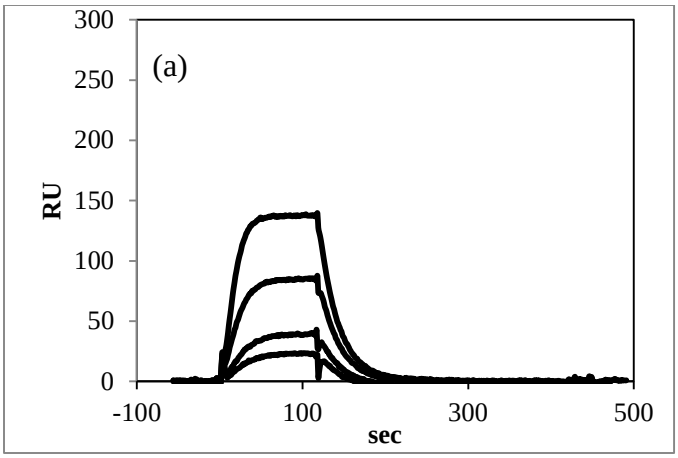

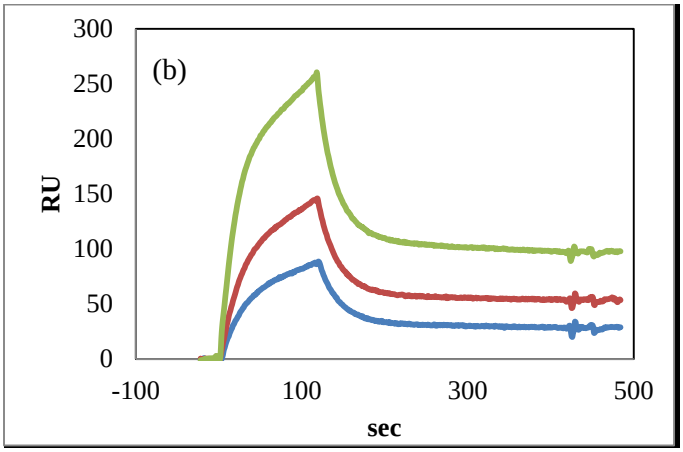

Fig 2.1 SPR binding curves of oligonucleotide-based ligands. (a) Free oligonucleotide with 40, 80, 200 and 400 nM; (b) G5-$(oligo)_6$ with 32.25, 62.5 and 125 nM.

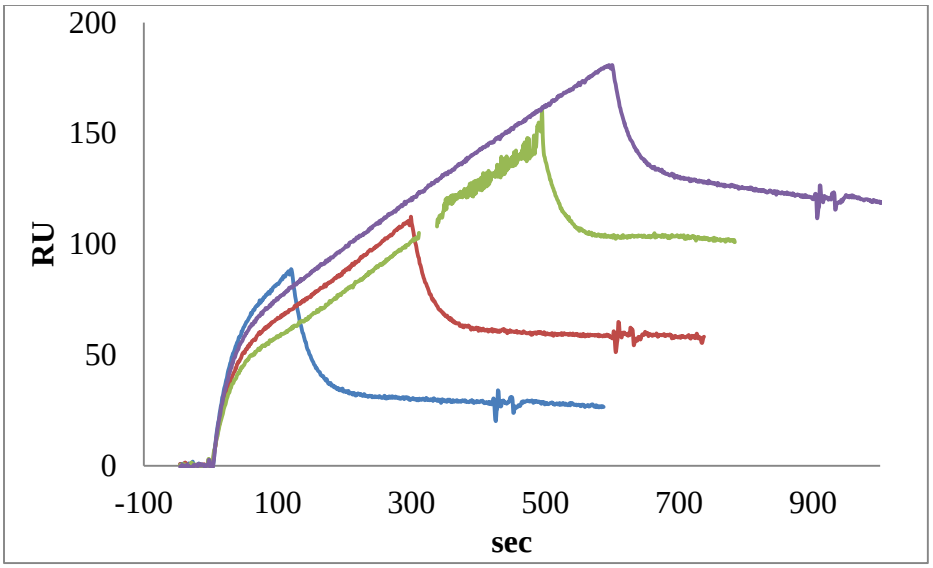

Fig.2.2 SPR binding curves of G5-$(oligo)_6$ with varied duration of association. The association times are 2, 5, 8 and 10 minutes, followed with 5 minutes of dissociation. The tested concentration of G5-$(oligo)_6$ was 62.5 nM.

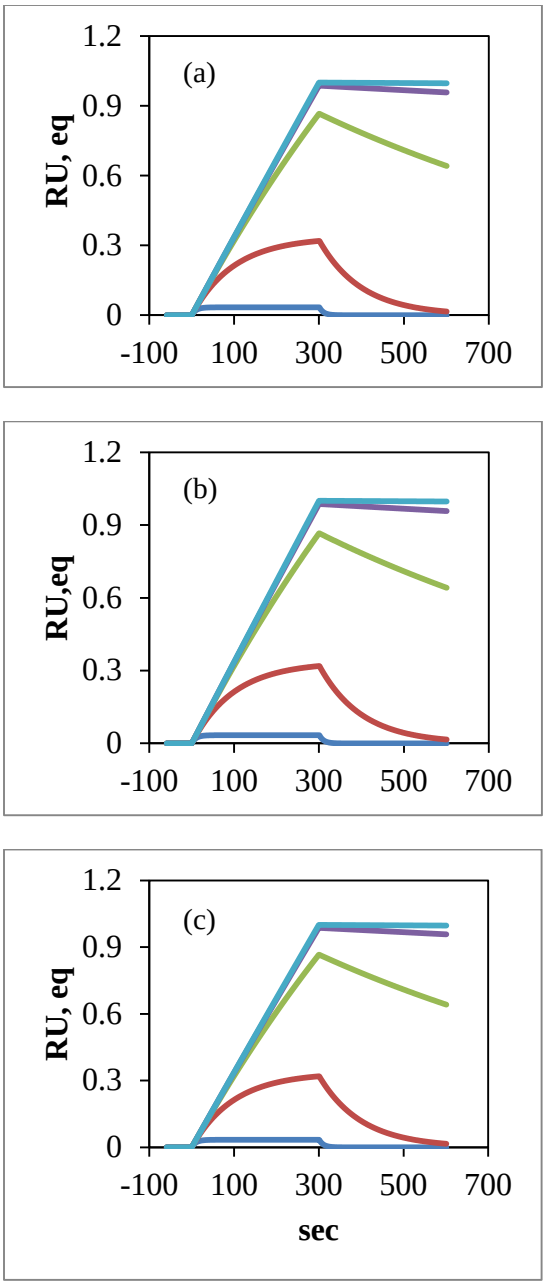

Fig. 2.3 Simulation binding curves of ligands with varied kinetic parameters determined by 1:1 Langmuir kinetic model. The dissociation constants (k_{off}) include 10^{-1}(blue), 10^{-2} (red), 10^{-3} (green), 10^{-4} (purple), and 10^{-5} (light blue) (s^{-1}); (a) $k_{on} = 10^3$, (b) $k_{on} = 10^4$, and (c) $k_{on} = 10^5$ ($M^{-1}s^{-1}$). The concentration is 62.5 nM, the durations of association and dissociation are 5 minutes, and RU, eq =RU/ RU_{max}.

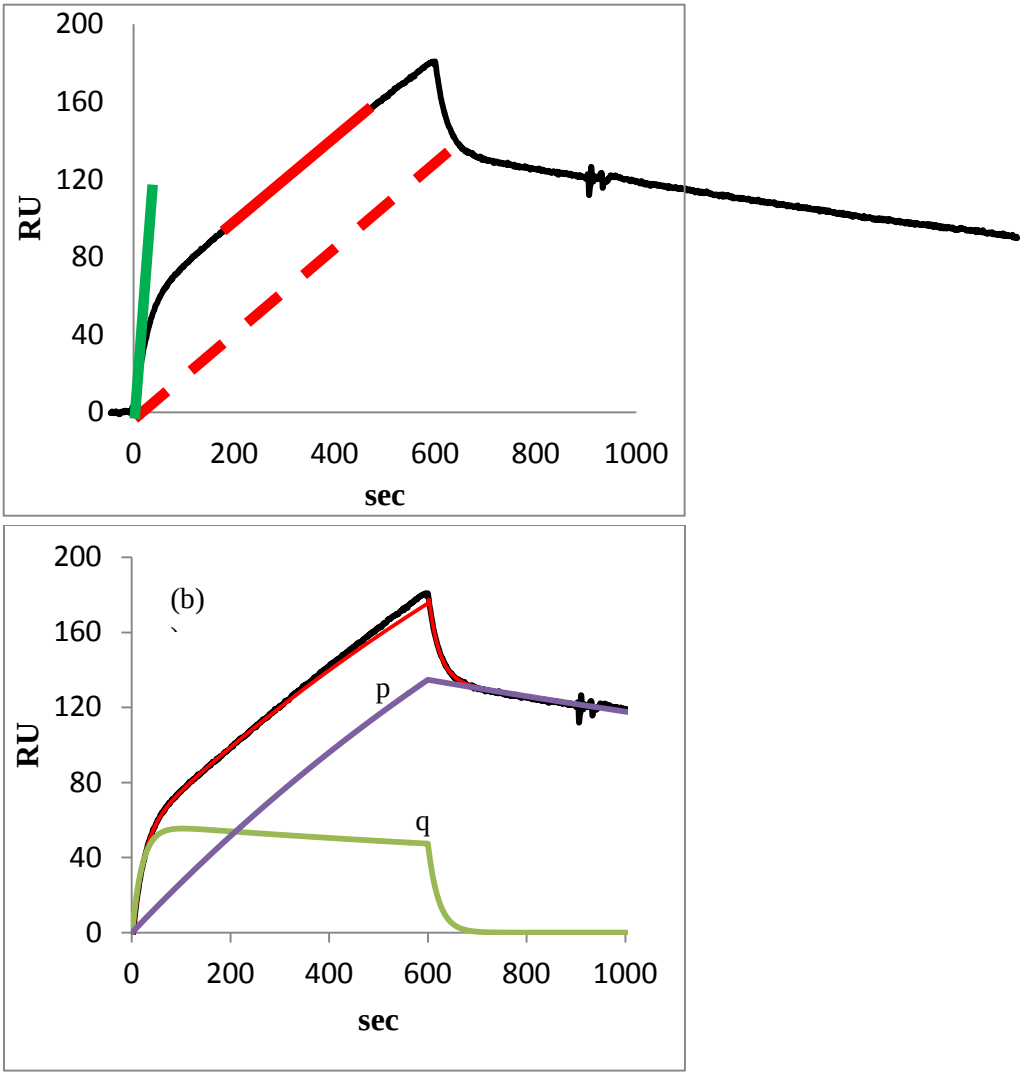

Fig 2.4 Avidity distribution of G5-(oligo)$_6$, determined by parallel initial rate analysis (a) and dual Langmuir kinetic analysis (b). (a) 1: initial rate of entire samples, 2: association rate of 2nd phase of association, and 2': extrapolated initial rate of the slow-dissociation subpopulation. (b) The non-linear regression resulted in χ^2 = 0.76 and showed 2 distinct kinetic patterns, p and q.

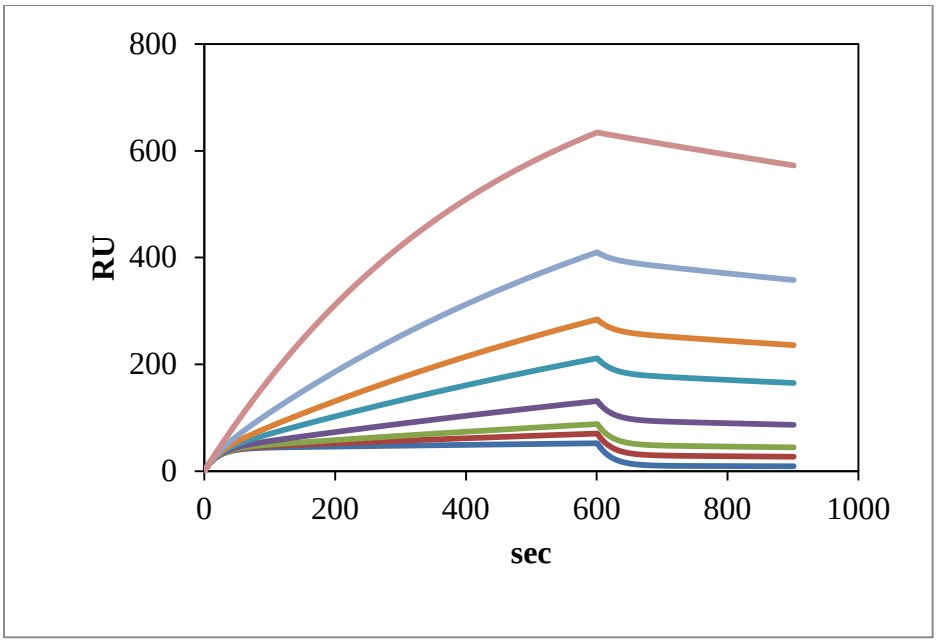

Fig. 2.5 Simulation binding curves of ligands with varied avidity distribution determined by the dual Langmuir kinetic model. The concentration is 62.5 nM and kinetic parameters of G5-$(oligo)_6$ served as k_{off} and k_{on} in this simulation. The percentages of slow-dissociation subpopulation are 1% (blue), 3% (red), 5% (green), 10% (purple), 20% (cyan), 30% (orange), 50% (dark blue), 100% (dark red). The durations of association and dissociation are 10 and 5 minutes, respectively.

2.4 Supplementary data

S2.1 potentiometric titration of 80% acetylated G5 PAMAMA (G5-Ac_{80}-NH_2) dendrimers.

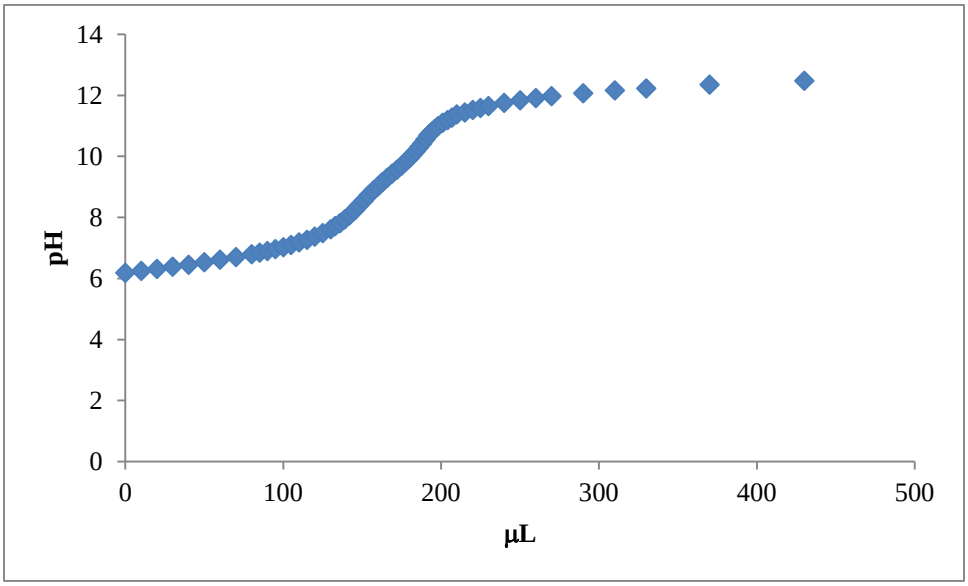

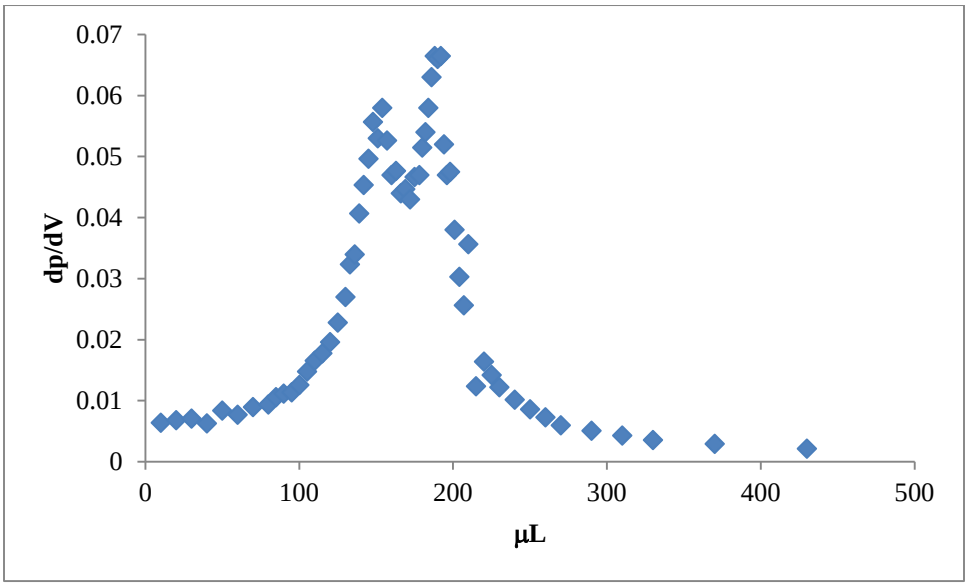

S2.2 MALDI TOF MS spectrometry of G5-$(oligo)_6$, the nomial MW= 34500.

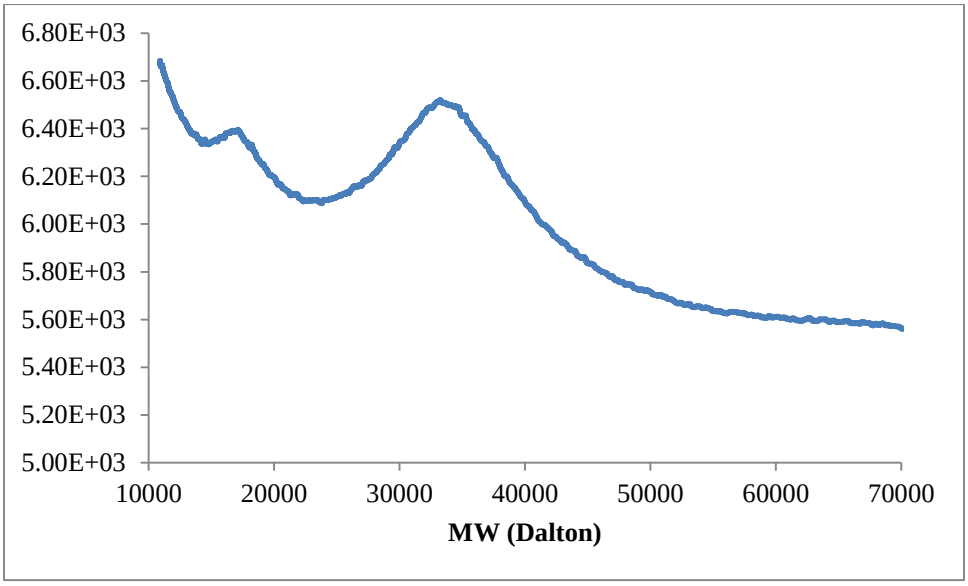

S2.3 UV-Vis spectrum of G5-(oligo)$_6$, measured at 0.05 mg/mL.

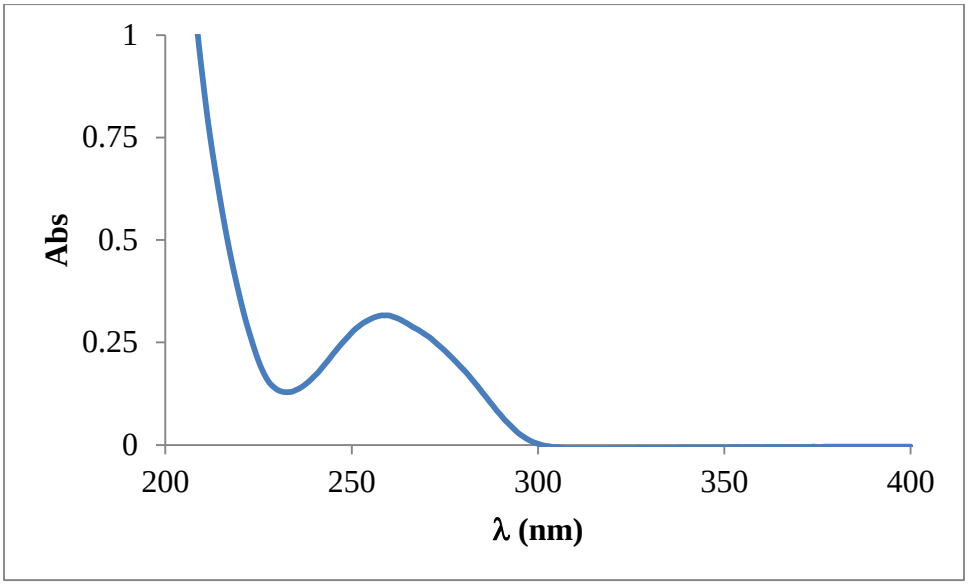

S 2.4 Fitting binding curves of G5-(oligo)$_6$ using 1:1 Langmuir model. The concentration of G5-(oligo)$_6$ was 62.5 nM. (χ2 = 369).

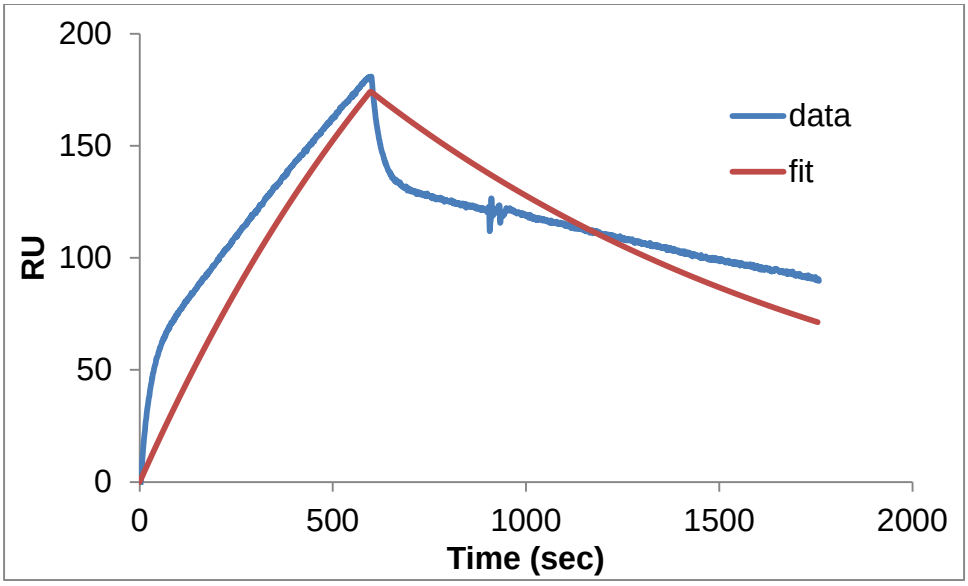

2.5 References

1. Mullen, D.G., *et al.* A Quantitative Assessment of Nanoparticle-Ligand Distributions: Implications for Targeted Drug and Imaging Delivery in Dendrimer Conjugates. *Acs Nano* **4**, 657-670 (2010).

2. Mullen, D.G., *et al.* Isolation and Characterization of Dendrimers with Precise Numbers of Functional Groups. *Chem-Eur J* **16**, 10675-10678 (2010).

3. Li, M.H., *et al.* Dendrimer-based multivalent methotrexates as dual acting nanoconjugates for cancer cell targeting. *Eur J Med Chem* **47**, 560-572 (2012).

4. Huang, B., *et al.* The facile synthesis of multifunctional PAMAM dendrimer conjugates through copper-free click chemistry. *Bioorg Med Chem Lett* **22**, 3152-3156 (2012).

5. Cline, E.N., *et al.* Paclitaxel-conjugated PAMAM dendrimers adversely affect microtubule structure through two independent modes of action. *Biomacromolecules* **14**, 654-664 (2013).

6. Mullen, D.G., *et al.* The implications of stochastic synthesis for the conjugation of functional groups to nanoparticles. *Bioconjugate Chem* **19**, 1748-1752 (2008).

7. Goonewardena, S.N., *et al.* Design considerations for PAMAM dendrimer therapeutics. *Bioorg Med Chem Lett* **23**, 2872-2875 (2013).

8. Edwards, P.R. & Leatherbarrow, R.J. Determination of association rate constants by an optical biosensor using initial rate analysis. *Anal Biochem* **246**, 1-6 (1997).

9. Nishikawa, M., Rattanakiat, S. & Takakura, Y. DNA-based nano-sized systems for pharmaceutical and biomedical applications. *Adv Drug Deliver Rev* **62**, 626-632 (2010).

10. McLaughlin, C.K., Hamblin, G.D. & Sleiman, H.F. Supramolecular DNA assembly. *Chem Soc Rev* **40**, 5647-5656 (2011).

11. Patwa, A., Gissot, A., Bestel, I. & Barthelemy, P. Hybrid lipid oligonucleotide conjugates: synthesis, self-assemblies and biomedical applications. *Chem Soc Rev* **40**, 5844-5854 (2011).

12. Persson, B., *et al.* Analysis of oligonucleotide probe affinities using surface plasmon resonance: A means for mutational scanning. *Anal Biochem* **246**, 34-44 (1997).

13. Hong, S., *et al.* The binding avidity of a nanoparticle-based multivalent targeted drug delivery platform. *Chem Biol* **14**, 107-115 (2007).

14. Tassa, C., *et al.* Binding affinity and kinetic analysis of targeted small molecule-modified nanoparticles. *Bioconjug Chem* **21**, 14-19 (2010).

15. Choi, S.K., *et al.* Dendrimer-based multivalent vancomycin nanoplatform for targeting the drug-resistant bacterial surface. *Acs Nano* **7**, 214-228 (2013).

16. Farokhzad, O.C., *et al.* Targeted nanoparticle-aptamer bioconjugates for cancer chemotherapy in vivo. *Proc Natl Acad Sci U S A* **103**, 6315-6320 (2006).

17. Wolfenden, M.L. & Cloninger, M.J. Carbohydrate-functionalized dendrimers to investigate the predictable tunability of multivalent interactions. *Bioconjugate Chem* **17**, 958-966 (2006).

18. Svenson, S. & Tomalia, D.A. Dendrimers in biomedical applications--reflections on the field. *Adv Drug Deliv Rev* **57**, 2106-2129 (2005).

19. Tomalia, D.A. Interview: An architectural journey: from trees, dendrons/dendrimers to nanomedicine. Interview by Hannah Stanwix. *Nanomedicine (Lond)* **7**, 953-956 (2012).

20. Choi, Y.S., Mecke, A., Orr, B.G., Holl, M.M.B. & Baker, J.R. DNA-directed synthesis of generation 7 and 5 PAMAM dendrimer nanoclusters. *Nano Lett* **4**, 391-397 (2004).

21. Choi, Y., Thomas, T., Kotlyar, A., Islam, M.T. & Baker, J.R. Synthesis and functional evaluation of DNA-assembled polyamidoamine dendrimer clusters for cancer cell-specific targeting. *Chemistry & Biology* **12**, 35-43 (2005).

22. Caminade, A.M., Turrin, C.O. & Majoral, J.P. Dendrimers and DNA: Combinations of two special topologies for nanomaterials and biology. *Chem-Eur J* **14**, 7422-7432 (2008).

CHAPTER 3

MODULATION OF MULTIVALENT INTERACTION: EFFECT OF VALENCE OF LIGAND-FUNCTIONALIZED NANOPARTICLES

3.1 Introduction

Multivalent ligand-receptor interaction is believed to be optimized when the binding moieties on synthetic multivalent ligands and multivalent receptors or surfaces have high affinity interactions.[1,2] Therefore, a variety of multivalent oligonucleotide ligands were developed to test this hypothesis by altering the sequence of synthetic multivalent ligands and then examine the effect of these modifications on the alterations in interaction caused by the number of ligands and the length and flexibility of intermediate linkers.[3-5] This work parallels prior work from other investigators.[6-9] For instance, Kitov and co-workers demonstrated that a synthetic pentavalent carbohydrate ligand can achieve a more than million-fold enhancement of the inhibition activity in neutralizing a five-member bacterial toxin. They also found this activity of inhibition would decrease with the valence of the synthetic carbohydrate ligands. Meanwhile, Zhang and co-workers additionally proved multivalent interactions were strongly subject to the length of intermediate linkers with similar pentavalent carbohydrate ligands. When the length of linkers is not sufficient to crosslink the binding moieties, the multivalent effect would become negligible, compared to the original monovalent interaction.

Given the ease of manipulation, the valence, the number of ligands, has been the most well-studied design factor of synthetic multivalent ligands that has been employed to enhance

binding avidities of multivalent nanoparticles.[10,11] For instance, Hong and co-workers utilized a series of folic acid-functionalized G5 PAMAM dendrimers which were functionalized with a variety of number of ligands to evaluate the effect of valence on their binding avidity. Their results showed that the multivalent enhancement of their binding avidity saturated when the nanoparticles functionalized with 5 and more folic acids, suggesting this valence (5 folic acids per dendrimer) would be an ideal design parameter that considered both targeting potency and effective consumption of targeting agents. Another study seems to agree with this suggestion that oligovalent nanoparticles can already perform enhanced avidity. Tassa and co-workers conducted an extensive survey on the binding avidity with a combinatorial library of ligand-functionalized iron oxide nanoparticles. They consistently found nanoparticles functionalized with 4 ligands in this library can show multivalent enhancement as high as nanoparticles with 4-fold higher valences.

However, a consensus on the ideal valence was not reached in studies examining different synthetic multivalent nanoparticle systems.[12-14] A trend regarding the relation of valence to avidity was revealed with a series of carbohydrate-functionalized dendrimers that were developed to target lectins. The results showed their interaction with lectins would not saturate in the same way as the increase in the number of ligands did on nanoparticles. The binding avidity of carbohydrate-functionalized dendrimers is positively associated with the quantity of functionalized carbohydrates even if the dendrimers were fully capped with carbohydrates. This discrepancy on the effect of valence suggests the mechanism of the multivalent interaction could be highly differentiated and dependent on the properties of the functionalized ligands.

In this chapter, a series of PAMAM dendrimers with varied numbers of ssDNA oligonucleotides were synthesized for examining the effect of valence on the binding avidities of synthetic multivalent nanoparticles. As described in Chapter 2, the avidity distribution and kinetic parameters of these synthetic multivalent nanoparticles were evaluated. We demonstrated that the avidity distribution of synthetic multivalent nanoparticles was significantly regulated by the number of functionalized ligands. In particular, the proportion of nanoparticles showing enhanced avidities would decrease with the valence of the ligands or even vanish when the valence could not support multivalent interactions. Comparing the results of Poisson simulation and the avidity distribution, we further suggested a cut-off value that initiates the multivalent interactions and potentially a threshold valence for the design of multivalent nanoparticle systems.

3.2 Experimental Methods

Chemicals and materials: Single-stranded DNA oligonucleotides (ssDNA oligos) were synthesized with 5'-end modifications and purified with a standard desalting process at Integrated DNA Technologies (Coralville, IA), including an 8-mer amino-terminated oligo, 5'-NH_2-C_6-TGCTGAGG, and a 25-mer biotinylated oligo 5'-biotin-TTTCTTCAGCATCTTATCCGAGTTTT. The generation 5 polyamidoamine (G5 PAMAM) dendrimer was purchased from Dendritech Inc. (Midland, MI) and purified as described in the synthesis section. All organic solvent, reagents and titration volumetric solutions (0.1M HCl and 0.1M NaOH) were purchased from Sigma Aldrich (St. Louis, MO) and used without further purification. Phosphate buffer saline (PBS) without calcium and magnesium was

purchased from Thermo Scientific (Logan, UT). 10K molecular cutoff (MWCO) centrifugal filters (Amicon Ultra-4) were purchased from Millipore (Billerica, MA). 10K MWCO dialysis membrane was purchased from Spectrum Laboratories (Rancho Dominquez, CA). Sensor chips SA for SPR measurements and HBS-EP (pH 7.4) buffer were purchased from GE Healthcare (Piscataway, NJ).

Synthesis and characterization of G5 PAMAM dendrimer-based multivalent nanoparticles: The synthesis and purification of functionalized G5 PAMAM dendrimer was identical to the procedures shown in Chapter 2, except for the method of ligand conjugation. In the conjugation process, the mixture of NHS-activated G5 PAMAM solution was evenly divided into three aliquots and then reacted with amino-terminated ssDNA oligos. Five and 10 equivalent ssDNA oligos (0.32 and 0.64 μmole) were individually added into aliquots with the NHS-ester activated dendrimer mixture in 0.4 mL pH 9 carbonate buffer for 16 hours at room temperature. After purification and recovery, the molecular weight of the G5 PAMAM dendrimer-based ssDNA oligo nanoparticles was determined by MALDI-TOF MS using a Micromass TofSpec-2E with positive ion mode as previously described. The number of attached ssDNA oligos was determined by UV-Vis spectra which were conducted in a 1 mL quartz cuvette using a Perkin Elmer Lamda 20 spectrophotometer. The equivalent concentration of ssDNA was calibrated using the OD_{260} of the specific DNA sequence. The mean number of conjugated ssDNA oligos per G5 PAMAM dendrimer was determined by using the quotient of the equivalent concentration of ssDNA that the oligonucleotide-functionalized dendrimer presented and the concentration of the nanoparticles that was calculated based on the MS-determined molecular weight of the functionalized nanoparticle.

SPR measurements and evaluation of avidity distribution: The kinetic analysis of multivalent nanoparticles was conducted using a BIAcore biosensor with identical experimental conditions as described in Chapter 2. Briefly, the SA surface of the sensor chip was immobilized with the 25-mer biotinylated ssDNA oligo, resulting in 1300 RU (1.3ng/mm^2) of immobilized ssDNA oligos. During SPR measurement, the 8-mer-ssDNA oligo-functionalized dendrimers dissolved in HBS-EP buffer were injected to both flow channels of the sensor chip, including the ssDNA oligo-immobilized channel and the reference channel, at a flow rate of 10 μL/min. After each measurement, the chip surface was regenerated using 5-10 μL pH 11 NaOH to ensure complete removal of the bound molecules before the next measurement. The final SPR sensograms were obtained by using the measurement after subtraction of the signal on the reference channel from the signal on the oligo-immobilized channel.

The avidity distribution of the synthetic multivalent nanoparticles was quantified using a method composed of a parallel initial rate analysis and dual Langmuir analysis as described in Chapter 2. In brief, the initial rate required for the parallel initial rate kinetic analysis was extracted by the first-order derivative at the initial point of the measured sensogram and using the average slope of the sensogram after association time at 2 minutes of association. In addition, kinetic parameters, including, k_{on}, k_{off} and K_D, of the ssDNA oligo-functionalized nanoparticles were determined using the dual Langmuir kinetic-binding model with BIAevaluation software. In this analysis, the concentrations of two tested ligands were defined as the product of the concentration of total dissolved ssDNA oligo-functionalized dendrimer and the molar fractions acquired by the parallel initial rate analysis described above.

Simulation of distributed valence on nanoparticles: The statistical model assumed that ligand conjugation with the nanoparticle obeys the Poissonian stochastic mechanism.[15,16] In this Poisson simulation, the total number of available attached sites on the dendrimer surface and the mean ligand number per dendrimer characterized with UV-Vis and MALDI-MS were used as factors to calculate the distribution. With this method, the ligand distribution was plotted, and the percentage of nanoparticles with specific valences was identified.

3.3 Results and Discussion

Synthesis of PAMAM dendrimer-based multivalent nanoparticles: For experimentally examining the effect of valence on binding avidity, two alternative ssDNA oligo-functionalized G5 PAMAM dendrimers with varied valences were synthesized. Based on results of MALDI MS and UV-Vis, the number of functionalized ssDNA oligos per dendrimer was characterized, which were 1.7 and 3.1, respectively. As described in Chapter 2, the low reaction yield of EDC coupling chemistry still hampered the fabrication of high-valence nanoparticles. Fortunately, taking the dendrimers with 6 ssDNA oligos together, these nanoparticles, in fact, can already be highly representative to demonstrate how multivalent effect is governed by the valence of the nanoparticle. Based on recent studies, the multivalent effect saturated as the valence was as low as 4 to 5 ligands per nanoparticle.[10,11] Therefore, the kinetic results obtained from nanoparticles functionalized with 2 to 6 ligands likely already cover most of the range in which the multivalent effect in the nanoparticles is significantly dependent on the valence of particles.

Evaluating avidity distribution of G5-(oligo)$_{1.7}$ and G5-(oligo)$_{3.1}$:. Researchers developing multivalent targeted nanoparticles have widely studied using the valence of a nanoparticle as a way to enhance their binding avidities. However, they examined the tested nanoparticle as a homogeneous system showing uniform binding avidity, which did not likely interpret the actual interacting behaviors of the complex ligand-nanoparticle systems appropriately. Therefore, we are strongly interested in examining the effect of valence on the interaction of nanoparticles from the aspect of avidity distribution by using our newly developed kinetic analysis as described in Chapter 2. First, we evaluated the interaction of G5-(oligo)$_{1.7}$ and G5-(oligo)$_{3.1}$ with their complementary surfaces, using an SPR biosensor. (Fig 3.1) The SPR sensograms depicted that, between these two multivalent nanoparticles, only G5-(oligo)$_{3.1}$ performed biphasic binding as G5-(oligo)$_{6,}$ showing the slow dissociation that characterized the enhanced avidity. In contrast, G5-(oligo)$_{1.7}$ reached the equilibrium of binding early in the association phase and then rapidly dissociated from the surface, suggesting this weak avidity is comparable to the affinity of the free ssDNA oligo. We found the multivalent effect deteriorated because of the insufficient valence on the nanoparticles.

Based on parallel initial rate analysis and dual Langmuir analysis, the avidity distribution and kinetic parameters of G5-(oligo)$_{3.1}$ were further quantitatively determined. (Table 3.1) There were fewer than 1% of slow-dissociation nanoparticles present in the G5-(oligo)$_{3.1}$, which is 10-fold fewer than this subpopulation existing in the G5-(oligo)$_{6}$. This result of a two-fold less valence leading to a 10-fold decrease in percentage of slow-dissociation nanoparticles revealed that avidity distribution of synthetic multivalent nanoparticles is highly sensitive to the valence. When the required valence is not attained, the avidity distribution is driven toward weak binding avidity. This infers that it would be

feasible to drive the avidity distribution of this system toward strong binding avidity if the valence can be effectively augmented.

Although the mean valence significantly changed the avidity distribution of the nanoparticles, we observed that nanoparticles with varied mean numbers of ligands fell within comparable kinetic parameters, wherein the weak binding avidity is comparable to the affinity of monovalent interaction and the strong binding avidity gained a 2-order-of–magnitude improvement. This coincident similarity of avidity enhancement appears to suggest that those nanoparticles with a different mean of ligand-to-nanoparticle ratio may perform multivalent interactions with similar strength and configuration of the complementary interactions. We believe that this kinetic similarity in fact resulted from similar structural properties of the multivalent nanoparticles, particularly the number of functionalized ligands on nanoparticles. Additionally, recent studies already showed the ligand-to-nanoparticle ratio in fact is heterogeneous and Poisson-distributed. Therefore, we hypothesize that the quantity of strong-avidity nanoparticles is associated with the percentage of densely functionalized nanoparticles that have a number of ligands higher than a required valence that initiates multivalent interactions.

The above hypothesis could be validated by the correspondence between the avidity distribution and ligand distribution in these oligonucleotide-functionalized multivalent nanoparticles. Based on the assumption that the multivalent effect is positively associated with the valence, we correlated the Poisson ligand distribution and the avidity distribution of the G5-$(oligo)_6$, and found that the 10% of the nanoparticles showing enhanced binding avidity are likely those particles presenting more than 9 ligands. (Fig. 3.2) If using this valence as a cut-off value, we also observed that in the G5-$(oligo)_{3.1}$ and the G5-$(oligo)_{1.7}$

there were just a few or no nanoparticles showing a valence higher than 9, suggesting the threshold valence in this multivalent nanoparticle system. This result offers quantitative evidence that the avidity distribution observed in our studies is mediated by the ligand distribution on the nanoparticles. Additionally, it provides a rational and quantitative approach to optimizing the binding avidity of multivalent nanoparticles. We could develop multivalent nanoparticles showing homogeneous strong binding avidity by increasing the ligand valence and controlling the entire ligand distribution to a level higher than the threshold valence required for the presence of a multivalent effect.

Table 3.1 Avidity distribution and kinetic parameters of oligonucleotide-functionalized nanoparticles.

Nanoparticles	**%**	**k_{on} ($M^{-1}s^{-1}$)**	**k_{off} (s^{-1})**	**K_D (M)**
G5-$(oligo)_6$	10	$3.10x10^4$	$3.37x10^{-4}$	$1.09x10^{-8}$
	90	$3.31x10^4$	$4.61x10^{-2}$	$1.39x10^{-6}$
G5-$(oligo)_{3.1}$	<1	$3.71x10^3$	$3.44x10^{-4}$	$9.26x10^{-8}$
	>99	$3.57x10^3$	$3.74x10^{-2}$	$1.05x10^{-5}$

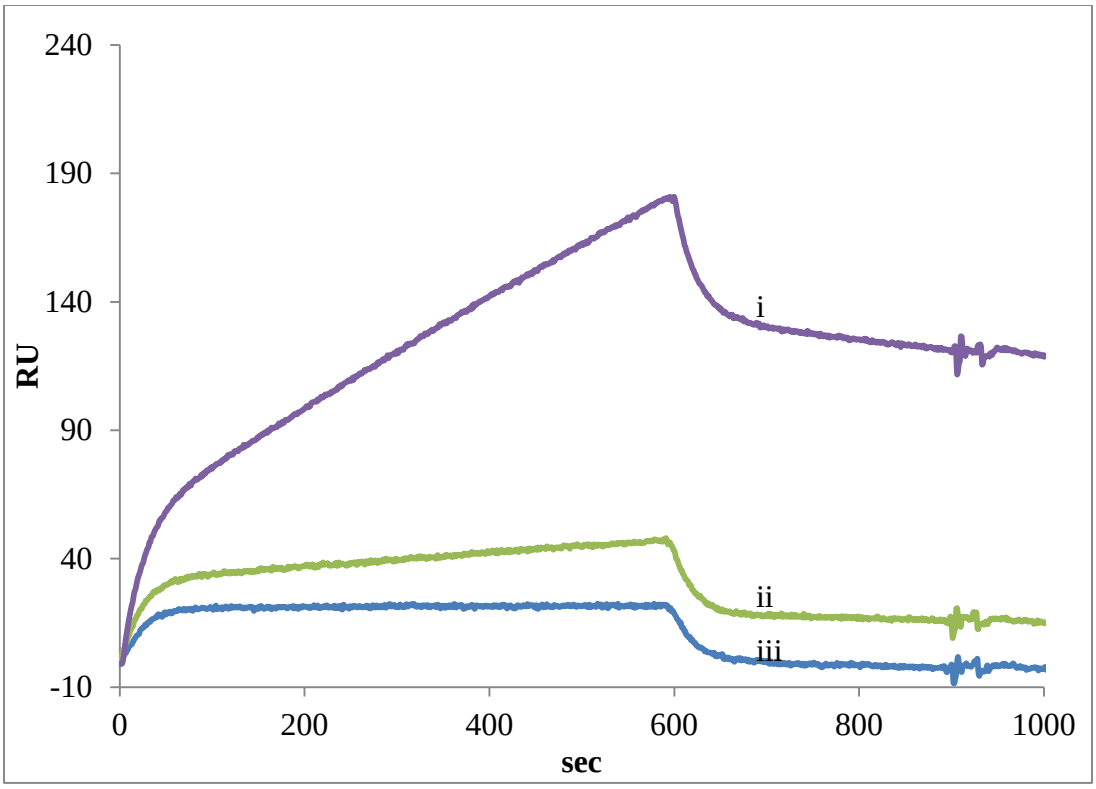

Fig. 3.1 SPR sensograms of oligonucleotide-functionalized nanoparticles. (i) G5-$(oligo)_6$ at 62.5 nM, (ii) G5-$(oligo)_{3.1}$ at 1 μM, and (iii) G5-$(oligo)_{1.7}$ at 1 μM.

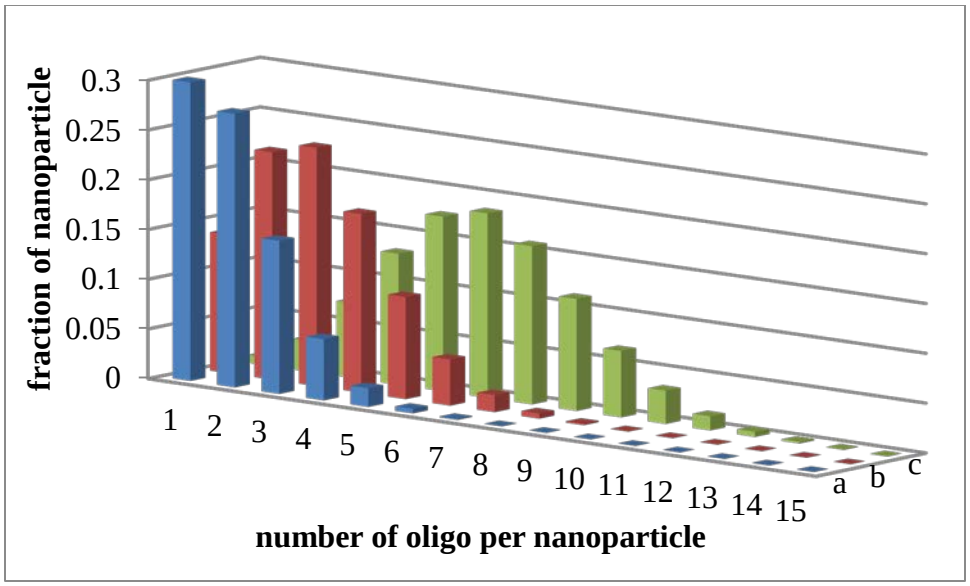

Fig. 3.2 Poisson simulation of ligand distribution on oligonucleotide-functionalized nanoparticles. (a) G5-$(oligo)_{1.7}$, (b) G5-$(oligo)_{3.1}$,and (c) G5-$(oligo)_{6}$.

3.4 Supplementary data

S3.1 MALDI TOF MS spectrometries of (a) G5-$(oligo)_{3.1}$ (MW= 32200) and (b) (G5-$oligo)_{1.7}$ (MW = 32400).

(a)

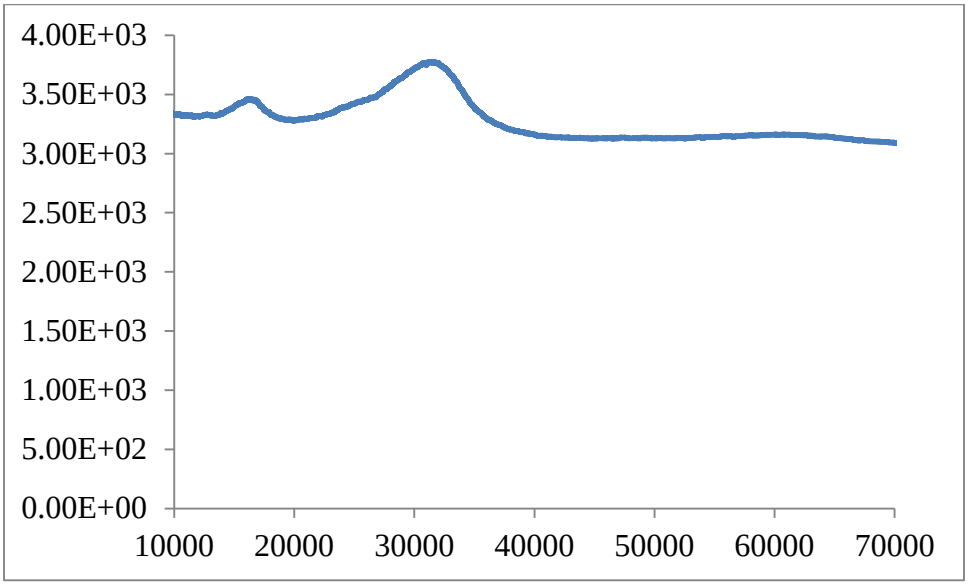

(b)

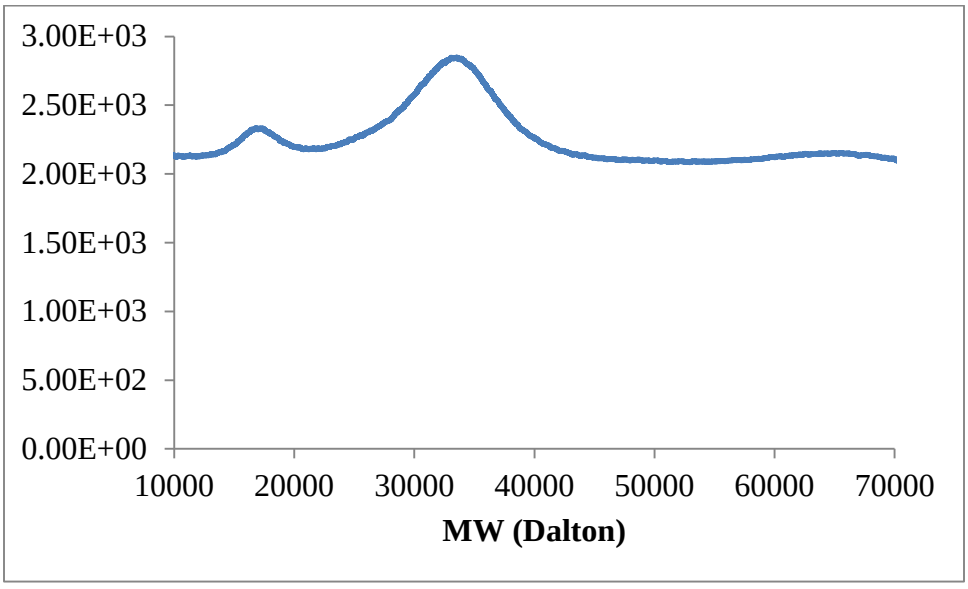

S3.2 UV-Vis spectra of (i) G5-$(oligo)_{3.1}$ and (ii) $(G5\text{-}oligo)_{1.7}$, measured at 0.05 mg/mL.

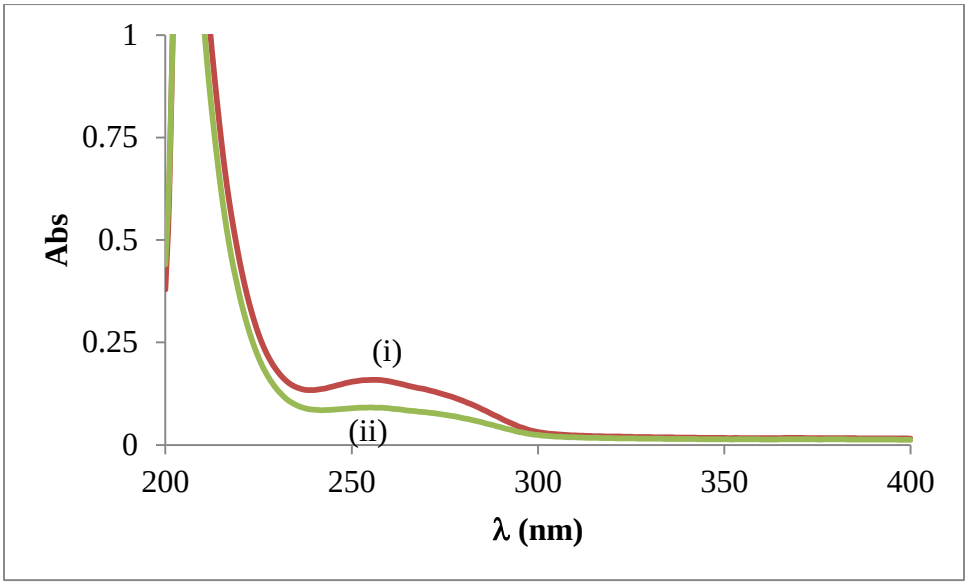

3.5 References

1. Mammen, M., Choi, S.K. & Whitesides, G.M. Polyvalent interactions in biological systems: Implications for design and use of multivalent ligands and inhibitors. *Angew Chem Int Edit* **37**, 2755-2794 (1998).

2. Pieters, R.J. Maximising multivalency effects in protein-carbohydrate interactions. *Org Biomol Chem* **7**, 2013-2025 (2009).

3. Zhang, Z.Y., Cheng, Q. & Feng, P.Y. Selective Removal of DNA-Labeled Nanoparticles from Planar Substrates by DNA Displacement Reactions. *Angew Chem Int Edit* **48**, 118-122 (2009).

4. Cutler, J.I., Zheng, D., Xu, X.Y., Giljohann, D.A. & Mirkin, C.A. Polyvalent Oligonucleotide Iron Oxide Nanoparticle "Click" Conjugates. *Nano Lett* **10**, 1477-1480 (2010).

5. Massich, M.D., Giljohann, D.A., Schmucker, A.L., Patel, P.C. & Mirkin, C.A. Cellular Response of Polyvalent Oligonucleotide-Gold Nanoparticle Conjugates. *Acs Nano* **4**, 5641-5646 (2010).

6. Kitov, P.I., *et al.* Shiga-like toxins are neutralized by tailored multivalent carbohydrate ligands. *Nature* **403**, 669-672 (2000).

7. Kitov, P.I., Shimizu, H., Homans, S.W. & Bundle, D.R. Optimization of tether length in nonglycosidically linked bivalent ligands that target sites 2 and 1 of a Shiga-like toxin. *J Am Chem Soc* **125**, 3284-3294 (2003).

8. Fan, E.K., *et al.* High-affinity pentavalent ligands of Escherichia coli heat-labile enterotoxin by modular structure-based design. *J Am Chem Soc* **122**, 2663-2664 (2000).

9. Zhang, Z.S., *et al.* Solution and crystallographic studies of branched multivalent ligands that inhibit the receptor-binding of cholera toxin. *J Am Chem Soc* **124**, 12991-12998 (2002).

10. Hong, S., *et al.* The binding avidity of a nanoparticle-based multivalent targeted drug delivery platform. *Chem Biol* **14**, 107-115 (2007).

11. Tassa, C., *et al.* Binding affinity and kinetic analysis of targeted small molecule-modified nanoparticles. *Bioconjug Chem* **21**, 14-19 (2010).

12. Woller, E.K., Walter, E.D., Morgan, J.R., Singel, D.J. & Cloninger, M.J. Altering the strength of lectin binding interactions and controlling the amount of lectin clustering using mannose/hydroxyl-functionalized dendrimers. *J Am Chem Soc* **125**, 8820-8826 (2003).

13. Mangold, S.L. & Cloninger, M.J. Binding of monomeric and dimeric Concanavalin A to mannose-functionalized dendrimers. *Org Biomol Chem* **4**, 2458-2465 (2006).

14. Wolfenden, M.L. & Cloninger, M.J. Carbohydrate-functionalized dendrimers to investigate the predictable tunability of multivalent interactions. *Bioconjugate Chem* **17**, 958-966 (2006).

15. Mullen, D.G., *et al.* A Quantitative Assessment of Nanoparticle-Ligand Distributions: Implications for Targeted Drug and Imaging Delivery in Dendrimer Conjugates. *Acs Nano* **4**, 657-670 (2010).

16. Mullen, D.G., *et al.* Isolation and Characterization of Dendrimers with Precise Numbers of Functional Groups. *Chem-Eur J* **16**, 10675-10678 (2010).

CHAPTER 4

EVALUATING PHYSICAL FACTORS TO INTERACTIONS OF MULTIVALENT NANOPARTICLES: THE EFFECT OF THE INTRINSIC AFFINITY OF LIGANDS

4.1 Introduction

Multivalent ligand-receptor interaction is governed by a variety of factors, including thermodynamic and kinetic parameters.[1-4] To improve the design of multivalent-targeted nanoparticles, these factors definitely need to be considered. The current approach to guide design has focused on studies that have used thermodynamic analyses to understand parameters as the entropy and enthalpy of multivalent interactions.[4-6] For instance, Dam and co-workers evaluated the binding interactions of a series of synthetic multivalent carbohydrate ligands and assessed their thermodynamic parameters. Although their analysis led to an increase in their understanding of the thermodynamic mechanisms, it is still difficult to translate these thermodynamic parameters into practical design factors for the creation of multivalent ligands or nanoparticles.

In contrast, kinetic factors, such as binding affinity, have a greater theoretical potential to aid in the practical design of multivalent nanoparticles. This argument is supported by facts which include 1) that most affinities of biological ligands have been evaluated once their biological activity has been identified, and 2) it is simple to correlate the final avidity of multivalent nanoparticles and the intrinsic affinity of the attached ligand and extract the effect of the intrinsic affinity without involving complicated thermodynamic

calculations.[1,7-9] In fact, the advancement of synthetic chemical biology and proteomics has revealed an abundance of novel ligands with specific interactions with biological receptors suitable for targeting.[10,11] To increase the value of these novel ligands in target therapy, it is important to enhance the ligand binding avidity by taking advantage of the multivalent effect. A systematic guideline for the effective combination of diverse ligands and nanoparticles that form strong-avidity nanoparticles would be very important. The affinity of a ligand could serve a single parameter that provides coherence to a targeting system and simplifies the expression of this guideline.

Unfortunately, at this date there are still few studies that have addressed the affinity of ligands in designing multivalent targeted nanoparticles. One study used PAMAM dendrimers functionalized with mannose and glucose to examine the effect of intrinsic ligand affinity on the multivalent interactions presented by the nanoparticles, suggesting that a stronger intrinsic ligand affinity would lead to stronger multivalent interactions.[12,13] However, another study with inorganic nanoparticle-based multivalent ligands showed the opposite trend: that the nanoparticles showed comparable binding avidity when functionalized with ligands with a variety of affinities.[8] These studies provide certain clues to explaining how ligand affinity is associated with the binding avidity of multivalent ligands or nanoparticles. Nonetheless, the contradictory results and conclusions reached under uncontrolled experimental conditions and with poorly defined materials impede the utility of using ligand affinity as a design factor of multivalent nanoparticles. Therefore, to overcome this current dichotomy, the key is to generate rules of design from a well-controlled system with defined materials and principles.

In the current studies we explored the effects of ligand affinity on the binding avidity of multivalent nanoparticles, using oligonucleotide-functionalized PAMAM dendrimers as model nanoparticles and an SPR biosensor to evaluate the interactions. By examining the relation between the ligand affinity and the avidity distribution of the multivalent nanoparticles, we aimed to provide design guidelines that are applicable for a broad range of ligands with varied affinities. The first approach was to use identical nanoparticles but change the ambient binding temperature to alter the affinities of oligonucleotides. The purpose of this approach was to avoid any deviations of the multivalent structure due to synthesis and to isolate the effects of the ligand affinity. The second approach was to synthesize model nanoparticles with a ligand showing varied affinity. The oligonucleotide was re-designed and assigned with a lower binding affinity than the oligonucleotides described in preceding chapters. The avidity distribution and kinetic parameters were then extracted and examined. Based on these studies, the results suggested that the lower affinity seems to promote multivalent interactions presented by the nanoparticles in these two approaches. In contrast, the avidity distribution only shifted significantly while nanoparticles functionalized with lower-affinity ligands, which showed a lower threshold valence for performing multivalent interactions.

4.2 Experimental Methods

Chemicals and materials: Single-stranded DNA oligonucleotides (ssDNA oligos) were synthesized with 5'-end modifications and purified with a standard desalting process at Integrated DNA Technologies (Coralville, IA), including an 8-mer amino-terminated oligo,

5’-NH_2-C_6-TGCTGAGG (Oligo1), 5’-NH_2-C_6-TAAGATGC (Oligo2) and a 25-mer biotinylated oligo 5’-biotin-TTTCTTCAGCATCTTATCCGAGTTTT. The generation 5 poly(amidoamine) (G5 PAMAM) dendrimer was purchased from Dendritech Inc. (Midland, MI) and purified as described in the synthesis section. Phosphate buffer saline (PBS) without calcium and magnesium was purchased from Thermo Scientific (Logan, UT). 10K molecular cutoff (MWCO) centrifugal filters (Amicon Ultra-4) were purchased from Millipore (Billerica, MA). 10K MWCO dialysis membrane was purchased from Spectrum Laboratories (Rancho Dominquez, CA). Sensor chips SA and HBS-EP (pH 7.4) buffer used in SPR measurements were purchased from GE Healthcare (Piscataway**,** NJ).

Synthesis and characterization of oligonucleotide-functionalized dendrimers: The synthesis and purification of the oligonucleotide-functionalized G5 PAMAM dendrimer were identical to the procedures shown in Chapter 2. In the conjugation process, the mixture of NHS-activated G5 PAMAM solution was evenly divided into three aliquots and then reacted with amino-terminated ssDNA oligos. 20 equivalent ssDNA oligos 1 and 2 (1.28 μmole) were individually added into aliquots with the NHS-ester activated dendrimer mixture in 0.4 mL pH 9 carbonate buffer for 16 hours at room temperature. After purification and recovery, the molecular weight of the G5 PAMAM dendrimer-based ssDNA oligo nanoparticles was determined by MALDI-TOF MS using a Micromass TofSpec-2E with positive ion mode, as previously described. The number of attached ssDNA oligos was determined by UV-Vis spectra which were conducted in a 1 mL quartz cuvette using a Perkin Elmer Lamda 20 spectrophotometer. The equivalent concentration of ssDNA was calibrated using the OD_{260} of the specific DNA sequence. The mean number of conjugated ssDNA oligos per G5 PAMAM dendrimer was determined by using the quotient of the equivalent

concentration of ssDNA that the oligonucleotide-functionalized dendrimer presented and the concentration of the nanoparticles that was calculated based on the MS-determined molecular weight of the functionalized nanoparticle.

SPR measurements and kinetic analysis: The kinetic analysis of oligonucleotides and multivalent nanoparticles was conducted using a BIAcore biosensor with identical experimental conditions as described in Chapter 2. Briefly, the SA surface on the flow channel 1 of the sensor chip was immobilized with the 25-mer biotinylated ssDNA oligo, resulting in 1300 RU (1.3 ng/mm^2) of immobilized ssDNA oligos. Meanwhile, the immobilization process would bypass the other flow channel, 2, for preparing a reference channel in the binding tests. During SPR measurement, the 8-mer-ssDNA oligo-functionalized dendrimers dissolved in HBS-EP buffer were injected into both flow channels of the sensor chip, including the ssDNA oligo-immobilized channel and the reference channel. After each measurement, the chip surface was regenerated using 5-10 μL pH 11 NaOH to ensure complete removal of the bound molecules before the next measurement. The final SPR sensograms were obtained by using the signal from the oligo-immobilized channel subtracted by the signal from the flow channel 2.

The avidity distribution of the synthetic multivalent nanoparticles was quantified using a method composed of a parallel initial rate analysis and dual Langmuir analysis as described in Chapter 2. In brief, the initial rate required for the parallel initial rate kinetic analysis was extracted by the first-order derivative at the initial point of the measured sensogram and using the average slope of the sensogram after association time at 2 minutes of association. In addition, the kinetic parameters, including, k_{on}, k_{off} and K_D, of the ssDNA oligo-functionalized nanoparticles, were determined using the dual Langmuir kinetic-binding

model with BIAevaluation software. In this analysis, the concentrations of two tested ligands were defined as the product of the concentration of the total dissolved ssDNA oligo-functionalized dendrimer and the molar fractions acquired by the parallel initial rate analysis described above. The kinetic parameters of the free oligos were determined with a 1:1 Langmuir kinetic model with BIAevaluation software.

Thermodynamic analysis: The thermodynamic binding parameters of the oligonucleotides and oligonucleotide-functionalized dendrimers were extracted based on the Gibbs free energy equation $\Delta G = \Delta H - T\Delta S$, where G, H, T, and S represented binding free energy, enthalpy, temperature and entropy, respectively. ΔG was converted by a dissociation constant, K_D, measured via Biacore, based on the integration form of the Arrehnius equation $\Delta G = RT*\ln(K_D)$, where R represents the gas constant (1.986 $calK^{-1}mol^{-1}$).[14] These parameters were extracted based on the result of the linear regression with $R^2 = 0.98$

Poissonian simulation of ligand distribution: The statistical model assumed that ligand conjugation with the nanoparticles obeys the Poissonian stochastic mechanism.[15] In this Poisson simulation, the total number of available attached sites on the dendrimer surface and the mean ligand number per dendrimer characterized with UV-Vis and MALDI-MS were used as factors to calculate the distribution. With this method, the ligand distribution was plotted, and the percentage of nanoparticles with specific valences was identified.

4.3 Results and Discussion

The effect of intrinsic ligand affinity, examined by changing ambient temperature: The binding of free oligonucleotides and multivalent nanoparticles was evaluated by BIAcore at a series of precisely-controlled temperatures with error less than 0.1^{o}C. The intrinsic affinities of oligo 1 were determined with 1:1 Langmuir kinetics and listed in Table 4.1. Nonetheless, the biphasic association was reproducibly present in this series of tests with gradually increasing temperature, documenting that the binary binding mechanism observed in room temperature in Chapter 2 was reproducible. (Fig. 4.1) Therefore the avidity distribution and the detailed kinetic parameters can be extracted using parallel initial rate analysis and a dual Langmuir kinetic model, as previously described and listed in Table 4.2. The excellent χ^2 indicates these models accurately interpreted the kinetic information measured by the biosensor. We found the avidity distribution was insignificantly altered due to the change of the intrinsic affinity of the functionalized ligand. All of the observed changes were less than 50% of the avidity distribution measured in room temperature. However, the effect of the intrinsic affinity of the ligand did play an important role in multivalency. The binding avidity of the subpopulation composed with slow-dissociation nanoparticles was significantly modified by the intrinsic affinity of the ligand. The multivalent enhancement β was inversely associated with the intrinsic affinity with more than a 10-fold difference in avidity. We believe this intrinsic affinity-avidity enhancement compensation can be explained by the fundamental principle of multivalent interaction, during which the initial singlet-bound ligand should have sufficient flexibility and mobility that it allows the unbound ligand on the substance to reach second receptors to form alternative affinitive bonds.

The binding kinetics of fast-dissociation nanoparticles also offers important information for the design of ligand-functionalized nanoparticles. This subpopulation performed binding comparable to its corresponding monovalent ligand. The difference between the affinity and this "monovalent-like" avidity is not as significant as this factor in slow-dissociation nanoparticles, and the ratio of these two parameters was presented with a 4-fold deviation. (Fig 4.2) Interestingly, we found this deviation is inversely associated with the intrinsic affinity of the functionalized ligand. We hypothesized this increase of the binding potential results from the transient formation of alternative affinitive bonding. The time of bonding is too short to prolong the time of the adherence and support a multivalent interaction. Based on our results, this formation of transient bonds is inversely associated with the intrinsic affinity of the ligand, which is in concert with the previous statement that the formation of alternative bonding can be promoted by the flexibility and mobility of the initially bound nanoparticle ligands. This type of transient binding is often observed in chemistry; for instance the time-averaged hybridized bond can be stated in non-integer numbers.[16] Our results suggest that this transient bonding might also happen in mesoscale interactions. The subpopulation of nanoparticles with valences below the threshold that promotes a multivalent effect would possibly form transient bonds, leading to partially enhanced binding avidity.

Thermodynamic binding parameters of heterogeneous multivalent nanoparticles: The temperature-dependent binding tests rendered the opportunity to understand the binding of synthetic multivalent nanoparticles from thermodynamic perspectives. The Gibbs binding energies were converted from the binding constant (K_D) measured by Biacore and the relation against temperature was plotted and shown as Fig. 4.3.

Additionally, the thermodynamic binding parameters were extracted from the result of a linear regression based on the Gibbs free energy equation $\Delta G = \Delta H - T\Delta S$ and listed in Table 4.3. The most obvious features that distinguish the three binding phenomena involving free oligo1 and fast- and slow-dissociation G5-$(oligo1)_6$ are the slopes in the Gibbs-energy plot, which reflect the binding entropies of these ligands. Interestingly, the fast-dissociation G5-$(oligo1)_6$ presented an intermediate entropy penalty between that of the free oligo1s and the multivalent-like G5-$(oligo1)_6$. This discovery of an intermediate entropy may provide evidence from a thermodynamic perspective that agrees with the result obtained through kinetic analysis that suggests that the "monovalent-like" nanoparticles might perform a type of interaction that is hybridized with monovalent and multivalent interactions.

The observation that the entropy of the multivalent interaction is less than this thermodynamic parameter of monovalent interaction seems to disagree with the recent experimental results attained in the study of synthetic multivalent carbohydrate ligands and multivalent carbohydrate-functionalized nanoparticles.[12,13] These results indicate that the trend of entropy-enthalpy compensation would be magnified with multivalent interactions. We believe the difference between both statements may actually infer the different mechanism of interactions. 1) In our system, the nanoparticles performing multivalent interaction were evaluated without consideration of those monovalent-like nanoparticles; in contrast, other experiments analyzed the interactions as uniform systems. 2) In these studies the interaction was measured on a surface, but in other experiments the interaction was measured within the solution system. 3) The interaction in our approach was measured in a flow (open) system that is different from the closed system others have used. The measurement time with a flow system is significantly different from this parameter with a

closed system. For example, in a Biacore system, the time that a ligand flows through the detection area would be in seconds, but the measurement in ITC would be typically more than 10 minutes. Clearly, the measurement in flow systems and on the surface would be more relevant to the physiological environment of targeted cellular surfaces in the circulatory system. Therefore, we believe our results can, accordingly, correctly elucidate the mechanism of multivalent interactions that happen within biological systems.

Synthesis and characterization of multivalent oligonucleotide-functionalized G5 PAMAM dendrimers: The synthesis scheme is identical to that which was used for synthesizing G5-(oligo1)$_6$, including the chemistry (EDC/NHS coupling), the reaction conditions (concentrations, times, temperatures) and materials (G5-NH_2-COOH and amino 8-mer oligonucleotides). The only difference is that the sequence of the oligo was redesigned.[17] We controlled variables that affect the conjugation with the intention of minimizing the inter-batch variations. The results of the characterization showed that the mean of conjugated oligos per G5 dendrimers was still about 6, suggesting that the process of amide bond conjugation was conducted in a way that is reproducible and the ligand distribution would possibly be similarly displayed.

The effect of intrinsic ligand affinity, examined by changing the sequence of the oligonucleotides: The biphasic association was shown in the binding process of G5-(oligo2)$_6$, suggesting that the binary binding mechanism was still valid in this system. (Fig. 4.4) Obviously, the transition between two phases of association was not as sharp as the changes in the previous binding sensograms. Based on the apparent observation of the slopes before and after this transition, as described in Chapter 2, we can postulate that the percentage of slow-dissociation nanoparticles in G5-(oligo2)$_6$ would be significantly higher than is in G5-

$(oligo1)_6$. The avidity distribution and kinetic parameters of G5-$(oligo2)_6$ was extracted by parallel initial rate analysis and the dual Langmuir kinetic model because biphasic binding subsequently supports this postulation. (Table 4.4) The result indicated that 40% of the nanoparticles in the G5-$(oligo2)_6$ performed multivalently enhanced interactions with 500-fold and 200-fold enhancement of binding avidity of the free oligos and the monovalent-like nanoparticles, respectively. The β was more than a 3-fold larger enhancement, compared to the avidity enhancement when using oligo1, which presented a 20-fold higher affinity. This observation confirms the results of binding performed by G5-$(oligo1)_6$ with temperature-adjusted low affinity and also suggests that the multivalent effect may be promoted by ligands with lower affinity.

Despite the similarity in terms of avidity enhancement, the significant difference of avidity distribution was found between G5-$(oligo1)_6$ at 35 ^oC and G5-$(oligo2)_6$ at 25 ^oC. The 40% multivalent-like nanoparticles in G5-$(oligo2)_6$ at 25 ^oC was 7-fold more than this subpopulation in G5-$(oligo1)_6$ at 35 ^oC. Compared to the avidity distribution and the Poisson distribution of functionalized ligand on the nanoparticles of G5-$(oligo2)_6$, the threshold valence to initiate the multivalent interactions was extracted and left-shifted to about 7. (Fig. 4.5) The decrease of threshold valence suggests that the requirement of ligand density is not as critical as when using oligo1, even if the binding affinity is similar. We believe that the different dissociation rate constant, k_{off}, in fact led to the remarkably distinct avidity distribution between two ligands with comparable affinity. The 3-fold smaller k_{off} of the free oligo2 suggests that the timeframe within which oligo2 dissociates from the hybridizing complex would be more extended than that of oligo1 at 35^oC. While multiple oligo2s were functionalized on dendrimers, the bound oligo2 would potentially provide more time to allow

additional nanoparticle oligo2 to approach collateral receptors, forming alternative affinitive bonds. Therefore, it would be possible for nanoparticles with less ligand density to perform multivalent interactions, just as the highly functionalized nanoparticles did.

Table 4.1 Kinetic parameters of oligo1 determined by a SPR biosensor, at varied temperatures.

Temperature	**k_{on} ($M^{-1}s^{-1}$)**	**k_{off} (s^{-1})**	**K_D (M)**
15 ºC	$4.16x10^{4}$	$1.05x10^{-3}$	$4.68x10^{-8}$
20 ºC	$6.29x10^{4}$	$1.10x10^{-2}$	$1.76x10^{-7}$
25 ºC	$5.36x10^{4}$	$4.34x10^{-2}$	$8.11x10^{-7}$
30 ºC	$6.39x10^{4}$	$1.05x10^{-1}$	$2.86x10^{-6}$
35 ºC	$2.71x10^{4}$	$7.56x10^{-1}$	$2.79x10^{-5}$

Table 4.2 Avidity distribution and kinetic parameters of G5-(oligo1)$_6$, measured at varied temperatures.

Temperature	**%**	**k_{on} ($M^{-1}s^{-1}$)**	**k_{off} (s^{-1})**	**K_D (M)**
15 °C	94.7	$3.76x10^{4}$	$7.49x10^{-3}$	$1.99x10^{-7}$
	5.3	$2.51x10^{4}$	$9.13x10^{-4}$	$3.64x10^{-9}$
20 °C	91.3	$3.21x10^{4}$	$1.26x10^{-2}$	$3.94x10^{-7}$
	8.7	$3.49x10^{4}$	$1.91x10^{-4}$	$5.46x10^{-9}$
25 °C	90	$3.31x10^{4}$	$4.61x10^{-2}$	$1.39x10^{-6}$
	10	$3.10x10^{4}$	$3.37x10^{-4}$	$1.09x10^{-8}$
30 °C	90.6	$8.05x10^{3}$	$2.81x10^{-2}$	$3.48x10^{-6}$
	9.4	$4.77x10^{4}$	$8.12x10^{-4}$	$1.70x10^{-8}$
35 °C	93.8	$6.67x10^{3}$	$4.34x10^{-2}$	$3.48x10^{-6}$
	6.2	$9.96x10^{3}$	$1.64x10^{-4}$	$1.65x10^{-8}$

Table 4.3 Thermodynamic binding parameters of G5-(oligo1)$_6$.

Ligand	**ΔH (kcal mol^{-1})**	**ΔS (kcal mol^{-1}K^{-1})**
oligo2	-55.0	-0.157
Fast-dissociation G5-(oligo2)$_6$	-32.2	-0.081
Slow-dissociation G5-(oligo2)$_6$	N.A.	N.A.

Table 4.4 Rate constants (k_{on} and k_{off}) and dissociation constant (K_D) of free oligo2 and G5-(oligo2)$_6$ determined by SPR kinetic analysis.

Ligands	**k_{on} ($M^{-1}s^{-1}$)**	**k_{off} (s^{-1})**	**K_D (M)**
oligo2	$1.93x10^4$	$2.64x10^{-1}$	$1.4x10^{-5}$
Fast-dissociation G5-(oligo2)$_6$	$1.62x10^4$	$1.82x10^{-2}$	$1.13x10^{-6}$
Slow-dissociation G5-(oligo2)$_6$	$1.57x10^4$	$4.55x10^{-4}$	$2.9x10^{-8}$

The kinetic parameters of free oligo were determined by 1:1 Langmuir kinetic model.
The kinetic parameters of G5-(oligo2)$_6$ were determined by dual Langmuir kinetic model.
χ^2 of these regressions were less than 1.

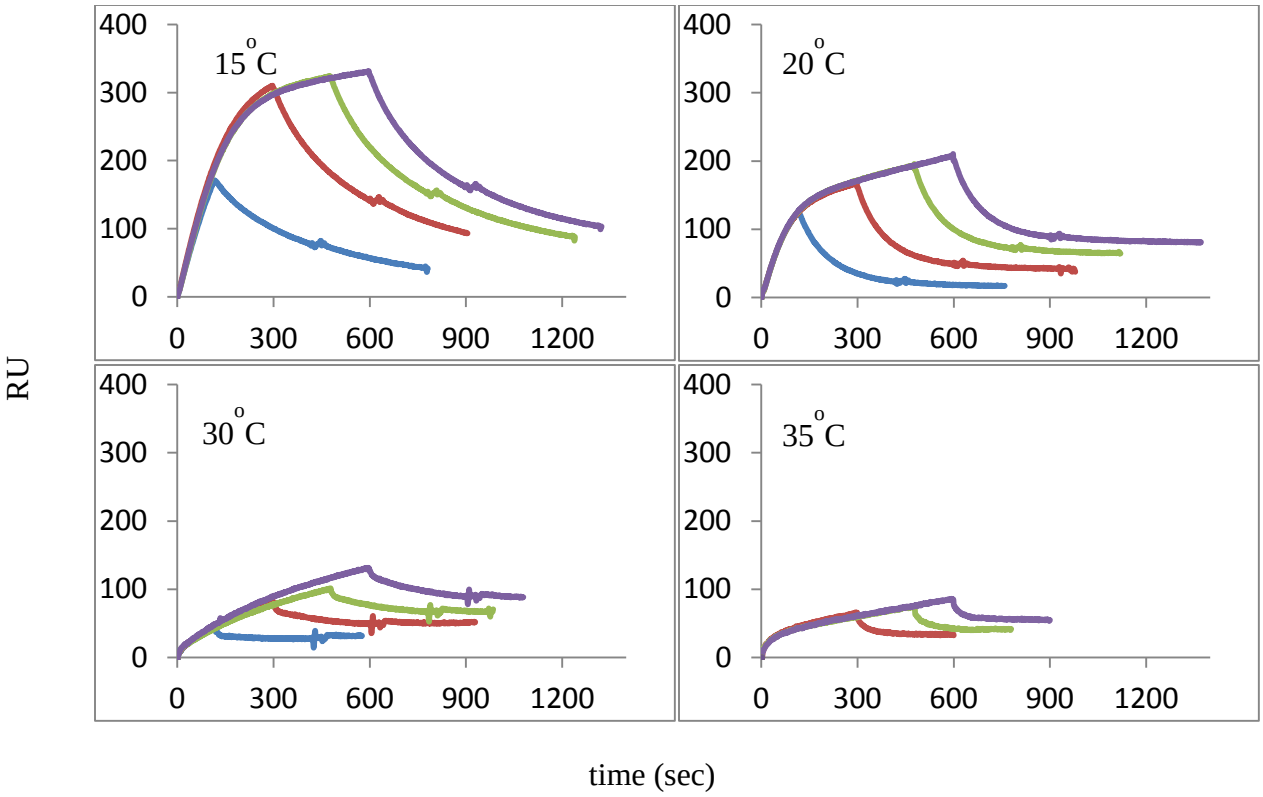

Fig. 4.1 SPR binding curves of G5-(oligo1)$_6$ with 62.5 nM at 15 ºC, 20 ºC, 30 ºC and 35 ºC. The durations of association include 2, 5, 8 and 10 minutes.

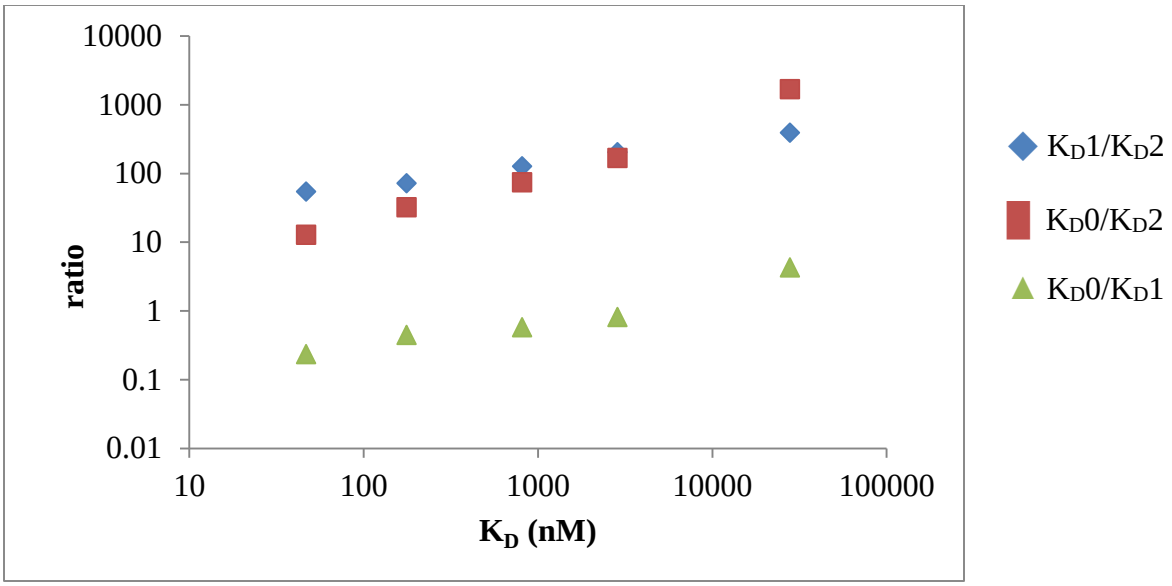

Fig. 4.2 Ratios of avidities of fast- and slow-dissociation nanoparticles in G5-$(oligo1)_6$ to affinities of oligo1. K_D0: the affinity of oligo1; K_D1: the avidity of fast-dissociation G5-$(oligo1)_6$; K_D2: the avidity of slow-dissociation G5-$(oligo1)_6$.

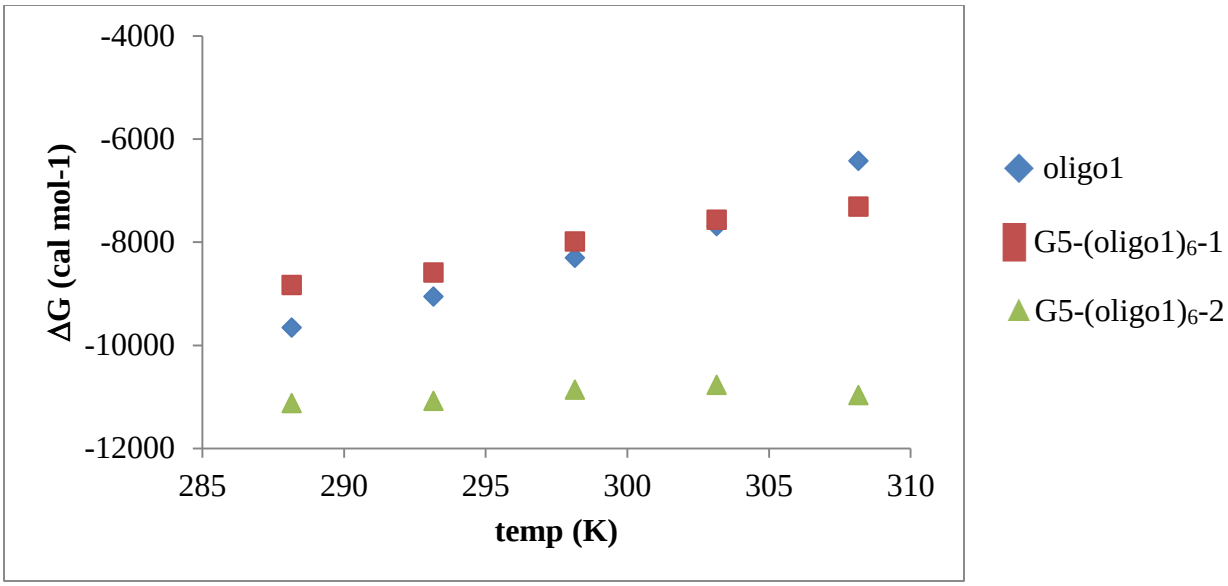

Fig. 4.3 The temperature dependence of Gibbs binding energies of fast- and slow-dissociation nanoparticles in G5-(oligo1)$_6$ and free oligo1. G5-(oligo1)$_6$-1 and G5-(oligo1)$_6$-2 represent fast- and slow-dissociation nanoparticles, respectively.

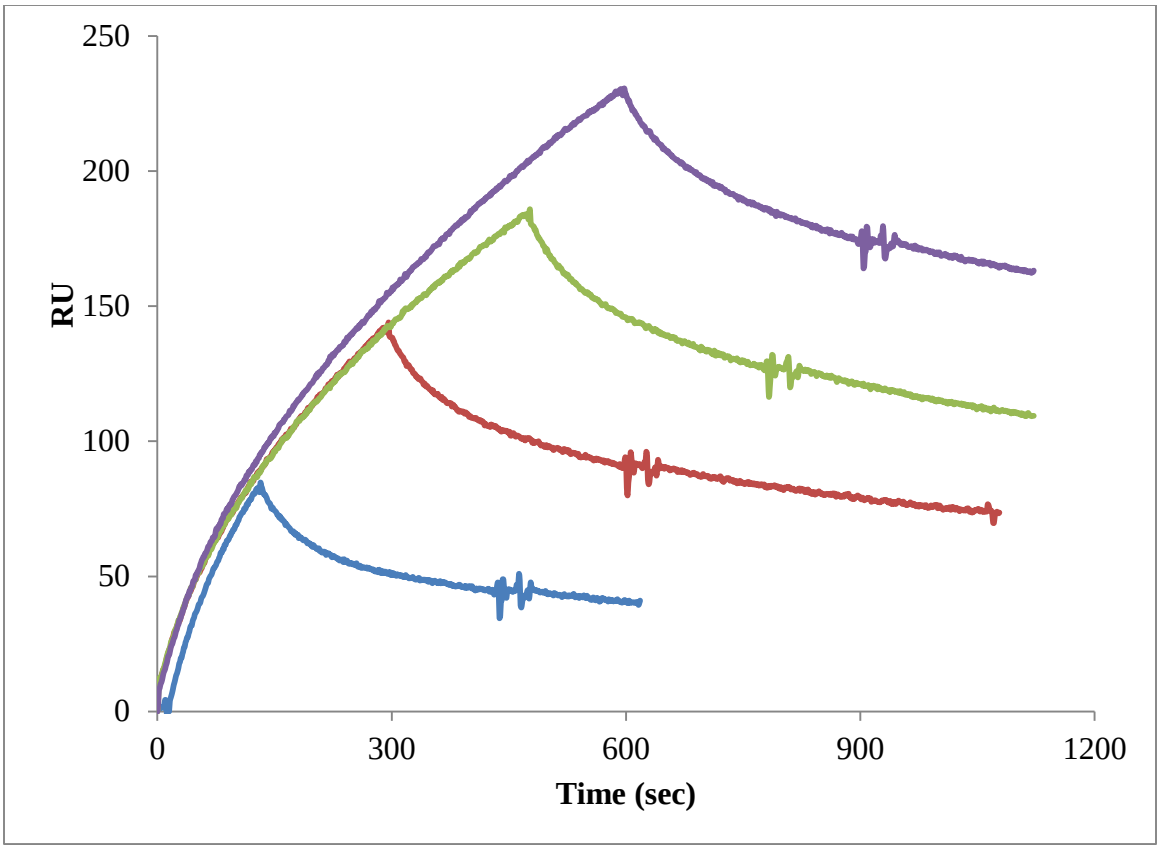

Fig. 4.4 SPR binding curves of G5-(oligo2)$_6$ with 62.5 nM at room temperature with durations of association at 2, 5, 8 and 10 minutes.

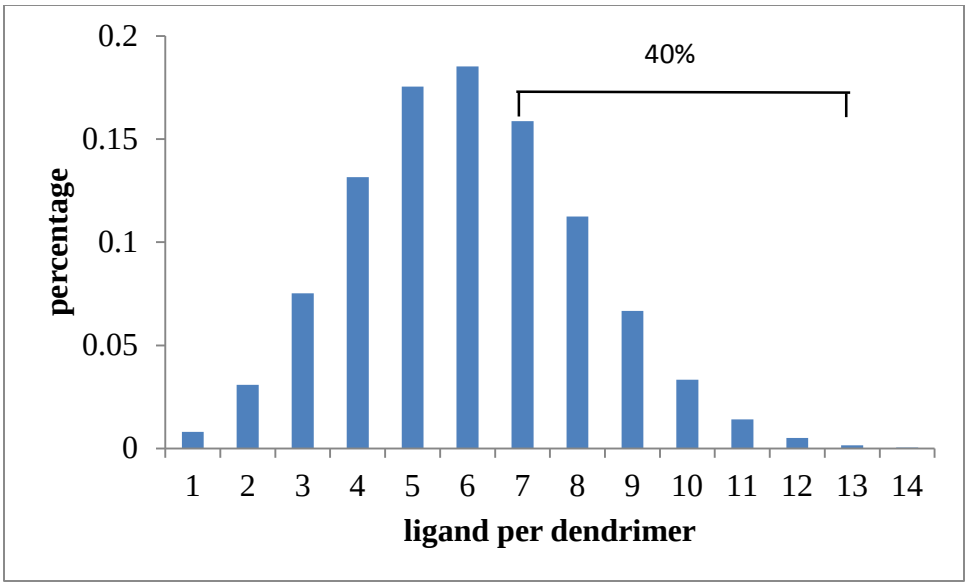

Fig. 4.5 Poisson simulation of ligand distribution on oligonucleotide-functionalized nanoparticles, G5-(oligo2)$_6$.

4.4 Supplementary data

S4.1 MALDI TOF MS spectrometry of G5-(oligo2)$_6$ (MW= 32300).

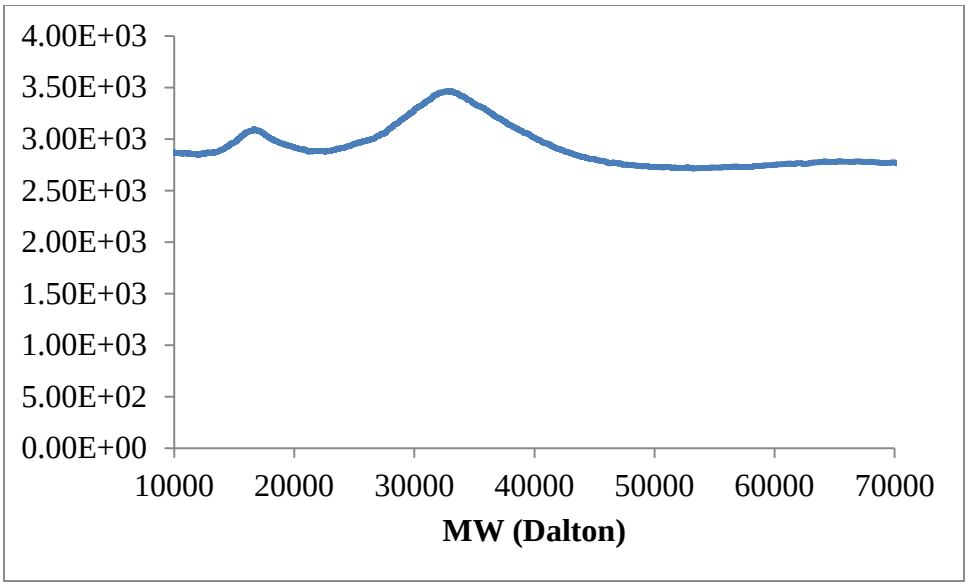

S4.2 UV-Vis spectra of G5-(oligo2)$_6$, measured at 0.1 mg/mL.

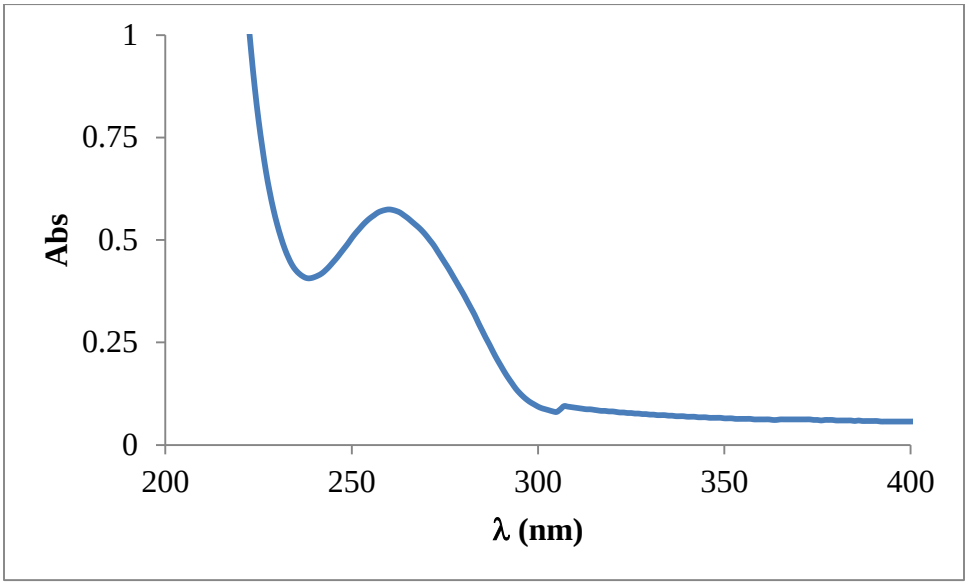

4.5 References

1. Mammen, M., Choi, S.K. & Whitesides, G.M. Polyvalent interactions in biological systems: Implications for design and use of multivalent ligands and inhibitors. *Angew Chem Int Edit* **37**, 2755-2794 (1998).

2. Kitov, P.I. & Bundle, D.R. On the nature of the multivalency effect: A thermodynamic model. *J Am Chem Soc* **125**, 16271-16284 (2003).

3. Krishnamurthy, V.M., Semetey, V., Bracher, P.J., Shen, N. & Whitesides, G.M. Dependence of effective molarity on linker length for an intramolecular protein-ligand system. *J Am Chem Soc* **129**, 1312-1320 (2007).

4. Kane, R.S. Thermodynamics of Multivalent Interactions: Influence of the Linker. *Langmuir* **26**, 8636-8640 (2010).

5. Dam, T.K., Roy, R., Das, S.K., Oscarson, S. & Brewer, C.F. Binding of multivalent carbohydrates to concanavalin A and Dioclea grandiflora lectin - Thermodynamic analysis of the "multivalency effect". *J Biol Chem* **275**, 14223-14230 (2000).

6. Dam, T.K., Roy, R., Page, D. & Brewer, C.F. Thermodynamic binding parameters of individual epitopes of multivalent carbohydrates to concanavalin a as determined by "reverse" isothermal titration microcalorimetry. *Biochemistry-Us* **41**, 1359-1363 (2002).

7. Hong, S., *et al.* The binding avidity of a nanoparticle-based multivalent targeted drug delivery platform. *Chem Biol* **14**, 107-115 (2007).

8. Tassa, C., *et al.* Binding affinity and kinetic analysis of targeted small molecule-modified nanoparticles. *Bioconjug Chem* **21**, 14-19 (2010).

9. Choi, S.K., *et al.* Dendrimer-based multivalent vancomycin nanoplatform for targeting the drug-resistant bacterial surface. *ACS Nano* **7**, 214-228 (2013).

10. Piggott, A.M. & Karuso, P. Quality, not quantity: The role of natural products and chemical proteomics in modern drug discovery. *Comb Chem High T Scr* **7**, 607-630 (2004).

11. Rashid, A., *et al.* Review: Diagnostic and therapeutic applications of rat basophilic leukemia cells. *Mol Immunol* **52**, 224-228 (2012).

12. Woller, E.K., Walter, E.D., Morgan, J.R., Singel, D.J. & Cloninger, M.J. Altering the strength of lectin binding interactions and controlling the amount of lectin clustering using mannose/hydroxyl-functionalized dendrimers. *J Am Chem Soc* **125**, 8820-8826 (2003).

13. Wolfenden, M.L. & Cloninger, M.J. Carbohydrate-functionalized dendrimers to investigate the predictable tunability of multivalent interactions. *Bioconjugate Chem* **17**, 958-966 (2006).

14. Navratilova, I., *et al.* Thermodynamic benchmark study using Biacore technology. *Anal Biochem* **364**, 67-77 (2007).

15. Mullen, D.G., *et al.* A Quantitative Assessment of Nanoparticle-Ligand Distributions: Implications for Targeted Drug and Imaging Delivery in Dendrimer Conjugates. *ACS Nano* **4**, 657-670 (2010).

16. Lendvay, G. On the correlation of bond order and bond length. *J Mol Struc-Theochem* **501**, 389-393 (2000).

17. Persson, B., *et al.* Analysis of oligonucleotide probe affinities using surface plasmon resonance: A means for mutational scanning. *Anal Biochem* **246**, 34-44 (1997).

CHAPTER 5

DEVELOPING HIGH-AVIDITY MULTIVALENT NANOPARTICLES WITH UNIFORM AVIDITY DISTRIBUTION

5.1 Introduction

Over several decades, many attempts have been made to develop synthetic multivalent nanoparticles as targeted delivery systems.[1-6] These efforts were based, in some part, on the presumption that using multiple targeting ligands to achieve an avidity interaction with target cells could enhance the binding of drug- carrying nanoparticles. This type of avidity interaction, which is responsible for events such as virus binding to cells, underlies many important processes in biology.[7] However, it became clear that only multivalent nanoparticles with certain specific factors, involving the valence and type/orientation of linkers, could generate a significant avidity enhancement.[8-10] Even when a multivalent effect is achieved, the improvements in avidity observed with synthetic nanoparticles are often substantially lower than the million-fold improvements in binding observed in natural systems.[11-15] The gap between the avidity in synthetic multivalent systems and that in natural interactions suggests there are design characteristics that must be determined to enhance nanoparticle systems for drug delivery.

Our results described in preceding chapters suggest there is a threshold valence that determines the occurrence of a multivalent effect. When the valence number is below this threshold, the nanoparticles cannot cause a multivalent interaction to occur. Additionally, nanoparticles with these low numbers of ligands could result in the creation of a weak-

binding subpopulation presented by multivalent nanoparticles. Conversely, this implies that, once all particles in a distribution have a valence that surpasses the threshold required for multivalency, the resulting population of nanoparticles should demonstrate uniformly strong binding avidity. Therefore, we hypothesize that uniformly high populations of multivalent-binding nanoparticles could be synthesized by increasing the average number of functionalized ligands to a number that ensures the entire population has high enough numbers of ligands to exceed the threshold valence required for avidity interactions, as illustrated in Figure 4.5.

This has been a synthesis that is difficult to accomplish with traditional coupling chemistry. Therefore, we needed to take advantage of newer chemistry approaches that can generate more efficient ligand conjugation. Click chemistry is a promising approach to improving the efficiency of ligand conjugation.[16,17] The term "click chemistry" generally describes conjugation chemistries with a variety of advantages, such as high reaction yield, low byproducts, stable ligation, and simple reaction conditions.[18] Initially, Cu (I)-catalyzed alkyne azide 1.3-dipolar cycloaddition (CuAAC) was the most widely used form of click chemistry, but there are already numerous successful examples of unique conjugation methods to functionalize ligands onto surfaces, such as of gold, silica, magnetic metal oxide, and polymer nanoparticles. [19-22]

Click chemistry has been extensively employed in the conjugation of ligands to dendritic polymers. Using CuAAC, small organic molecules, including chemotherapeutics, fluorescent dyes, nucleoside antagonists, and targeting ligands, were coupled to monofunctional or multifunctional dendrimer-based nanoparticles.[23-26] Larger molecules, oligomer-peptides, and PEG have also been effectively clicked to dendrimers.[27,28] However,

the copper catalyst can be retained in the polymer core and cause cytotoxicity in subsequent biological studies.[29] Fortunately, this concern can be resolved by using copper-free click chemistry that employs a cyclo-addition involving a selective reaction between the cyclooctyne and azide groups.[30,31] (Fig 5.1) Huang et. al. from our laboratory employed copper-free, strain-promoted alkyne-azide cycloaddition (SPAAC) chemistry to enhance the valence of dual-functional methotrexate (MTX)-functionalized PAMAM dendrimers. These clicked nanoparticles have consistently high numbers of attached MTX, which could not be accomplished by typical amide or ester couplings. In addition, these dendrimers also retained high water solubility, which is important for subsequent biological studies.

In the current studies, we employ the copper-free SPAAC conjugation method to enhance the number and consistency of oligonucleotides conjugated to PAMAM dendrimers. We first prepared G5 PAMAM dendrimers that were functionalized with multiple cyclooctyne linkers. Then, azide-oligonucleotides were synthesized, purified, and recovered. These molecules were then coupled to the dendrimer using the click process. The binding activity of the resulting population of multivalent nanoparticles was then examined using an SPR biosensor with kinetic parameters and avidity distribution being analyzed. Our results indicated that the copper-free click chemistry accomplished a nearly complete conjugation reaction and attached, on average, 13 oligonucleotides onto each dendrimer. The kinetic analyses demonstrated the degree to which a consistently high valence promotes multivalent interactions, illustrated by a 50,000-fold avidity enhancement and uniform avidity distribution.

5.2 Experimental Methods

Chemicals and materials: Single-stranded DNA oligonucleotides (ssDNA oligos) were synthesized with 5'-end modifications and purified with a standard desalting process at Integrated DNA Technologies (Coralville, IA), including an 8-mer amino-terminated oligo, 5'-NH_2-C_6-TGCTGAGG, an azido-8-mer oligo, and a 25-mer biotinylated oligo, 5'-biotin-TTTCTTCAGCATCTTATCCGAGTTTT. Generation 5 poly(amidoamine) (G5 PAMAM) dendrimers were purchased from Dendritech Inc. (Midland, MI) and purified as described in the Synthesis section. All organic solvents and reagents were purchased from Sigma Aldrich (St. Louis, MO) and used without further purification or modification. Phosphate buffer saline (PBS) without calcium and magnesium was purchased from Thermo Scientific (Logan, UT). 10K molecular cutoff (MWCO) centrifugal filters (Amicon Ultra-4) were purchased from Millipore (Billerica, MA). 10K MWCO dialysis membrane was purchased from Spectrum Laboratories (Rancho Dominquez, CA). Sensor chips SA and HBS-EP (pH 7.4) buffer were purchased from GE Healthcare (Piscataway, NJ).

Synthesis of azido-ssDNA oligonucleotide conjugates: 5-azidopentonoic acid (110 mg, 769 μmole) was dissolved in 2 mL DMSO and reacted with N-N'-dicyclohexylcarbodiimide (DCC) (206 mg, 1 mmole) and NHS (115 mg, 1 mmole) pre-dissolved in 0.5 mL in DMSO for 4 hours at room temperature. The mixture of the reaction solution was then filtered to remove any undissolved solid. The clear filtrate was collected and reacted with the amino-8-mer oligo (13 mg, 5 μmole) pre-dissolved in 800 μL pH 9 buffer (0.2 M $NaHCO_3$) for 16 hours at room temperature.

Purification of azido-ssDNA oligonucleotide conjugates: The azido-oligo conjugate was purified by RP-HPLC on a Waters Delta 600 HPLC system with a photodiode array detector. The reaction mixture was injected into a C18 silica-based Waters Atlantis T3 column (250 x 4.6 mm) with a gradient of acetonitrile in ammonium acetate (5 to 50% buffer B over 32 minutes, flow rate 1 mL/minute) in which buffer A was 0.1 M ammonium acetate at pH 7 and buffer B was 0.1 M ammonium acetate at pH 7, with 50% acetonitrile. Elution was monitored by UV absorption at 260 nm. After HPLC purification, the conjugate was desalted using a MidiTrap Sephadex G10 column (GE healthcare) and lyophilized for 3 days.

Synthesis of cyclooctyne-functionalized G5 PAMAM dendrimers: Partially acetylated G5 PAMAM dendrimer was synthesized according to the literature. Briefly, G5-NH_2 (233.0 mg, 8.85 μmole) and triethylamine (76.0 mg, 752 μmole) were dissolved in anhydrous MeOH (50 mL). The solution was kept in an ice-water batch for 0.5 hours. Acetic anhydride (76.8 mg, 752 μmole) in Methanol (50 ml) was added slowly (2-hour expansion). The mixture was further stirred at room temperature for 16 hours. Organic solvents were removed by rotary evaporation and the residue was re-dissolved in water. The sample was purified using 10,000 MWCO centrifugal filtration devices. Purification consisted of ten cycles (20 minutes at 4800 rpm) using PBS (5 cycles) and DI water (5 cycles). The purified dendrimer samples were lyophilized to yield as white solids (245 mg, 89%). The ^{1}H NMR integration determined that the mean number of acetyl groups per dendrimer was 80.1.

Partially acetylated G5 dendrimer G5-NHAc-NH_2 (125.0 mg, 4.2 μmole) and *N*,*N*-Diisopropylethylamine (DIPEA) (16.2 mg, 126 μmole) were dissolved in anhydrous DMSO (0.5 mL). Cyclooctyne-NHS (23.9 mg, 62.8 μmole) purchased from Berry & Associates (Dexter, MI) in DMSO (0.5 mL) was added slowly with stirring. The mixture was then

stirred at room temperature for 24 hours. The sample was purified using 10,000 MWCO centrifugal filtration devices. Purification consisted of ten cycles (20 minutes at 4800 rpm) using PBS (5 cycles) and DI water (5 cycles). The purified dendrimer samples were lyophilized to yield as white solids (121 mg, 85%). The number of cyclooctynes on the dendrimers was determined with ^{1}H NMR spectra measured on a 500 MHz Varian vnmrs NMR system equipped with a multinuclear 5-mm probe. ^{1}H chemical shifts are reported in parts per million from TMS.

Synthesis of oligonucleotide-clicked G5 PAMAM dendrimers: The cyclooctyne-functionalized dendrimer (2.7 mg. 0.075 μmole) dissolved in DIW (0.5 mL) was reacted with azido oligonucleotides (3.5 mg, 1.25 μmole) synthesized as described above for 16 hours at room temperature. The mixture of the reaction solution was purified using 10K MWCO centrifugal filters in PBS and DIW for 4 cycles each. The recovered dendrimer-ssDNA conjugates were lyophilized for 3 days to yield a white solid (5.54 mg) with yield ~ 80%.

Characterization of oligonucleotide-clicked G5 PAMAM dendrimers: The molecular weight of G5 PAMAM dendrimer-based ssDNA oligo nanoparticles was determined by MALDI-TOF MS using a Micromass TofSpec-2E with positive ion mode as previously described. The number of attached ssDNA oligos was determined by UV-Vis spectra, which were conducted in a 1-mL quartz cuvette, using a Perkin Elmer Lamda 20 spectrophotometer. The equivalent concentration of ssDNA was calibrated using OD_{260} of the specific DNA sequence. The mean number of conjugated ssDNA oligos per G5 PAMAM dendrimer was determined by using the quotient of an equivalent concentration of ssDNA that the oligonucleotide-functionalized dendrimer presented and the concentration of the

nanoparticles that was calculated based on the MS-determined molecular weight of the functionalized nanoparticles.

SPR measurements and kinetic analysis: The kinetic analysis was conducted using a BIAcore X (Pharmacia Biosensor AB, Uppsala, Sweden) equipped with a sensor chip SA, which was pre-coated with streptavidin on the surface, for the capture of biotinylated ssDNA oligos. Before the immobilization process, the SA surface was pre-conditioned with exposure to three 1-minute injections containing 50 mM NaOH. The 25-mer biotinylated ssDNA oligo solution (1 mg/mL) in HBS-EP buffer was then injected only into flow channel 1 for 10 minutes, resulting in 1300 RU (1.3 ng/mm^2) of immobilized ssDNA oligos. After the capturing process, a 1-minute injection of 10 mM NaOH was used to reduce the non-specific binding that occurred during prior injections.

During SPR measurement, the 8-mer ssDNA oligo and the oligo-functionalized dendrimer dissolved in HBS-EP buffer were injected into both flow channels of the sensor chip, including the ssDNA oligo-immobilized channel described above and another channel without immobilization of the oligonucleotides as the reference channel, at a flow rate of 10 μL/min. After each measurement, the chip surface was regenerated using 5 μL injections of pH 2 HCl-glycine buffer or 5-10 μL pH 11 NaOH for the sample of 8-mer ssDNA oligos or the G5 ssDNA oligo-functionalized nanoparticles, respectively, to ensure complete removal of bound molecules before the next measurement. The final SPR sensograms were obtained by using the measurement after subtraction of the signal on the reference channel from the signal on the oligo-immobilized channel. After this process of referencing, the kinetic parameters, including the k_{on}, k_{off} and K_D, of the free ssDNA oligo, were determined using the Langmuir 1:1 kinetic model with default setting in BIAevaluation software.

Poissonian statistical simulation: The statistical model assumed that ligand conjugation with the nanoparticles obeys the Poissonian stochastic mechanism.[32] In this Poisson simulation, the total number of available attached sites on the dendrimer surface and the mean ligand number per dendrimer characterized with UV-Vis and MALDI-MS were used as factors to calculate the distribution. With this method, the ligand distribution was plotted, and the percentage of nanoparticles with specific valences was identified.

5.3 Results and Discussion

Synthesis and characterization of azido-ssDNA oligonucleotide conjugates: After the DCC-catalyzed conjugation, the reaction mixture was purified using C18 RP-HPLC. Given the increasing hydrophobicity of the conjugate, due to the attached azide-segment, we were able to completely resolve the conjugated from the non-conjugated ssDNA oligo, as the two molecules showed a difference of 28 minutes in retention time. (Fig. 5.1) After appropriate fractions were collected, the conjugate composed of an azide functional group, an 8-mer ssDNA oligonucleotide and a C_{11} intermediate linker was recovered. Comparing this to the chromatograph of a commercial azido oligonucleotide with similar structure (except for an extra carbon atom in the linker), the retention time was nearly identical, suggesting a comparable structure with complete conjugation of the azido linker. Subsequently, the synthesized conjugates were desalted using Sephadex G-10, and this process yielded a 60% recovery of the oligo conjugate.

Synthesis and characterization of cyclooctyne-functionalized G5 PAMAM dendrimers: The synthesis of cyclooctyne-functionalized G5 PAMAM dendrimer (G5-Oct)

is shown in Fig 5.2. In brief, G5-$(NH)_2$ was partially acetylated with acetic anhydride to neutralize 75% of the surface primary amines. This step reduced undesired electrostatic interactions in subsequent assays and also enhanced the solubility of the dendrimer in organic solvent. The partially acetylated G5 PAMAM dendrimer was coupled with a 15-molar equivalence of cyclooctyne-NHS ester linker in DMSO in the presence of DIEPA. The average number of conjugated cyclooctynes was determined by ^{1}H NMR using a method developed by our laboratory. By referencing the internal standard peak representing acetamide (1.84 ppm), the alkyl proton signal (3.10 and 3.41 ppm) in the cyclooctyne linker was used to determine the number of cyclooctynes. (Fig. 5. 3) This analysis showed that the coupling reaction resulted in a mean of 13 conjugated cyclooctynes per dendrimer. The G5-Oct_{13} left sufficient active sites for further ligand coupling reactions and also retained high water solubility, which was crucial to the conjugation process with oligonucleotides.

Synthesis and characterization of oligonucleotide-clicked G5 PAMAM dendrimers: The non-copper click chemistry process was conducted in DIW, without pH adjustment, metal catalyst, heating or cooling. After 10K MWCO ultrafiltration, 80% of the oligo-functionalized G5 dendrimer was recovered. Based on MW and the concentration of oligo, as determined by MALDI MS and UV-Vis, the mean oligo per G5 dendrimer was 13. Given the molar ratios of the reactants, this suggested that all of the oligos were clicked to the dendrimer, indicating the efficiency of the click chemistry conjugation. Moreover, despite having 13 attached ligands via a hydrophobic linker, the functionalized G5 PAMAM dendrimer still maintained superior water solubility. This was demonstrated by the lyophilized solid dendrimer's ability to be rapidly dissolved in water, preparing a concentrated aqueous stock at 10 mg/mL.

Fortunately, from these results we were successful using the approach of high-reaction yield click chemistry to achieve our goal of creating high-valency, ligand-functionalized nanoparticles. Additionally, there are two major reasons that lead us to select the use of copper-free click chemistry over copper-catalyzed protocols. First, using copper-free click chemistry can resolve the concern of cytotoxicity that is caused by residual copper ions retained in the polymer conjugate.[29] Second, this type of chemistry holds no possibility of nucleic acid hydrolysis and crosslinking of oligonucleotides due to multivalent ions.[33] Thus, this synthesis should be most likely to yield active, conjugated oligos with sufficient valence on the dendrimer to achieve a multivalent effect.

Evaluation of binding avidity of oligonucleotide-clicked G5 PAMAM dendrimers: In the binding curves of G5-Oct-$(oligo)_{13}$, we can clearly observe a variety of features that revealed marked improvements in avidity with this particular functionalized nanoparticle. (Fig. 5.4) The features of this binding include: 1) a straight association curve that showed a continuous increase without decrease in the apparent binding rate, even after 10 minutes of injection, 2) the bound nanoparticles rarely dissociated from the surface, even after a high-speed flush and 5 minutes of dissociation, and 3) the SPR binding signal can be detected, even with sub-nM sample concentrations. None of these characteristics were observed in the binding measurement of synthetic multivalent nanoparticles made with traditional conjugation chemistry and suggest unusual strong binding avidity for the G5-Oct-$(oligo)_{13}$ nanoparticles.

Based on 1:1 Langmuir kinetic analysis, the binding parameters of the G5-Oct-$(oligo)_{13}$ nanoparticles were determined and are listed in Table 5.1. These kinetic parameters provide quantitative support for the extraordinary strength of the binding activity apparent

from our observations. The pM-level K_D identified in these calculations is the strongest binding avidity we believe has been reported for synthetic multivalent nanoparticles.[14,15,34] Based on our survey containing a variety of ligand-functionalized nanoparticles with the number of ligands as high as 20 per particle, the strongest avidity reached just 0.25 nM. The only exception was a dendrimer coupled with 5 cell adhesion molecules (CAMs) that on average showed 0.58 pM in avidity.[35] However, examining the SPR sensograms of this engineered dendrimer, we found that in order to obtain a comparable measured response unit as G5-Oct-$(oligo)_{13}$, it is necessary to increase the concentration by 20-fold, suggesting that the G5-Oct-$(oligo)_{13}$ in fact performed a stronger binding. Additionally, the results of the binding sensograms of the CAM-functionalized dendrimers repeatedly showed spikes in the fitted curves in the beginning of dissociation. This feature suggests that these fitted curves did not match the experimental data well and may overlook the dissociation during this duration, thus leading to overestimating the strength of the binding avidity.

While our studies are unique, the use of highly valent nanoparticles to enhance binding avidity is not a new concept. Researchers have functionalized hundreds of ligands onto nanoparticles in an attempt to generate an increase in the targeting potential for nanoparticle systems. For example, PAMAM dendrimers functionalized with 10 folates or hundreds of carbohydrates were synthesized to target their folate receptors and lectins, respectively. However, the avidities of these highly-functionalized dendrimers were not as high as expected.[35] We believe that the superior binding avidity enhancement of G5-Oct-$(oligo)_{13}$ over these other systems may result from the following factors: 1) G5-Oct-$(oligo)_{13}$ nanoparticles have sufficient long linkers (~20 atoms) to extend the hydrophilic oligos beyond the surface of the molecule into the liquid phase, which prevents the oligos from

attaching to or being embedded into the dendrimer surface, and 2) oligos are negatively-charged molecules that would demonstrate repulsive forces against each other, preventing undesired ligand-ligand or nanoparticle-nanoparticle aggregation.[36-38] The above features ensure that the functionalized oligos on dendrimers are freely available and therefore almost all of the surface bound ligands can effectively interact with complimentary molecules. In our specific example, there would be an average of 13, 8-mer oligos on dendrimers that can effectively hybridize with 25-mer oligos on the SPR surface. In contrast, those carbohydrate- or folate-functionalized dendrimers either lack proper linkers or tend to form aggregations due to the hydrophobicity of the ligand.[30,39] Therefore, increases in the numerical valence did not improve the multivalent effects.

A Correlation of ligand distribution with the binding avidity of oligonucleotide-clicked G5 PAMAM dendrimers: G5-Oct-$(oligo)_{13}$ still contains a heterogeneous population of oligonucleotide functionalized dendrimers even though the click-chemistry conjugation was highly efficient. This distribution resulted from the initial step of the click chemistry, the amide-bond conjugation of the cyclooctynes to the dendrimer surface. Based on a Poissonian simulation, the ligand distribution of G5-Oct_{13} can be assessed and plotted as in Fig. 5.5. This Poisson distribution suggests that more than 99% of the dendrimers bear 7 to 21 oligos. Unlike prior work with dendrimers functionalized with traditional conjugation chemistry (which demonstrated heterogeneous binding), G5-Oct-$(oligo)_{13}$ showed a continuous, linear increase in association with the complementary oligo-covered SPR surface. This suggests that multivalent interactions occurred in the entire population of nanoparticles in this system. This implies that the entire population of dendrimers existing in G5-Oct-$(oligo)_{13}$ surpassed the threshold valence required for multivalent interaction. Therefore,

referring to the Poissonian ligand distribution of G5-Oct-$(oligo)_{13}$, the threshold valence would be equal to the minimal valence of dendrimer in the population, which is about 6 to 7.

Interestingly, we also found that the threshold valences for G5-$(oligo)_6$ and G5-Oct-$(oligo)_{13}$ are not identical. The threshold valence of G5-Oct-$(oligo)_{13}$ is lower than the value determined from studies with G5-$(oligo)_6$. We believe that this lower threshold valence suggests that the longer linkers in G5-Oct-$(oligo)_{13}$ may also promote more efficient multivalent effects. The 500-fold avidity enhancement in G5-Oct-$(oligo)_{13}$ also may support an important role of linker length in promoting multivalent effects. This phenomenon has been reported in an oligo-nanogold system, where a 20-mer-oligonucleotide linker significantly promotes stronger binding avidity to the nanoparticles than did the 10-mer-oligonucleotide linker, despite a similar-length complementary sequence.[36]

Table 5.1 Kinetic parameters of G5-Oct-$(oligo)_{13}$, determined by 1:1 Langmuir kinetic analysis using a SPR biosensor.

Ligands	**k_{on} ($M^{-1}s^{-1}$)**	**k_{off} (s^{-1})**	**K_D (M)**
oligo	$5.36x10^{4}$	$4.34x10^{-2}$	$8.11x10^{-7}$
G5-Oct-$(oligo)_{13}$	$1.43x10^{4}$	$1.93x10^{-9}$	$1.35x10^{-11}$

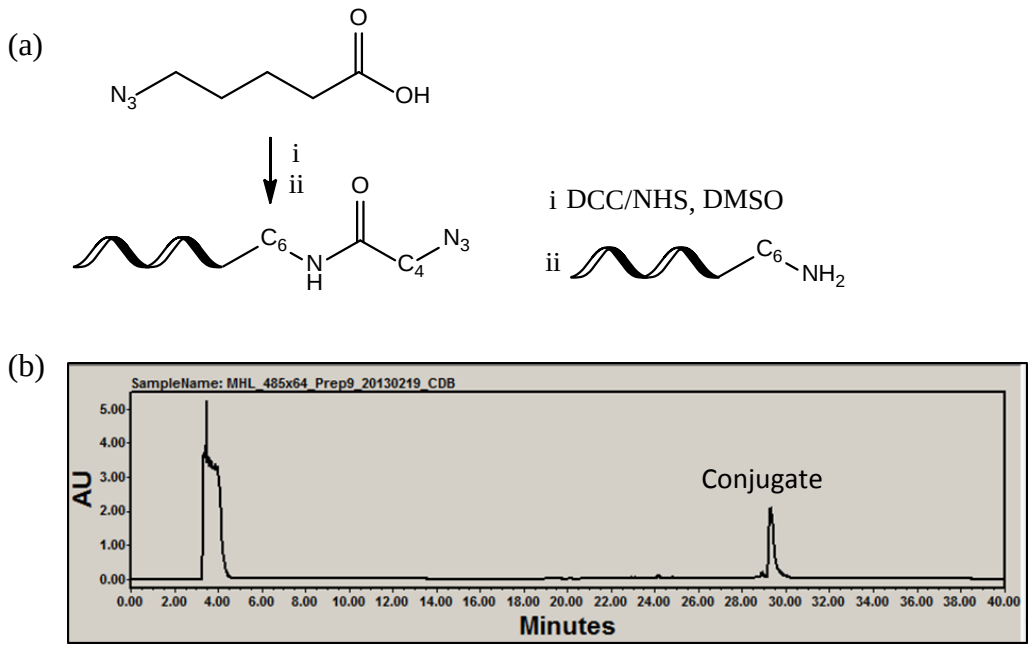

Fig. 5.1 The synthesis and purification of the azido-oligonulceotide conjugate.

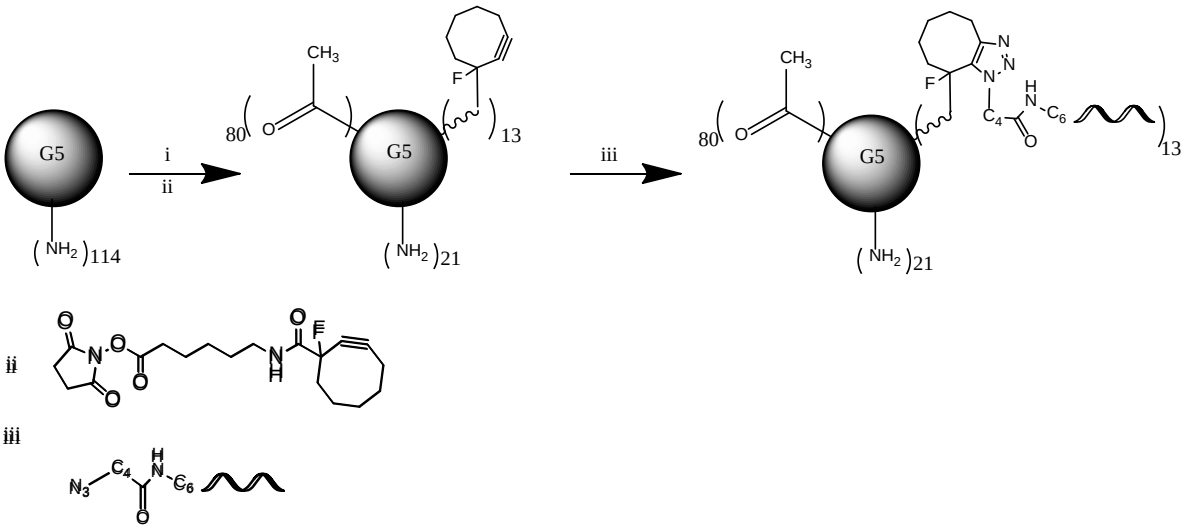

Fig. 5.2 The synthesis of G5-Oct-(oligo)$_{13}$: (i) acetic anhydride, triethylamine; (ii) cyclooctyne-NHS, DIPEA, DMSO; (iii) azido-oligonucleotide, pH 9 carbonate buffer.

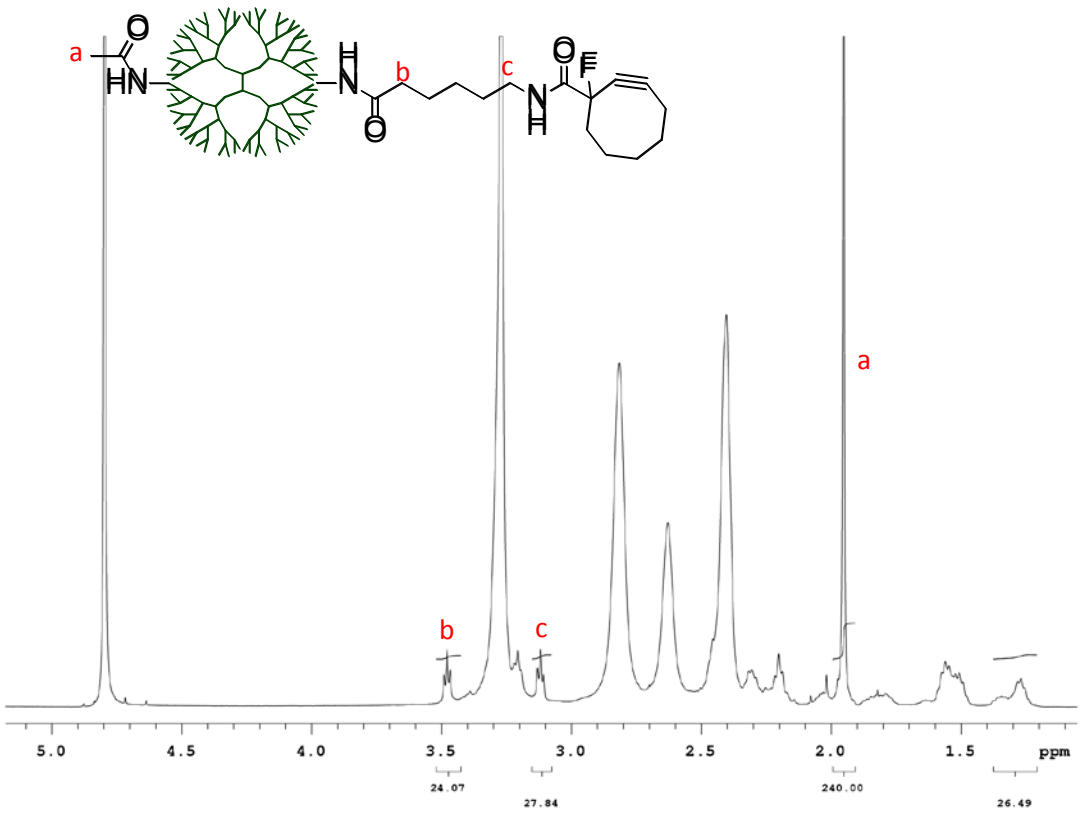

Fig. 5.3 ^{1}H NMR spectrum of G5-Oct$_{13}$. (a) δ=1.84 ppm; (b) δ=3.42 ppm; (c) δ=3.10 ppm.

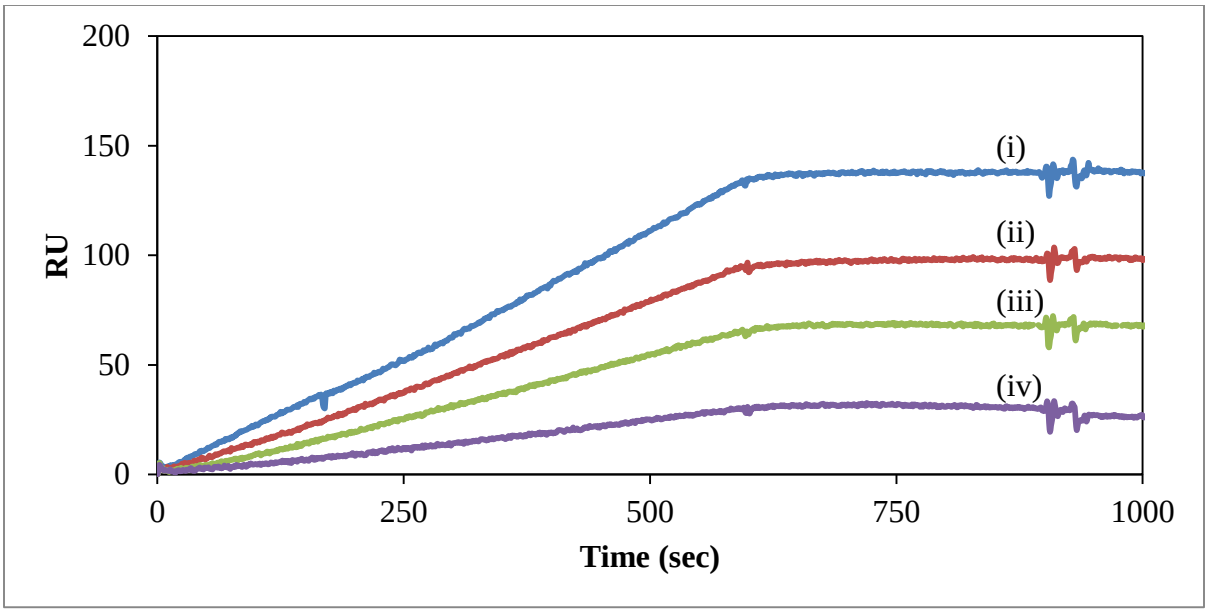

Fig. 5.4 SPR sensograms of G5-Oct-$(oligo)_{13}$. (i) 1 nM; (ii) 500 pM; (iii) 250 pM; (iv) 125 pM.

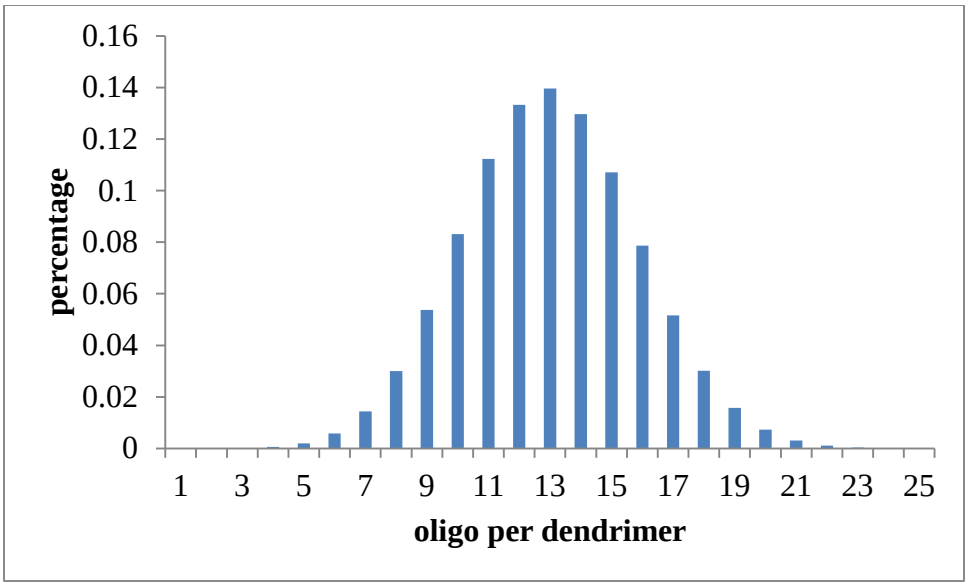

Fig. 5.5 Poisson simulation of ligand distribution on oligonucleotide-functionalized nanoparticles, G5-Oct-$(oligo)_{13}$.

5.4 Supplementary data

S5.1 HPLC chromatograph of the commercial azido-oligonucleotide conjugate.

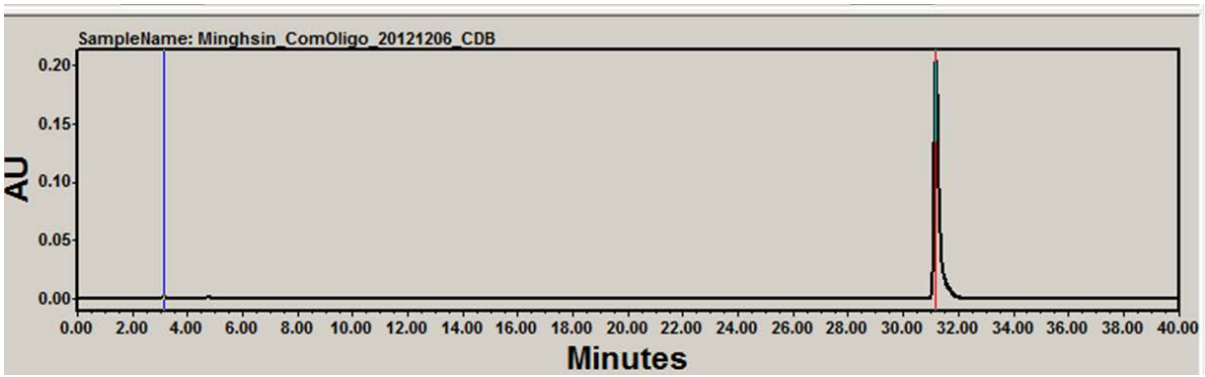

S5.2 SEC desalting process with 100 uL azido-oligonucleotide conjugate at 1 mg/mL.

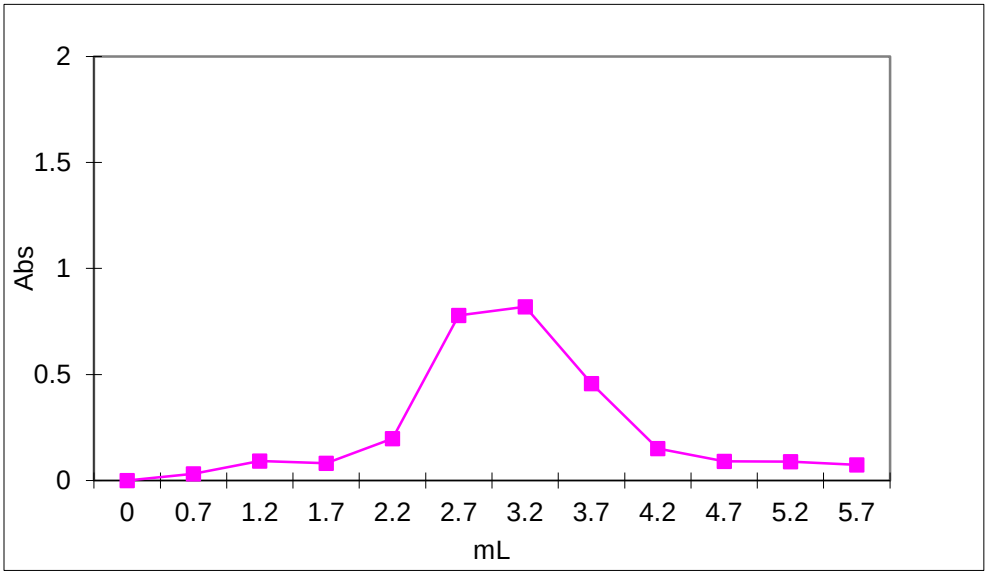

S5.3 MALDI TOF MS spectrometry of (a) G5-Oct-(oligo)$_{13}$ (MW= 49900).

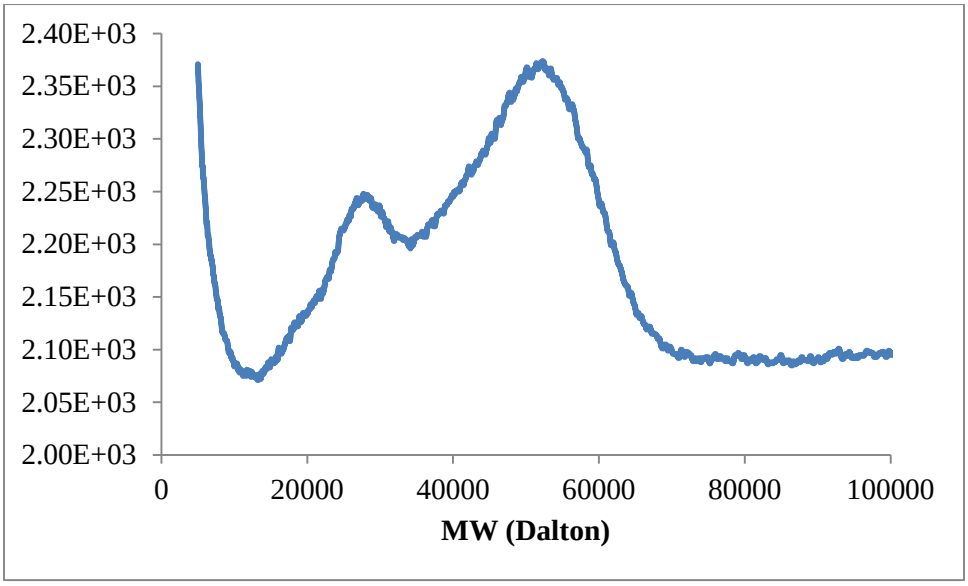

S5.4 UV-Vis spectrum of G5-Oct-(oligo)$_{13}$.

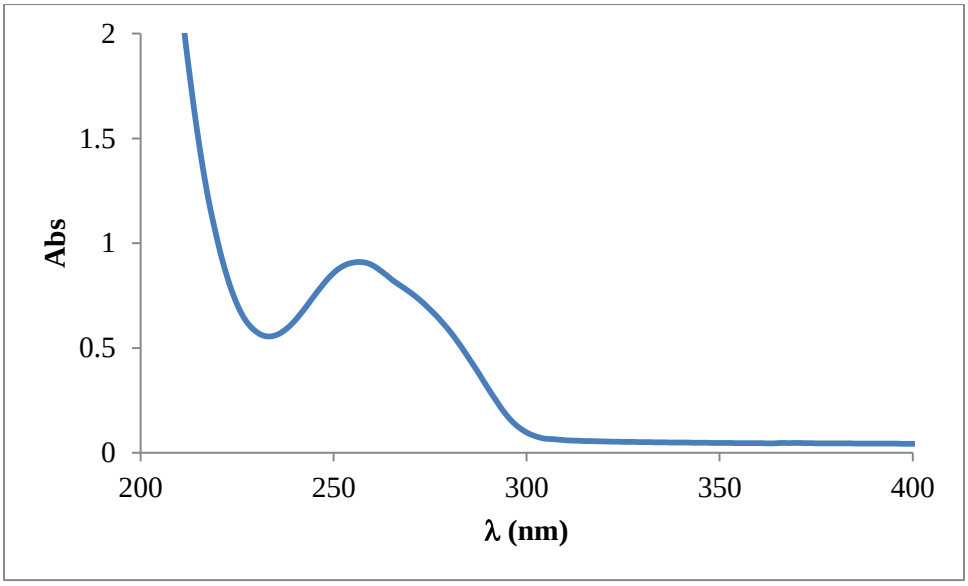

5.5 References

1. Brannon-Peppas, L. & Blanchette, J.O. Nanoparticle and targeted systems for cancer therapy. *Adv Drug Deliv Rev* **56**, 1649-1659 (2004).

2. Peer, D., *et al.* Nanocarriers as an emerging platform for cancer therapy. *Nat Nanotechnol* **2**, 751-760 (2007).

3. Debbage, P. Targeted drugs and nanomedicine: present and future. *Curr Pharm Des* **15**, 153-172 (2009).

4. Yu, M.K., Park, J. & Jon, S. Targeting Strategies for Multifunctional Nanoparticles in Cancer Imaging and Therapy. *Theranostics* **2**, 3-44 (2012).

5. Zhang, X.Q., *et al.* Interactions of nanomaterials and biological systems: Implications to personalized nanomedicine. *Adv Drug Deliv Rev* **64**, 1363-1384 (2012).

6. Rizzo, L.Y., Theek, B., Storm, G., Kiessling, F. & Lammers, T. Recent progress in nanomedicine: therapeutic, diagnostic and theranostic applications. *Curr Opin Biotechnol* (2013).

7. Mammen, M., Choi, S.K. & Whitesides, G.M. Polyvalent interactions in biological systems: Implications for design and use of multivalent ligands and inhibitors. *Angew Chem Int Edit* **37**, 2755-2794 (1998).

8. Duncan, R. Polymer conjugates as anticancer nanomedicines. *Nature Reviews Cancer* **6**, 688-701 (2006).

9. Kumar, P., Khan, R.A., Choonara, Y.E. & Pillay, V. A prospective overview of the essential requirements in molecular modeling for nanomedicine design. *Future Med Chem* **5**, 929-946 (2013).

10. Sengupta, S. & Kulkarni, A. Design principles for clinical efficacy of cancer nanomedicine: a look into the basics. *ACS Nano* **7**, 2878-2882 (2013).

11. Fan, E.K., *et al.* High-affinity pentavalent ligands of Escherichia coli heat-labile enterotoxin by modular structure-based design. *J Am Chem Soc* **122**, 2663-2664 (2000).

12. Kitov, P.I., *et al.* Shiga-like toxins are neutralized by tailored multivalent carbohydrate ligands. *Nature* **403**, 669-672 (2000).

13. Kitov, P.I., Shimizu, H., Homans, S.W. & Bundle, D.R. Optimization of tether length in nonglycosidically linked bivalent ligands that target sites 2 and 1 of a Shiga-like toxin. *J Am Chem Soc* **125**, 3284-3294 (2003).

14. Tassa, C., *et al.* Binding affinity and kinetic analysis of targeted small molecule-modified nanoparticles. *Bioconjug Chem* **21**, 14-19 (2010).

15. Li, M.H., *et al.* Dendrimer-based multivalent methotrexates as dual acting nanoconjugates for cancer cell targeting. *Eur J Med Chem* **47**, 560-572 (2012).

16. Hein, C.D., Liu, X.M. & Wang, D. Click chemistry, a powerful tool for pharmaceutical sciences. *Pharm Res-Dordr* **25**, 2216-2230 (2008).

17. Lallana, E., Sousa-Herves, A., Fernandez-Trillo, F., Riguera, R. & Fernandez-Megia, E. Click Chemistry for Drug Delivery Nanosystems. *Pharm Res-Dordr* **29**, 1-34 (2012).

18. Kolb, H.C., Finn, M.G. & Sharpless, K.B. Click chemistry: Diverse chemical function from a few good reactions. *Angew Chem Int Edit* **40**, 2004-+ (2001).

19. Brennan, J.L., *et al.* Bionanoconjugation via click chemistry: The creation of functional hybrids of lipases and gold nanoparticles. *Bioconjugate Chem* **17**, 1373-1375 (2006).

20. Ranjan, R. & Brittain, W.J. Tandem RAFT polymerization and click chemistry: An efficient approach to surface modification. *Macromol Rapid Comm* **28**, 2084-2089 (2007).

21. White, M.A., Johnson, J.A., Koberstein, J.T. & Turro, N.J. Toward the syntheses of universal ligands for metal oxide surfaces: Controlling surface functionality through click chemistry. *J Am Chem Soc* **128**, 11356-11357 (2006).

22. O'Reilly, R.K., Joralemon, M.J., Wooley, K.L. & Hawker, C.J. Functionalization of micelles and shell cross-linked nanoparticles using click chemistry. *Chem Mater* **17**, 5976-5988 (2005).

23. Zong, H., *et al.* Bifunctional PAMAM dendrimer conjugates of folic acid and methotrexate with defined ratio. *Biomacromolecules* **13**, 982-991 (2012).

24. Wu, P., *et al.* Multivalent, bifunctional dendrimers prepared by click chemistry. *Chem Commun (Camb)*, 5775-5777 (2005).

25. Wan, T.C., *et al.* Polyamidoamine (PAMAM) dendrimer conjugate specifically activates the A3 adenosine receptor to improve post-ischemic/reperfusion function in isolated mouse hearts. *BMC Pharmacol* **11**, 11 (2011).

26. Schlick, K.H., Morgan, J.R., Weiel, J.J., Kelsey, M.S. & Cloninger, M.J. Clusters of ligands on dendrimer surfaces. *Bioorg Med Chem Lett* **21**, 5078-5083 (2011).

27. Wangler, C., *et al.* Multimerization of cRGD Peptides by Click Chemistry: Synthetic Strategies, Chemical Limitations, and Influence on Biological Properties. *Chembiochem* **11**, 2168-2181 (2010).

28. Gopin, A., Ebner, S., Attali, B. & Shabat, D. Enzymatic activation of second-generation dendritic prodrugs: Conjugation of self-immolative dendrimers with poly(ethylene glycol) via click chemistry. *Bioconjugate Chem* **17**, 1432-1440 (2006).

29. Baskin, J.M., *et al.* Copper-free click chemistry for dynamic in vivo imaging. *P Natl Acad Sci USA* **104**, 16793-16797 (2007).

30. Huang, B.H., *et al.* Copper-free click conjugation of methotrexate to a PAMAM dendrimer platform. *Tetrahedron Lett* **52**, 1411-1414 (2011).

31. Goonewardena, S.N., *et al.* Design considerations for PAMAM dendrimer therapeutics. *Bioorg Med Chem Lett* **23**, 2872-2875 (2013).

32. Mullen, D.G., *et al.* A Quantitative Assessment of Nanoparticle-Ligand Distributions: Implications for Targeted Drug and Imaging Delivery in Dendrimer Conjugates. *ACS Nano* **4**, 657-670 (2010).

33. Sreedhara, A. & Cowan, J.A. Catalytic hydrolysis of DNA by metal ions and complexes. *J Biol Inorg Chem* **6**, 337-347 (2001).

34. Choi, S.K., *et al.* Dendrimer-based multivalent vancomycin nanoplatform for targeting the drug-resistant bacterial surface. *ACS Nano* **7**, 214-228 (2013).

35. Thomas, T.P., *et al.* Polyvalent dendrimer-methotrexate as a folate receptor-targeted cancer therapeutic. *Mol Pharm* **9**, 2669-2676 (2012).

36. Zhang, Z.Y., Cheng, Q. & Feng, P.Y. Selective Removal of DNA-Labeled Nanoparticles from Planar Substrates by DNA Displacement Reactions. *Angew Chem Int Edit* **48**, 118-122 (2009).

37. Cutler, J.I., Zheng, D., Xu, X.Y., Giljohann, D.A. & Mirkin, C.A. Polyvalent Oligonucleotide Iron Oxide Nanoparticle "Click" Conjugates. *Nano Lett* **10**, 1477-1480 (2010).

38. Massich, M.D., Giljohann, D.A., Schmucker, A.L., Patel, P.C. & Mirkin, C.A. Cellular Response of Polyvalent Oligonucleotide-Gold Nanoparticle Conjugates. *Acs Nano* **4**, 5641-5646 (2010).

39. Mangold, S.L. & Cloninger, M.J. Binding of monomeric and dimeric Concanavalin A to mannose-functionalized dendrimers. *Org Biomol Chem* **4**, 2458-2465 (2006).

CHAPTER 6

CONLCUSIONS AND OUTLOOK

This dissertation has systematically investigated factors that regulate the multivalent binding of nanoparticles and in particular explored how the heterogeneity of nanoparticle populations alter binding distributions of these particles. These studies have resulted in a comprehensive analysis of the structure-function relationship that underlies binding and can inform the design of targeted drug delivery carriers. The binding avidity of nanoparticles could be specifically and greatly optimized by using a combination of these design parameters, depending on the properties of the targeting ligands on the nanoparticle.

In Chapter 2, the kinetic behavior of heterogeneous binding synthetic multivalent nanoparticles was evaluated. We developed the means to perform kinetic analyses to identify the binding subpopulations in ligand-functionalized nanoparticles and to evaluate the avidity distribution of our materials. We documented that only a small portion of ligand-functionalized nanoparticles actually gain avidity enhancement due to their multivalent structure. Based on a kinetic simulation for this heterogeneous binding, we realized that the percentage of strong binding nanoparticles existing in the population is really the key that determines the quantity of nanoparticles that are attached and retained on a targeted surface as a result of targeted delivery. Our approach toward modeling this activity can offer binding information in a real-time fashion and would be valuable in future applications of high-

throughput screening of different targeting systems on synthetic multivalent targeting nanoparticles.

In Chapter 3, a series of PAMAM dendrimers with varied numbers of ssDNA oligonucleotides were synthesized as a test system to examine the effect of valence on the binding avidity of synthetic multivalent nanoparticles. We demonstrated that the avidity distribution of the multivalent nanoparticles was related to the number of functionalized ligands per nanoparticle. In particular, the proportion of nanoparticles showing enhanced binding avidity would decrease as the valence of the ligands on the nanoparticle decreased, and avidity increases would vanish when the valence became lower than three. Comparing the results of Poisson simulation of ligand distribution and the experimentally derived avidity distribution, we validated the threshold valence that initiates the multivalent interactions and showed its potential to provide a rational and quantitative approach to optimize the binding avidity of multivalent nanoparticles. It became apparent that as compared to the heterogeneous binding observed with most nanoparticle systems, one could develop multivalent nanoparticles with homogeneous, strong binding avidity by increasing the ligand valence and making sure that every particle had a ligand number higher than the threshold valence required for the presence of multivalent binding.

In Chapter 4, we explored the effects of intrinsic ligand affinity on the binding avidity of multivalent nanoparticles, using oligonucleotide-functionalized PAMAM dendrimers as model nanoparticles. The first approach was to use identical oligonucleotides on the nanoparticles but to change the ambient binding temperature to alter the affinity. The second approach was to synthesize model nanoparticles with different sequence oligonucleotide ligands to vary affinity. Both results suggested that lower affinity ligands seemed more

effective in promoting multivalent interactions. Therefore when selecting targeting ligands to build multivalent nanoparticles to a targeted receptor, one could use lower-affinity ligands and yield higher targeted binding of the nanoparticles. However, the second approach, characterized with ligands with a slower dissociation rate, showed an avidity distribution present with a higher percentage of "multivalent-avidity" nanoparticles and a lower threshold valence for performing multivalent interactions. This result further suggests that, compared to the affinity of ligand, the dissociation rate may play a more important role in promoting multivalent interactions.

In Chapter 5, we employed copper-free SPAAC "click chemistry" conjugation to enhance the number and consistency of oligonucleotides that we conjugated to PAMAM dendrimers. The purpose of this was to assure that the vast majority of the particles in the nanoparticle population surpassed the threshold valence required for multivalent interactions. Our results indicated that the copper-free click chemistry accomplished a nearly complete conjugation reaction of free ligands to dendrimers and attached sufficient oligonucleotides onto each dendrimer to support uniform multivalent interactions. This eliminated the subpopulation showing the "monovalent-like" binding avidity due to inadequate numbers of ligands. The kinetic analyses demonstrated the superior binding resulting from a consistently high valence, illustrated by a 50,000-fold avidity enhancement and 14-pM K_D. In addition to design valence, based on this successful approach, we can also suggest guidelines to design synthetic multivalent nanoparticles, including: 1) proper linkers would promote multivalent interactions, resulting in enhancing the binding avidity or decreasing the threshold valence of multivalent interactions, and 2) the well-dispersed ligands on nanoparticles such as

oligonucleotides may promote higher multivalent interactions due to less opportunity to cause ligand-ligand or ligand-nanoparticle aggregation.

In this dissertation, I have demonstrated that multivalent interactions of ligand-functionalized nanoparticles are significantly regulated by a variety of design parameters, including the number of ligands (valence), the length of the linkers, and the affinity of the ligands. However, when examining the effect of these design parameters using single-factor analyses one cannot probe the cooperative effect of multiple design parameters. To approach the actual optimized design of synthetic multivalent nanoparticles, it is necessary to conduct a multivariate analysis that considers multiple design parameters simultaneously, which will be a future goal of our work.

One of the future goal of our studies is to employ the "design of experiment (DOE)" method to facilitate the optimization process. In fact, DOE methods have been used in optimizing drug delivery systems and targeted-delivery carries.[1-4] The requirement of the amount of nanoparticles with varied combinations of design parameters can be significantly reduced. For instance, if we intend to optimize the design of multivalent nanoparticles considering valence, the length of linker, the affinity of ligand and the size of dendrimer as design parameters, by using the most popular DOE method, the Taguchi design, we only need to prepare a library of synthetic multivalent nanoparticles with 9 combinations of variables (three levels of each parameter). (Table 6.1) If using a traditional optimizing method, this library would need to contain full combinations with all design parameters, involving 3^4 (81) species of nanoparticles.

Another goal of this work is to design and synthesize the optimized multivalent nanoparticles with other types of biological targeting ligands, such as small molecule vitamins (folic acid). It is obvious that there will be a number of challenges that will need to be addressed in this process. First, one must retain the binding affinity of the targeting ligand, and thus one should retain the intact structure of the binding moiety. To accomplish this, the coupling chemistry for the attachment of the linkers should not change the structure. Second, ligand-ligand aggregation for enhancing needs to be avoided to maximize the number of ligands that maintain their original affinity. Using hydrophilic linkers attached to the ligands may help separate each targeting ligand, but only if solubility of the nanoparticle is maintained. Additionally, we aim to create a receptor-immobilized surface with uniform density and orientation for the evaluation of binding avidities. This improvement of our model system will prevent aberrant measurements from heterogeneity in the sensor surface so that the effects of heterogeneity of the nanoparticles can be isolated and identified.

Table 6.1 Design of experiment using Taguchi method.

	Size of nanoparticle	Length of linker	Affinity of ligand	Valence of nanoparticle
L1	1	1	1	1
L2	1	2	2	2
L3	1	3	3	3
L4	2	1	2	3
L5	2	2	3	1
L6	2	3	1	2
L7	3	1	3	2
L8	3	2	1	3
L9	3	3	2	1

1: level 1 (highest); 2: level 2 (medium); 3: level 3 (lowest)

6.2 References

1. Singh, B., Kumar, R. & Ahuja, N. Optimizing drug delivery systems using systematic "Design of experiments." Part I: Fundamental aspects. *Crit Rev Ther Drug* **22**, 27-105 (2005).

2. Mahmoudi, M., Simchi, A., Imani, M., Milani, A.S. & Stroeve, P. Optimal Design and Characterization of Superparamagnetic Iron Oxide Nanoparticles Coated with Polyvinyl Alcohol for Targeted Delivery and Imaging. *J Phys Chem B* **112**, 14470-14481 (2008).

3. Emami, J., Rezazadeh, M., Varshosaz, J., Tabbakhian, M. & Aslani, A. Formulation of LDL Targeted Nanostructured Lipid Carriers Loaded with Paclitaxel: A Detailed Study of Preparation, Freeze Drying Condition, and In Vitro Cytotoxicity. *J Nanomater* (2012).

4. Nayebsadrian, M., *et al.* Screening the Most Effective Variables on Physical Properties of Folate-Targeted Dextran/Retinoic Acid Micelles by Taguchi Design. *J Nanomater* (2012).